Marta Laņģe
2024 | Riga

Clinical Validation of Non-contact Skin Evaluation and Imaging Technologies

Doctoral Thesis

Submitted for the Doctoral degree in Physics and Astronomy

Subfield: Medical Physics

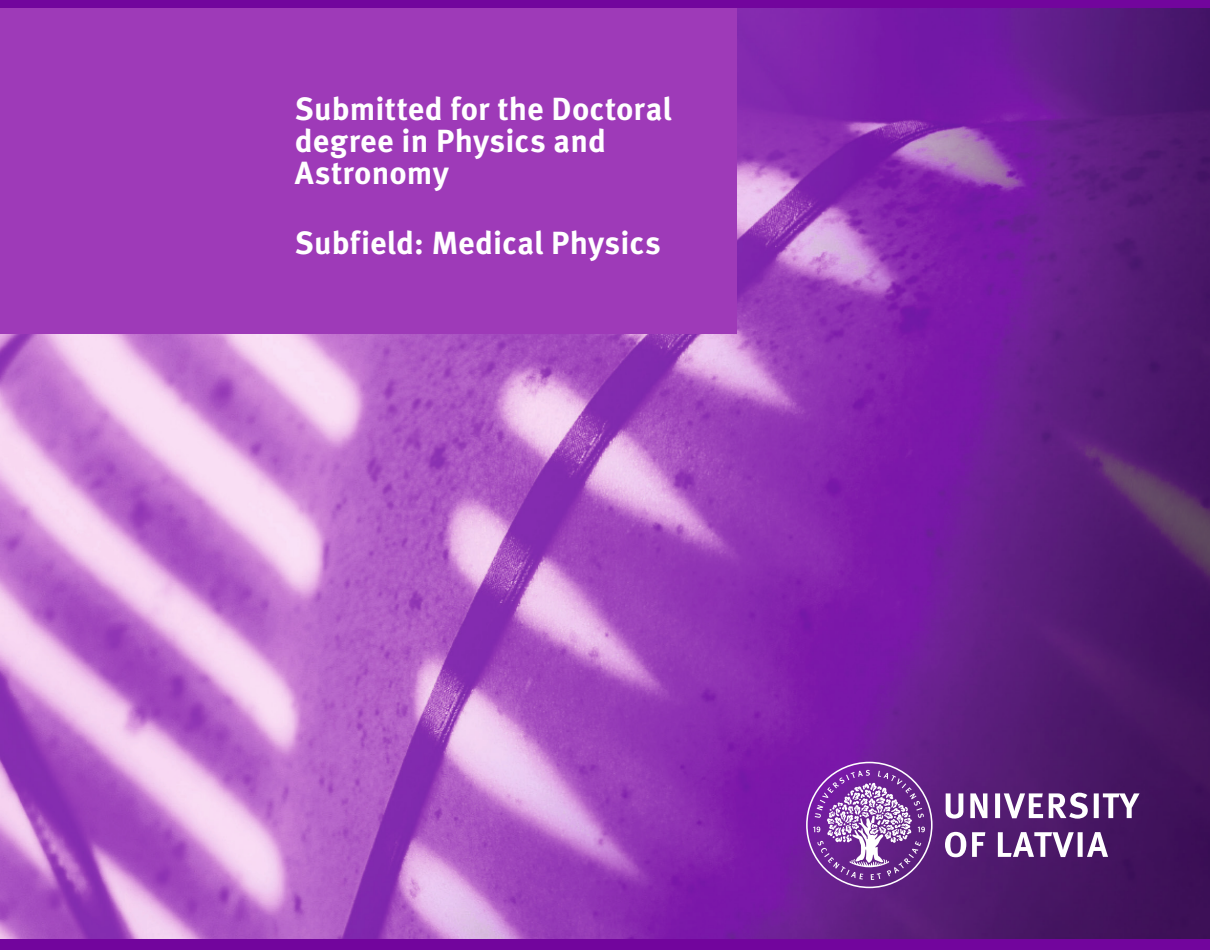

UNIVERSITY OF LATVIA

UNIVERSITY OF LATVIA

FACULTY OF PHYSICS, MATHEMATICS AND OPTOMETRY

Marta Laņģe

CLINICAL VALIDATION OF NON-CONTACT SKIN EVALUATION AND IMAGING TECHNOLOGIES

DOCTORAL THESIS

Submitted for the Doctoral degree in Physics and Astronomy
Subfield: Medical Physics

Riga
2024

The doctoral thesis was carried out at the Biophotonics laboratory, Institute of Atomic physics and spectroscopy, Faculty of Physics, mathematics and optometry, University of Latvia from 2014 to 2023.

Form of the thesis: dissertation in medical physics.

Supervisor: professor Dr. habil. phys. Jānis Spīgulis.

Reviewers:
1) Dr. phys. Gunta Krūmiņa, University of Latvia;
2) Dr. phys. Aleksejs Kataševs, Riga Technical university;
3) Dr. Walter Blondel, Université de Lorraine, France.

The thesis will be defended at the public session of the doctoral committee of Physics and astronomy, University of Latvia on 12th of September, 2024 at 3 Jelgavas Street, Rīga.

The thesis is available at the library of the University of Latvia, 19 Raiņa Boulevard, Rīga.

Chairman of the Doctoral Committee _____ / Gunta Krūmiņa /
(signature)

Secretary of the Doctoral Committee _____ / Sintija Siliņa /
(signature)

Cover design: Līga Bērziņa

ANOTĀCIJA

Šajā promocijas darbā ir aplūkoti risinājumi aizdomīgu izmaiņu agrīnai atklāšanai veidojumos uz cilvēku ādas, cenšoties mazināt ādas vēža gadījumu skaita pieaugumu un tā diagnostiku vēlīnā stadijā. Turklāt ir pētītas iespējas noteikt brīdi, kad anestēzija ir kļuvusi efektīva pirms ķirurģiskajām procedūrām, izmantojot bezkontakta attēlošanu.

Ir izstrādāti, ieviesti un klīniski apstiprināti trīs tehnoloģiskie risinājumi bezkontakta attēlveidošanas metožu pielietošanai *in-vivo* ādas izmaiņu noteikšanai: divi risinājumi ādas vēža skrīningam: viedtālruņa autofluorescences attēlošanas sistēma un pārnēsājama gaismu emitējošu diožu ādas skrīninga ierīce, un trešais: bezkontakta fotopletizmogrāfijas monitoringa ierīce reģionālās anestēzijas novērtēšanai. Promocijas darba mērķis ir izstrādāt un klīniski validēt optiskās ādas attēlošanas tehnoloģijas neinvazīvu ādas veidojumu izšķiršanai un reģionālās anestēzijas efektivitātes novērtēšanai. Galvenās izmantotās metodes ir: difūzās atstarošanas attēlošana, autofluorescences attēlošana un bezkontakta fotopletizmogrāfija. Dažādos pētījumu posmos tika iegūti vairāk nekā četri tūkstoši multispektrālu attēlu, un piedalījās vairāk nekā 550 brīvprātīgo pacientu.

Nozīmīgākie secinājumi ir šādi: autofluorescences intensitātes attiecība varētu būt indikators iespējamam vēža recidīvam un tam, cik labi dzīst ādas vēža pēcoperācijas rēta; viedtālruņa autofluorescences attēlveidošanas sistēma un pārnēsājamas gaismas diožu ādas skrīninga ierīces ir noderīgi instrumenti dermatologam klīnisko lēmumu pieņemšanas procesā; bezkontakta fotopletizmogrāfijas anestēzijas monitoringa ierīce ir apstiprināta lietošanai klīniskajā vidē ādas mikrocirkulācijas novērošanai.

Atslēgas vārdi: autofluorescence, attēlošana, neinvazīvs, pēcoperāciju rētas, skrīnings, ādas vēzis.

ABSTRACT

In this doctoral thesis solutions for early detection of suspicious changes in human skin lesions have been discussed, trying to reduce the challenge of increasing skin cancer cases and its detection only at a late stage. In addition, the possibilities of determining the moment when anesthesia has become effective before the surgical procedures by using contactless imaging have been studied.

Three technological solutions for the application of non-contact imaging methods for detecting changes of *in-vivo* skin have been developed, implemented and clinically validated: two solutions for skin cancer screening: a smartphone autofluorescence imaging system and a portable light emitting diode skin screening device, and the third: remote photoplethysmography anesthesia monitoring device for evaluating regional anesthesia. The goal of the thesis is to develop and clinically validate optical *in-vivo* skin imaging technologies for non-invasive skin lesion differentiating and assessing the effectiveness of regional anesthesia. The main used methods are: diffuse reflectance imaging, autofluorescence imaging and remote photoplethysmography. There were more than four thousand multispectral images acquired during different stages of research, and more than 550 volunteer patients participated.

The most significant conclusions are: autofluorescence intensity ratio could be an indicator of possible cancer recurrence and how well the skin cancer post-operative scar is healing; a smartphone autofluorescence imaging system and a portable light emitting diode skin screening devices are valid tools for the dermatologist in clinical decision making; the remote photoplethysmography anesthesia monitoring device is approved to be used in clinical environment for monitoring the skin microcirculation.

Keywords: autofluorescence, imaging, non-invasive, post-operative scars, screening, skin cancer.

CONTENTS

Abbreviations 7

Introduction 8

1 Literature review 10
- 1.1 Human skin 10
  - 1.1.1 Benign malformations of the skin 10
- 1.2 Skin pathologies 12
  - 1.2.1 "Ugly Duckling" principle and ABCDE evaluation 13
  - 1.2.2 Types of skin cancer 13
  - 1.2.3 Skin cancer incidence in Latvia 14
- 1.3 Post-operative scars 16
- 1.4 Fitzpatrick scale 18
- 1.5 Current situation regarding skin screening 19
  - 1.5.1 Skin screening protocols 19
  - 1.5.2 Rapid changes in lifestyle and technology 20
- 1.6 Commercial diagnostic imaging devices for dermato-oncology 21
  - 1.6.1 Dermatoscope 21
  - 1.6.2 High frequency ultrasound imaging 21
  - 1.6.3 Optical coherence tomography imaging 22
  - 1.6.4 FotoFinder 23
  - 1.6.5 Devices that use multiscpectral illumination 24
- 1.7 Non-contact diagnostic imaging techniques: the basics 24
  - 1.7.1 Diffuse reflectance imaging 24
  - 1.7.2 Autofluorescence 27
  - 1.7.3 Combined imaging: diffuse reflection and autofluorescence 28
  - 1.7.4 Photoplethysmography technology 29

2 Methodology of measurements and data processing 33
- 2.1 Portable LED skin screening device for skin malformation diagnostics 33
  - 2.1.1 Autofluorescence and diffuse reflection imaging 33
  - 2.1.2 Patient selection 34
  - 2.1.3 Image acquisition and analysis 34
  - 2.1.4 Post-operative scar imaging 34
  - 2.1.5 Imaging parameters 35
  - 2.1.6 Device setup 36
  - 2.1.7 Parameter p' 39
- 2.2 Smartphone AF imaging system for skin malformation diagnostics 39
  - 2.2.1 Experimental setup 40
  - 2.2.2 Image processing technique 40
  - 2.2.3 Patient selection 40
  - 2.2.4 Measurement protocol 41

2.3 Regional anesthesia effectiveness evaluation with PPG imaging 41
2.3.1 Application of remote PPG in anesthesiology 41
2.3.2 Remote PPG monitoring device for regional anasthesia 42
2.3.3 Video processing 43
2.3.4 Measurement procedure and patient selection 44

3 Results 45
3.1 Validation results of smartphone AF imaging system 45
3.2 Validation results of the portable LED skin screening device 48
3.2.1 Malignant lesion evaluation 48
3.2.2 Post-operative scar evaluation 53
3.3 Validation results of the remote PPG monitoring device 57

4 Discussion 61
4.1 Smartphone autofluorescence imaging system 61
4.2 Portable LED skin screening device 61
4.3 Screening of post-operative scars 62
4.4 Remote PPG monitoring device 62

5 Conclusions 64

Thesis for the defense 66

List of publications 67

Participation in conferences 68

References 71

Acknowledgements 78

Annex 1 80

Annex 2 81

Annex 3 82

Annex 4 83

ABBREVIATIONS

AF – autofluorescence
AI – artificial intelligence
a.u. – arbitrary units
AVI – autio video interleave
BCC – basal cell carcinoma
CMOS – Complementary metal-oxide-semiconductor
FDA – Food and Drug Administration
IR – infrared
I.R. – intensity ratio
LAN – local area network
LED – light emitting diode
Li-on – lithium ion
LOC – Oncology Centre of Latvia
MM – malignant melanoma
NAD – nicotamide adenine dinucleotide
OEM – original equipment manufacturer
QSXGA – Quad Super Extended Graphics Array
RA – regional anesthesia
RGB – red, green, blue
ROI – region of interest
PPG – photoplethysmography
SCC – squamous cell carcinoma
SDRAM – synchronous dynamic random-access memory
SK – Seborrheic keratosis
TOS – Hospital of Traumatology and Orthopedics
USB – universal serial bus
USA – United States of America
UV – ultraviolet

INTRODUCTION

The motivation for choosing the topic is the increasing numbers of skin cancer patients whose diagnosis unfortunately is made quite late (at stages III and IV), educating society about healthy skin and skin cancer issues, showing the importance of yearly skin screening for all age groups, as well as bringing society's awareness about habits of sunbathing and using sun protection.

Regarding the remote regional anesthesia (RA) monitoring, the motivation is to introduce non-contact evaluation system that can help improve the patient's experience during the surgery, as well as save the hospital's resources and make their work more efficient.

In addition, author's personal interest in developing innovative, easy-to-use, and accessible diagnostic equipment to help people bring awareness of their physical health condition faster, easier and more affordable across various geographical areas.

This doctoral thesis consists of three parts, aiming to reach **the goal of the thesis**: to develop and clinically validate optical *in-vivo* skin imaging technologies for differentiating skin lesions and assessing the effectiveness of RA.

The **objectives** of this work are:

1. To participate in the design and validation of non-invasive, portable light emitting diode (LED) skin screening device (further in text **portable LED skin screening device**) with diffuse reflectance (DR) and fluorescence features. During the validation acquire various clinical multispectral images of skin cancer lesions: malignant melanoma (MM), basal cell carcinoma (BCC), etc., as well as benign lesions: nevus, seborrheic keratosis (SK) and hemangioma, post-operative scar images and others;
2. To participate in clinical validation of smartphone autofluorescence (AF) imaging system (further in text **smartphone AF imaging system**). During validation acquire clinical multispectral images of various skin lesions: both malignant and benign;
3. To clinically test and validate remote photoplethysmography (PPG) imaging device to evaluate the effectiveness of regional anesthesia (RA) before surgery (further in text **remote PPG monitoring device**).

The **innovation** of this work are the first attempts to evaluate post-operative scar healing after skin cancer surgery with multispectral imaging in different time periods to detect possible cancer recurrence. In addition, the mentioned three different optical *in-vivo* skin imaging technologies have been validated at a clinical environment.

The main **methods** used for clinical measurements are:

Spectral imaging – image acquisition at different spectral bands: red (R), green (G), blue/violet (B), infrared (IR) to acquire information about skin chromophores.

DR imaging – a quantitative technique, determining optical absorption and optical scattering, using visible and near IR light to evaluate the chromophores in skin.

AF imaging – analysing skin fluorophore distribution images acquired at 405 nm (violet) illumination that induces certain tissue AF and can provide clinical information about the lesion.

Remote PPG – an imaging method that reveals information about skin blood pulsations for characterization of blood oxygenation level and blood volume changes in dermis.

The work described in this thesis was done over the time period 2014–2023 at the Biophotonics Laboratory, Institute of Atomic physics and spectroscopy, University of Latvia; the clinical validation studies were performed in collaboration with Oncology Centre of Latvia (LOC), Dermatology Department, Semmelweis University in Budapest, Hungary, as well as Hospital of Traumatology and Orthopedics (TOS) in Riga, Latvia. In total, there were more than 553 volunteer patients included in 11 different studies, and more than four thousand images acquired of different skin lesions and conditions.

The work would not have been possible without the support of scientific research project grants (please, see the complete list of grants in the Acknowledgements paragraph).

The main results have been presented in: 14 published papers cited in *Scopus, Web of Science, Web of Conferences* and *PubMed* databases, as well as at international conferences with10 oral and 8 poster presentations. The author has received awards in 5 international contests and scientific events for the topics presented in this work.

This doctoral thesis consists of 83 pages in total (76 pages – the work; 7 pages – references), 4 annexes, 53 figures and 135 references.

1 LITERATURE REVIEW

1.1 Human skin

Skin is the largest human organ, weighing about 5 kg and covering an area of about 2 m^2 [1].

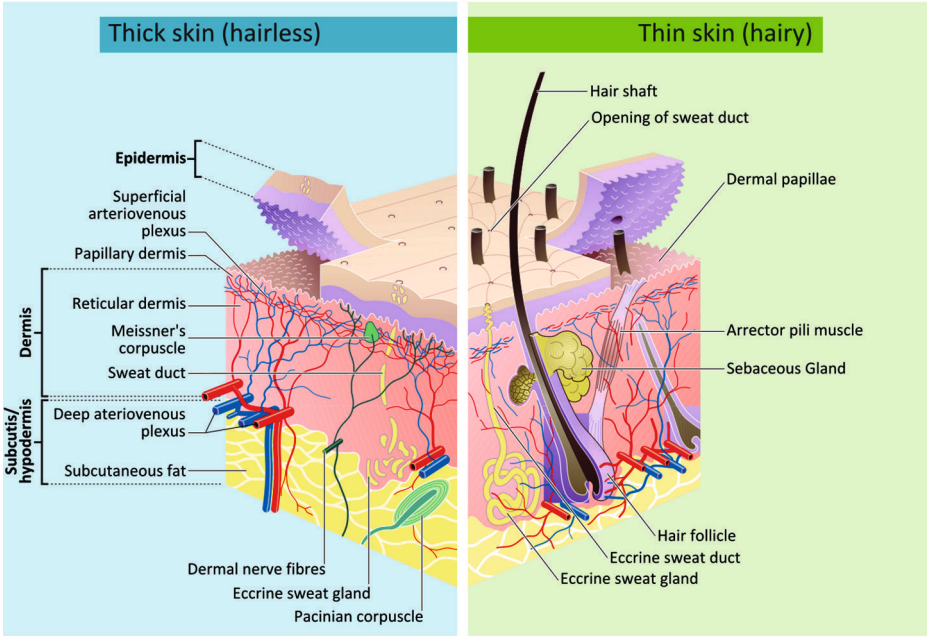

Figure 1. **Human skin layers** [2]

It consists of three main layers: epidermis, dermis and hypodermis (Figure 1 on the left). Epidermis is the outermost layer, comprising constantly renewing layers of cells, for instance, keratinocytes. Dermis is the inner layer composed of dense connective tissue, containing the nerves and blood vessels that supply the skin. Hypodermis is the layer of loose connective tissue under the skin [1].

1.1.1 Benign malformations of the skin

There are various benign and harmless lesions on human skin. Some of them can appear due to lifestyle or health issues or with time as human skin ages. Although maybe sometimes visually similar to the malignant lesions, sometimes these lesions can be misdiagnosed as harmful, causing unnecessary medical expenses and medical procedures for the patient. Here some of the most common benign lesions with its features are described.

1.1.1.1 Melanocytic nevus

Melanocytic nevus is the most common benign lesion on human body, also called as *birthmark* or a *mole*.

Melanocytic nevi are neoplasms composed of melanocytes – cells of human body that produces pigment in epidermis [3].

Figure 2. **Nevus. Clinical colour image of a patient. Photo by Dr. Luca Fesus**

Normally, there are up to 50 nevi on human body. These are usually subdivided into: congenital, common, dysplastic, blue, Spitz nevus, etc.

1.1.1.2 Seborrheic keratosis

Seborrheic keratosis (SK) is very common benign epithelial skin tumours encountered in the adult population; they show an increasing incidence with age, which reaches a peak at ~60 years [4]. SK is a slow-growing lesion, typically raised and sometimes has a rough texture. These growths are neither viral nor bacterial and, therefore, cannot spread [5].

Different histologic and clinical subtypes have been identified. The great variability of SK raises some difficulties in diagnosis. Dermoscopy is the preferred non-invasive diagnostic method, in particular to differentiate pigmented SK from other pigment tumours, including MM [4].

Due to the fact that SK usually has a superficial layer consisting of keratinocytes that give a strong autofluorescent (AF) signal [6], it is possible to distinguish it from MM, using the AF imaging. AF features can be a great diagnostic factor when differencing SK from BCC and MM [P10].

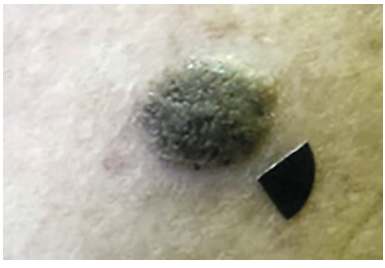

Figure 3. **Clinical image of SK and a marker sticker for scale and image stabilisation Photo by M. Lange**

1.1.1.3 Hemangioma

Hemangioma is a benign lesion consisting of endothelial cells and has vascular features. Visually, it appears as a red, purple or dark red spot on the skin [7]. Hemangiomas can occur anywhere on the body [8]. Darker hemangiomas can sometimes be misdiagnosed for other pigmented lesions, so using the DR multispectral imaging at G channel, hemangiomas can be easily distinguished because one of haemoglobin (oxyhemoglobin and deoxyhemoglobin) absorption spectra maximum peaks is at 550 nm (thus the G channel) in the visible region [9].

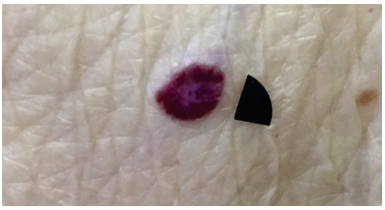

Figure 4. **Clinical image of Hemangioma. Photo by M. Lange**

1.1.1.4 Sun-damaged skin

Sun-damaged spots on the skin due to photoaging appear with time when the acquired UV light amount has caused DNA changes at a cellular level in dermis. Visually these lesions look like brown spots, broken capillaries, and uneven skin texture [10].

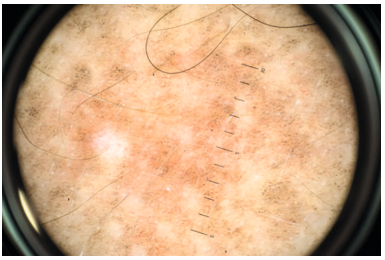

Figure 5. **Dermoscopy image of sun damaged skin** [11]

1.2 Skin pathologies

Skin cancer is the most common type of cancers [12]. If diagnosed early, skin cancer is treatable. As the majority of the cases are discovered in later stages of cancer, regular screening at primary care level is essential.

According to the World Health Organization, screening is defined as "the presumptive identification of unrecognized disease in an apparently healthy, asymptomatic population by means of tests, examinations or other procedures that can be applied rapidly and easily to the target population. A screening programme must include all the core components in the screening process from inviting the target population to

accessing effective treatment for individuals diagnosed with disease" [13]. Skin cancer screening programs and protocols vary widely depending on the country.

According to the Centre's for Disease Control and Prevention [14] estimate, skin cancer is one of the most common kind of cancer in the United States of America (USA); managing and treating the disease is a huge burden to the healthcare system. Unfortunately, often the skin cancer is being diagnosed at a late stage, so it is essential to develop early diagnostic and screening methods [P9]. In Latvia also the skin cancer (MM, BCC, etc.) often is diagnosed at the III or only IV stage, because the early skin screening unfortunately is not being performed or is ineffective [15].

In Latvia, according to the Centre for Disease Prevention and Control, the average new MM cases diagnosed in time period from 2010 till 2019 (for years: 2018 and 2019 there is only preliminary data) were 10.8+/–0.8 per population 100 000 or 214+/–15 yearly [16].

To compare with, in the USA in 2019, new cases of MM were 88 059 and rate per 100 000 population is 22.7 (95% Cl = 22.5 – 22.8) [14].

1.2.1 "Ugly Duckling" principle and ABCDE evaluation

Suspicious lesions on the skin, first of all, can be self-diagnosed at home by regularly checking visual changes of the body, especially before and after summer season. It is important to check for any changes or new formations on the skin by searching for the "ugly duckling" – a lesion that clearly stands out.

A widely used ABCDE principle is easily memorable, checking the suspicious lesion for features, like: A – **a**symmetry; B – uneven **b**orders; C – different in **c**olor; D – **d**iameter larger than 5mm (or height); E – **e**volving (changing in size); Also, it is important to notice any ulceration, itching or trauma [17].

1.2.2 Types of skin cancer

1.2.2.1 Malignant melanoma

MM arises from the melanocytes (pigment-producing cells) in the skin. Sunlight exposure especially in childhood, episodes of blistering sunburn, using tanning beds and a family history, as well as fair skin type are increasing factors for cancer. Unfortunately, MM often metastasize and is lethal for 0.6 per 100 000 population worldwide (data of 2020, according to World Cancer Research Fund International) [18].

(A) MM
Large MM on men's right breast. Photo by Dr. Szabolcs Bozsányi

(B) BCC [19]
Nodulo-cystic BCC on the forehead

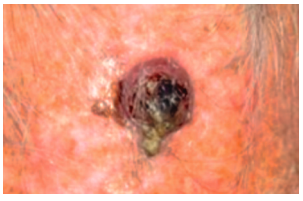

(C) SCC [20]
SCC on an 80-year old male's scalp

Figure 6. **Examples of typical skin cancers: (A) MM, (B) BCC, (C) SCC** [19], [20]

1.2.2.2 Basal cell carcinoma and Squamous cell carcinoma

BCC and Squamous cell carcinoma (SCC) are both usually caused by cumulative UV light exposure, see the comparison in Figure 6. BCC arises from the basal cell layer and is rare before the age of 40. It accounts for around 80% of skin cancers [21]. The lesion appears as raised, smooth, pink or browny-grey bump with a pearly border, which may have visible blood vessels of it. It grows slowly and very rarely metastasizes. SCC arises from the squamous cell layer. It may rarely also be due to chemical cancerogens or ionizing radiation, including UV light, usually occurs to patients older than 60. SCC accounts for ~16% of all skin cancers. The lesion is a raised, hard, pinkish and scaling patch that may ulcerate, bleed and crust. It slowly enlarges, sometimes developing into a large mass, and rarely metastasizes [1].

1.2.3 Skin cancer incidence in Latvia

The healthcare system of Latvia use the classification system ICD-10 Version: 2016 for disease classification [22]. The skin cancer types are divided as: C43 as MM of the skin and its subtypes and C44 that includes: BCC and SCC, and subtypes.

In Latvia on average there are approximately 200 newly discovered MM (C43) and 1300 non-melanoma cancer (C44) cases per year (see Figure 7) [15]. At first, the numbers might seem unalarming. However, population of Latvia is less than two million, from which 68% are the urban and 32% is the rural area [23]. The incidence of MM is about 10 cases and for non-melanoma skin cancer about 65 cases per 100 000 inhabitants (average in time period from 2010 till 2017, Figure 7) [15]. The primary healthcare availability, including proper dermatological examination, in rural areas should be essentially improved. That is one of the reasons MM and BCC is diagnosed at late stages.

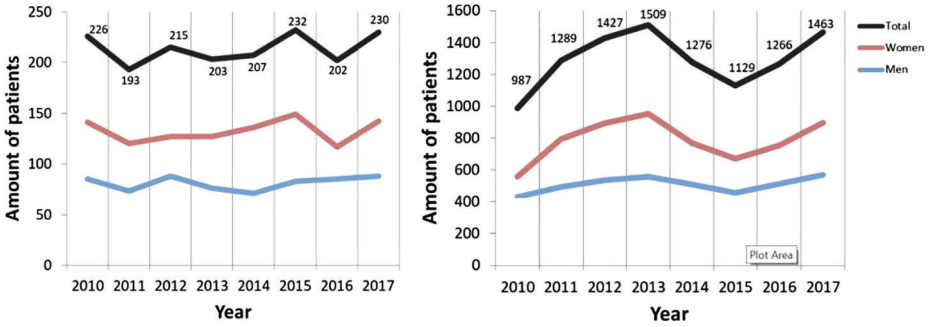

Figure 7. **Skin cancer statistics in Latvia from 2010 till 2017: incidence for MM (code C43) (on the left) and non-melanoma skin cancers (code C44) (on the right); the absolute amount of patients with first-time diagnosis** [15]

In order to keep up to date, author has added the latest statistics of skin cancer cases in Latvia in Annex 3 for more precise insight.

In the Strategy report of Society Health for 2001–2010 (G. Rozentale and colleagues) one of the aims was defined as: "The mortality in the population of age group of 65 and younger from visual localization type of cancers must be decreased by at least 15%".

The report shows an increase of the mortality from MM and other skin cancer types from 2001–2009. The mortality trend is increasing, and the defined aim of the Society Health Strategy was not reached. As a conclusion the report states that mortality from MM is 4 times higher compared to other skin cancer types. Also, by discovering the MM at a late stage, the first year mortality is three times higher [24].

So far there have been government funded cancer prevention programs only for breast, cervical and colorectal cancer in Latvia [25]. For skin cancer prevention, in 2018 there was a social campaign organized by The Centre for Disease Prevention and Control of Latvia that included an outreach to the society by providing information about the risks of extensive UV exposure, the use of tanning beds, as well as the first visual signs of skin cancer [26].

The actual self-check and skin lesion evaluation is the patient's own responsibility. If there is a concerning mole, there are several options in the existing healthcare system:

1) Patient turns to the family doctor for a consultation and if necessary, gets referred to the dermatologist or dermato-oncologist (can take up to two months of waiting time) of a government paid medical care;
2) Patient can visit the private sector dermatologist (waiting time up to two weeks, but the patient's cost will be approximately 10 times higher);
3) If the suspicious lesion is considered high risk, the patient is under the category of "urgent" and by using the "Green Corridor" the patient shall receive full check-up and diagnosis within several working days, but in the reality that it is not always the case.

The most common cancer type in women in Latvia (time period from year 2006 to 2015) after breast cancer (20%) is skin cancer including MM (14%); in men skin cancer is less common, but still frequent (10%). After successfully treated, the 5-year survival was the highest for skin cancer lesions, including MM, 71.3% for men and 77.2% for women, when compared with other types of cancer, for instance: breast, prostate, cervical, stomach, etc. [27].

In Figures 8 and 9 the distribution of MM (code C43) and most common C44 diagnosis which are BCC and SCC are shown. The MM is mostly being discovered at I and

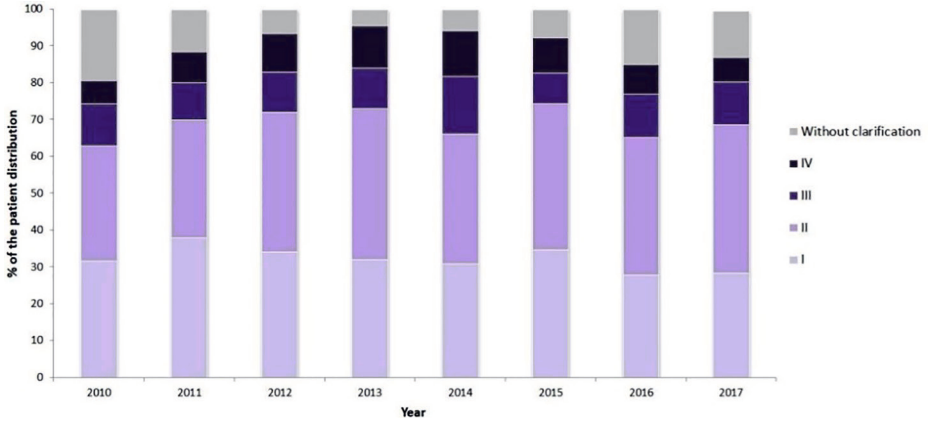

Figure 8. **Distribution of the patients (%) with MM stages I–IV in Latvia 2010–2017** [15]

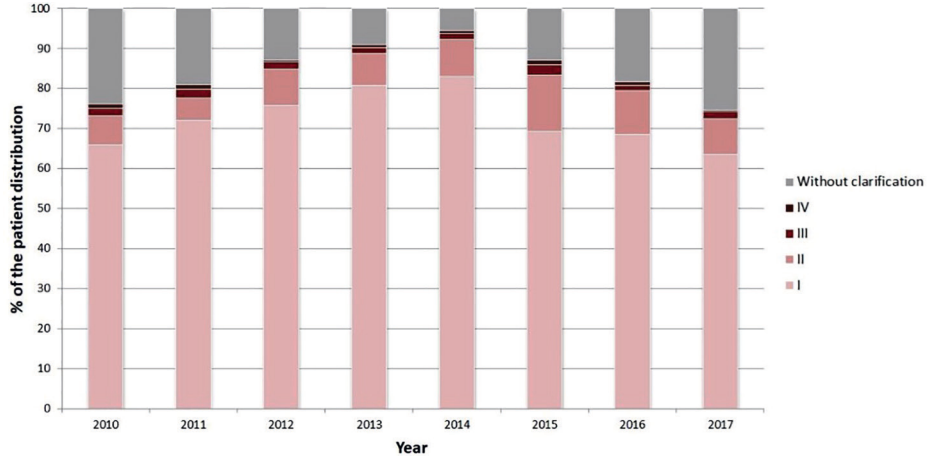

Figure 9. **Distribution of the patients (%) with non-melanoma cancer stages I–IV in Latvia 2010–2017** [15]

II stage, however, there is still a significant number of cases discovered at late stages: III (11.4%) and IV (9.1%), and what is more concerning, more than 10% of the histology diagnosis are "without clarification". For BCC and other C44 cancer types, luckily most are discovered at stages I (72.4%) and II (9.2%). Unfortunately, again diagnosis "without clarification" shows in more than 15% of the results [15].

1.3 Post-operative scars

Among the skin cancers, the MM accounts for ~1% of the cases while it is responsible for the majority of deaths. The BCC is the most common form of skin cancer with a very low mortality rate [28]. After removal of these skin cancers there is a risk of cancer local recurrence (see visual example in Figure 10). Recurrence range varies and is reported from 2.9% to 67% for BCC and up to 41.4% for MM [29], [30], [31].

Post-operative scar evaluation and follow-up is an essential part of the treatment plan. The monitoring of local cancer recurrence within the scar, ideally, should be integrated into the post-operative follow-up process of cancer patients, intended for effective treatment outcome and timely detection of tumour recurrence.

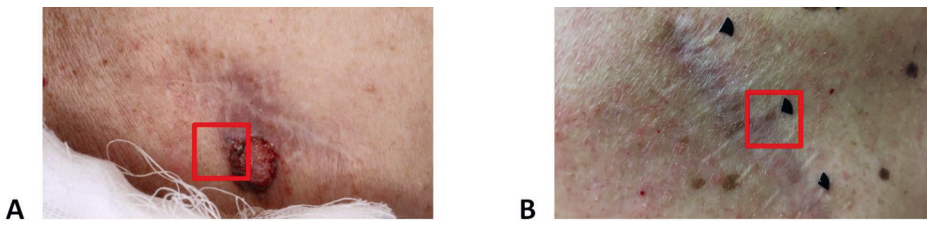

Figure 10. **Clinical images showing examples of (A) recurrent and (B) healthy healing scar after MM surgery. Field of view (2.0 × 2.0 cm) marked with a red rectangle** [P4]

Currently, post-surgical/therapy scar follow-up in clinical practice is presented by subjective visual examination of the scar followed by a dermoscopic evaluation.

However, a serious limitation of this approach is a large number of false positive results. In particular, the diagnostic accuracy of skin lesions mainly depends on the dermatologist's experience and can vary according to different estimates in the range of 29–88% [32].

Moreover, the lack of clinical guidelines of imaging methods for follow-up of the post-operative scars in combination with the still not so widely used dermoscopy practice leaves an impact on clinical practice quality. Such a great and varying number of recurrences is a signal that recurrent cases are not always reported accordingly, there is a lack of trusted, transparent, verified, easy-to use system in the whole process of steps: lesion diagnosis, imaging, surgery, histology, treatment and regular follow-up. According to Lawrence, L Yu et al. there are still challenges with proper lesion staging, taking into account metastasis that are found in the site of primary excision that are often considered as cutaneous or subcutaneous melanoma recurrences [33].

The reason why post-operative surgical scars are particularly interesting is the complexity and number of physiological processes behind the wound while it is healing. As it is not possible to see and evaluate the process as it happens visually, and for each patient it can be different, to distinguish whether the scar heals properly, can be a challenge. Normally, there are four basic stages of wound healing: 1) Hemostasis, 2) Inflammation, 3) Proliferation and 4) Maturation (see Figure 11) [34].

The healing process takes time; still, it is crucial to evaluate healing, especially after skin cancer removal. The process is complex, and the healing stages can vary from patient to patient, the most intense healing takes place during the first year after surgery (see Figure 12).

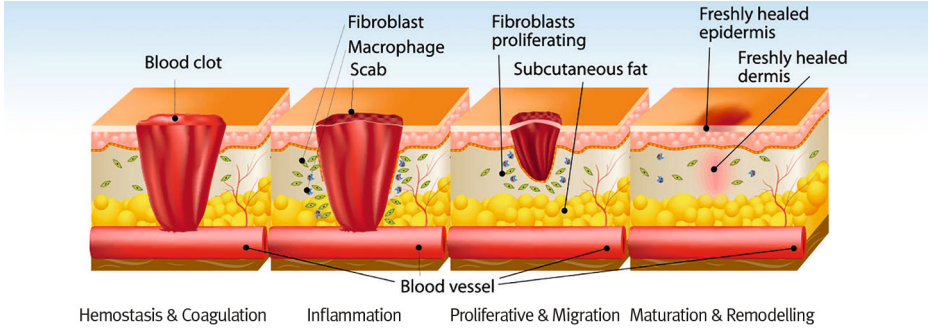

Figure 11. **Wound healing stages** [34]

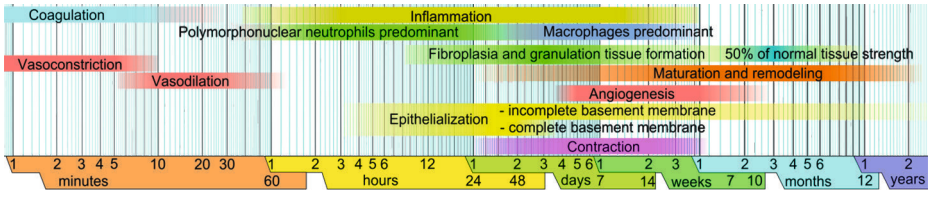

Figure 12. **Phases of wound healing. Limits vary within faded intervals, mainly by wound size and healing conditions, but image does not include major impairments that cause chronic wounds. Image author: Mikael Häggström** [35]

The blood vessels dilate after homeostasis is achieved. This allows white blood cells, nutrients, enzymes, antibodies, and other beneficial elements reach the affected area to accelerate wound healing. The second stage in the wound healing process is proliferation in which new, healthy granulation tissue replaces the wound. It is important that the blood vessels receive enough nutrients and oxygen to form granulation tissue. The tissue consists of a mixture of collagen and extracellular matrix, which helps develop a new network of blood vessels. During the process, the color of granulation tissue will change. If it is pink or red, it usually means that it is healthy. It indicates infection when the color of granulation tissue is rather dark. Maturation or remodelling is the end stage of the wound healing process. It takes place soon after the wound has closed up. This stage may continue for a couple of years and involves repair of the dermal tissues to improve their tensile strength. During this stage, functional fibroblasts will replace non-functional one and the number of blood vessels in the area will also decrease gradually. Factors that can affect wound healing, include: age and immune system response, as well as medication effects, nutrition, stress, infection, etc. [34].

1.4 Fitzpatrick scale

In dermatology for human skin classification very widely used is the Fitzpatrick scale (see Figure 13), developed by Thomas B. Fitzpatrick. It is a way to classify different skin types and their response to UV irradiation, measuring from I to VI, showing that cancer risk is much higher to Fitzpartick scale I phototype of fair skin, compared to those of Fitzpatrick scale V and VI with much darker skin [36].

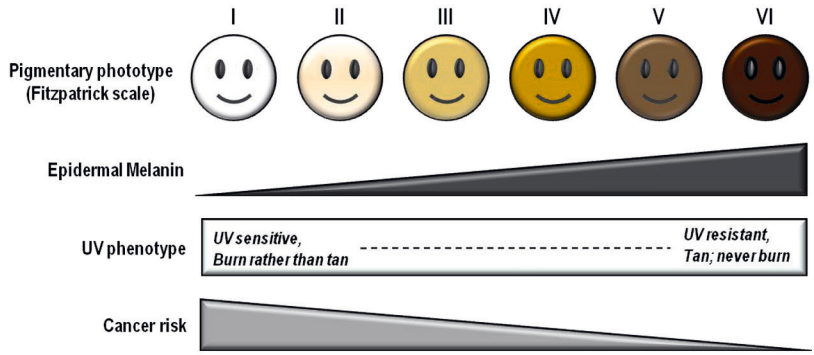

Figure 13. **The Fitzpatrick phototype scale** [37]

Due to the higher concentration of melanocytes in the skin people of Fitzpatrick prototype V and VI have higher protection from UV damage. Still, there are skin cancer cases also among people with darker skin tones and they get diagnosed at later stages. Also, SCC is more common in Back and BCC in Hispanic populations [38]. Below in Figure 14 the world map and skin tone distribution is shown.

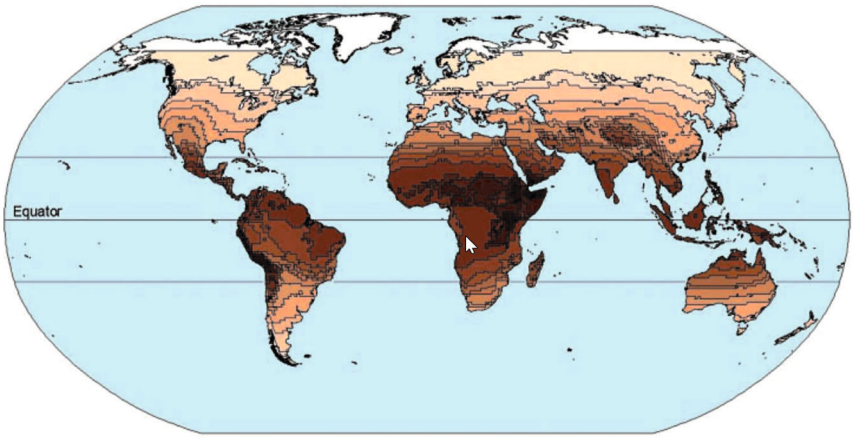

Figure 14. **ENVIRONMENT AND HUMAN SKIN COLORATION, Map of skin color reflectance predicted from multiple regression. Map is generalized to reduce number of polygons** [39]

Perceived skin color is mainly composed of dermis scattering, melanin and vascular absorption which are different among individuals due to the differences of skin chromophore concentrations [36], [40].

1.5 Current situation regarding skin screening

1.5.1 Skin screening protocols

Taking the situation in Latvia as an example, where most of the clinical validation of the methods took place, according to the National Health Service of the Republic of Latvia, currently there is no specific skin cancer screening programme. The national guidelines state that currently it is enough with regular visual self-inspection or with regular general practitioner's check-ups for healthy patients or patients with no skin cancer history. In The National Guidelines for skin cancer the wider public screening is not recommended due to the lack of worldwide evidence-based research that would support it as effective, however patients with BCC, SCC and MM in family anamnesis, the regular self-check is recommended [41].

In Latvia, before the summer season, often in May which is also the Euro melanoma awareness month, [https://www.euromelanoma.org/intl] there are events organised by private sector dermatologists and skin cancer patient support non-profit organisation "One Step Ahead of Melanoma" (in latvian: Melanomas pacientu atbalsta biedrība "Soli priekšā melanomai") for society to be aware of skin cancer and be able to do free skin check-up by a professional dermatologist [42].

As skin cancer is considered to be easily diagnosed compared with other types of cancers, because it is visual, still there are many cases when cancer is discovered at very late stages, patients do not perform regular self check-ups, family doctors lack experience or training in basic dermatology diagnostics, and time/staff resources, as well as some dermatologists lack experience with cancerous lesions, since daily they

are dealing more with aesthetic issues and procedures. It is essential to make the right diagnosis and choose the appropriate skin lesion removal procedure in order to ensure the best and safest outcome for the patient.

Still, in the government healthcare provided hospitals, for instance, in Latvia the current diagnosis is mostly performed as a visual examination, with a dermatoscope in the best case, and the preliminary diagnosis is subjective and not quantitative. If a lesion is considered as suspicious, cytology and/or histology is performed.

The care and diagnostics provided in private dermatology clinics is more costly and not always available to the general population due to the comparatively much higher price. Equipment such as "FotoFinder" (FotoFinder Systems GmbH) and similar visual quantitative diagnostic tools are only available in some private clinics.

For now, regarding skin cancer there are recommendations for early detection, but not yet for screening.

In Germany the project GEKID reports MM incidence rise from approximately 14 to 18 cases per 100 000 population since 2007–2008 when the national screening was introduced. The SCREEN project concludes that screening programme is not justified [43]. So far the skin cancer control in a national cancer policy/strategy is effective only in USA [44]. Still, the US Preventive Task Force Recommendations regarding skin cancer in the report in 2009 state that there is not enough evidence for both: benefits and risks of early cancer diagnostics and screening. Regarding the screening tests is said that: "There is insufficient evidence to assess the balance of benefits and harms of whole-body skin examination by a clinician or patient skin self-examination for the early detection of skin cancer" [45]. As expressed by many dermatologists, skin cancer early detection and screening is still essential. Also, Shawn Allen, MD mentions the confusion and lack of consensus regarding proper guidelines of skin cancer early diagnosis [46].

1.5.2 Rapid changes in lifestyle and technology

Elevated exposure to the UV radiation is a high risk factor for skin cancer in Caucasian populations [47]. In the past 30 years the beauty standards in the society have changed, and a dark tanned skin is considered a symbol of health and good looks, especially for young women. This cultivated beauty trend inspires tanning bed companies to produce more powerful and effective UV lamps and tanning devices. Luckily, a lot of national health organizations have started to act and make restrictions for artificial UV tanning, especially for young people, as well as drawing the attention to the harm of extensive tanning at a young age. For instance, in Latvia the use of tanning beds is restricted for children younger than 18 years. This law is becoming effective in 2019 [48]. Before there was no specific restriction regarding tanning beds on a national level.

Nowadays in the digital age, fast information and data exchange is a daily routine. This accounts also for medicine. Digital technologies are available in medicine already in the past two decades. With the era of smartphones now it is very easy to reach the doctor within seconds, and with special mobile applications even exchange images, as well as use numbers of other telemedicine solutions. The field of deep learning image recognition algorithms is developing rapidly as well. The use of picture archiving and communication system (PACS) for radiology images has been well practiced in almost every hospital. Now, with the development of the accessibility of good quality imaging devices and smartphones at a reasonable price, the imaging field in dermatology is expanding too [49], [50].

1.6 Commercial diagnostic imaging devices for dermato-oncology

Depending on the size and patient flow of the dermatology clinic, here are the most common, commercially available, approved and widely used skin imaging devices and modalities for skin lesion diagnostics and management.

1.6.1 Dermatoscope

Most common, widely available is the dermascope, also called dermatoscope (see Figure 15). Starting with the appearance of skin surface microscopy possibilities, the dermatoscope was developed in 1989 [51].

(a)

(b)

Figure 15. **(a) Dermatoscope. HEINE** [52] **(b) in action during the skin examination** [53]

This tool still is the most simple and effective diagnostic tool in every dermatologist's pocket. The dermatoscope consists of a light source (polarized or non-polarized) and a magnifier (usually 10-fold). It is commonly used with a liquid medium between the instrument and the skin to avoid surface reflection and for better structural visualisation of the lesion.

Pros: cost-effective, simple to use, portable. Cons: requires training and an experienced dermatologist to make a precise diagnosis. Still, used together with ABCDE Rule, it is only 65–80% sensitive [54].

1.6.2 High frequency ultrasound imaging

The high frequency ultrasound imaging (Figure 16) as a non-invasive technique was introduced in dermatology in 1979, using at least 10 MHz frequency sound waves, allowing high-resolution imaging of the skin, helping the physicians to assess lesions in real-time for diagnostic and surgical purposes [55]. US images are acquired by using the probe with a transducer can both: produce the US waves and detect the echoes reflected back. The transducers consist of arrays of piezoelectric crystals that can produce sound waves when the electric field is applied to them and vice-versa - the sound waves are reflected back to the transducer by boundaries between tissues

in the path of the beam (for instance, the boundary between fluid and soft tissue or tissue and bone). When these echoes hit the transducer, they generate electrical signals that are sent to the US scanner. Using the speed of sound and the time of each echo's return, the scanner calculates the distance from the transducer to the tissue boundary. These distances are then used to generate two-dimensional images of tissues and organs [56].

Figure 16. **(On the left) High-frequency ultrasound machine with 7.5–15 MHz multi frequency probe with color and pulsed Doppler ultrasonography. And unltrasound probes (on the right)** [57]

Pros: fast and safe, many modalities. Cons: ultrasound device is expensive, available only in big clinics, requires extra training.

1.6.3 Optical coherence tomography imaging

The optical coherence tomography (OCT) (Figure 17) use in dermatology appeared in the late 90ties mostly diagnosing carcinomas [58]. The application is not a routine diagnostic tool in a typical dermatology clinic, but mostly can be found in research facilities.

Figure 17. **Skin imaging with OCT** [59]

OCT is an optical three-dimensional (3D) morphological imaging technology that captures vertical slice images in biological tissue using IR light. OCT now exhibits the tissue penetration and image contrast necessary to make it more broadly useful in the skin, which consists of multilayers of epidermis and extracellular matrix-rich dermis. There are OCT systems optimized for skin imaging use near-IR laser light in one of the "water absorption windows" with a wavelength of 1300 nm, where absorption of light by water is reduced, to achieve good image penetration up to 1.5 mm beneath the surface of the skin with of coherent light interference to "see" into the tissue (much deeper than is possible with conventional/confocal microscopy) and to obtain precise, high-resolution information about the skin microstructure and the exact depth of skin layers and structures [60], [61].

One of the latest and best-in-class line-field OCT device for skin imaging is *Deep Live* by *Damae Medical*, providing both: histology-like vertical images, as well as 3D imaging modality, allowing the dermatologist to evaluate the patient's lesion *in-vivo*, and acquiring patient's optical digital biopsies [62].

Pros: good for detecting tumour margins. Cons: challenges of insufficient resolution; diagnostics of MM is still developing, expensive, requires specific training [63], [64].

1.6.4 FotoFinder

FotoFinder (Figure 18), *FotoFinder Systems GmbH* is an automated full-body, high resolution imaging device, and its latest models have artificial intelligence (AI) modules inbuilt, helping the physician to make the decision regarding the diagnostics faster. Widely used in clinics and in research facilities. It includes a video dermatoscope – a full high definition video camera, providing sharp, high resolution clinical images at a calibrated illumination with both polarized and non-polarized light.

Figure 18. **FotoFinder (FotoFinder Systems GmbH) Imaging setup (on the left) and example of the image library (on the right)** [65]

Pros: Good quality full body images; possibility to image patients in time (dynamic observation), digital dermoscopy, AI. Cons: expensive, bulky and not portable [65].

1.6.5 Devices that use multiscpectral illumination

Multispectral digital skin lesion analysis uses visible and IR light to image pigmented skin lesions suspicious for MM along with computer algorithms that characterize the images and determine the likelihood of lesion malignancy.

1.6.5.1 MelaFind

The two most studied multispectral digital skin lesion analysis techniques include: *MelaFind* (MELA Sciences Inc, Irvington, New York) and SIAscopy (Spectrophotometric Intracutaneous Analysis).

MelaFind was a Food and Drug Administration (FDA) in USA approved handheld device that irradiates the skin with 10 spectral wavelengths ranging from 430 nm to 950 nm. This algorithm recognizes changes in orientation, colour, and texture to measure overall morphologic disorganization, then it scores the lesion based on these features and advises for or against biopsy [66]. This can serve the dermatologist as tool for decision making process in diagnostics.

MelaFind was recalled from the market in 2015, because some of its software wasn't included in its pre-market approval from the FDA [67].

Pros: provides spectral information of the lesion, non-invasive, fully automatic. Cons: accuracy issues, not approved by FDA.

1.6.5.2 SIAscope

A second system is spectrophotometric intracutaneous analysis, also known as SIAscopy. SIAscopes are handheld devices that illuminate the skin with 400 nm to 1000 nm wavelength light. The associated computer algorithm analyses the distribution and amount of tissue chromophores, including eumelanin, haemoglobin, and collagen.

MoleMate, an FDA-approved SIAscope designed for primary care providers, uses the primary care scoring algorithm for lesion analysis [68]. Walter and colleagues, however, found no evidence that using *MoleMate* in the primary care setting had improved the appropriateness of referral for skin lesions [69]. Nevertheless, primary care providers who used MoleMate earned higher patient satisfaction scores than providers who did not use this new technology. Further investigation of SIAscopy is necessary to determine its role in dermatology and primary care [66].

Pros: provides information about cromophores, pain-free, satisfied patients, non-invasive, hand-held. Cons: *MoleMate* with its software is at a high price level.

The previously mentioned commercially available devices are widely used by dermatologists, depending on the needs and scope of their clinic, patient flow and specialization. Still, the dermatology imaging device market does not offer big variety of highly trustable, yet affordable multispectral skin imaging solutions that would include big AI capability and high accuracy level in regards of the lesion differentiation, at the same time accessible price level also for smaller clinics or public hospitals in rural areas.

1.7 Non-contact diagnostic imaging techniques: the basics

1.7.1 Diffuse reflectance imaging

When illumination is applied to the skin, single photons depending on their energy can travel in the skin. An example showed in Figure 19 demonstrates different reflection

types: direct reflection, total internal reflection, diffuse reflection and total internal reflection [70]. Knowing these photon features, DR imaging is a quantitative technique that allows both optical absorption and optical scattering to be determined from images of DR. Using visible (380 to 700 nm) and near IR (715 to ~1000 nm) light can determine the chromophores in the superficial part of the skin [71].

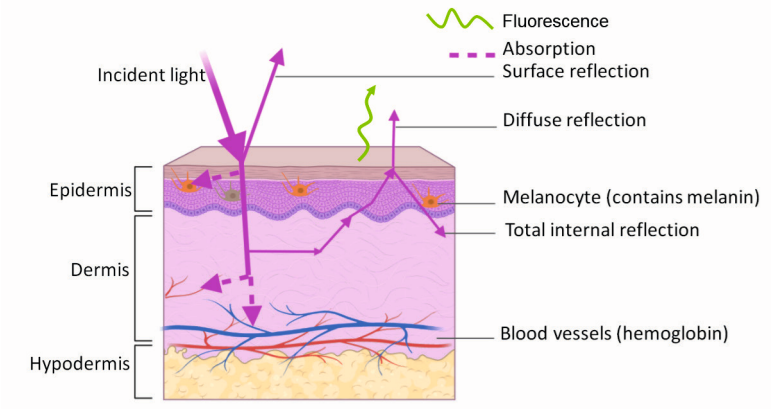

Figure 19. **Light pathways in skin and different types of light reflection. Figure made with BioRender tool** [73]

Due to the Beer-Lambert law that relates to the optical attenuation after passing through the sample (skin) and absorptivity of the tissue, it is possible to determine the absorption of light in certain chromophores. Absorption of electromagnetic radiation is how matter takes up photon's energy [74]. The absorbance of an object quantifies how much of the incident light is absorbed by it (instead of being reflected or refracted). This may be related to other properties of the object through the Beer–Lambert law. Beer's law states that under certain conditions, linear absorption coefficient is a product of the molar concentration of the absorbing substance and its molar absorption coefficient [75].

Bouguer–Lambert law states that the loss of light intensity when it propagates in medium is directly proportional to intensity and path length:

$$I = I_o\, e^{(-\mu b)} \tag{1}$$

where:
I = intensity of transmitted light,
Io = intensity of incident light,
b = the thickness of the sample (the path length),
μ = the attenuation coefficient.

The Beer's law states that: (A) absorbance is proportional to light path length or the thickness of the medium (b) in [cm], molar absorptivity (ε) of the medium or the extinction coefficient [cm^{-1} M^{-1}], and concentration of the medium (c):

$$A = \varepsilon bc \tag{2}$$

As each chromophore of the skin have a different molar absorption coefficient (ε) at specific wavelength, it is possible to determine what chromophore signals can be detected of the skin surface.

The three main chromophores of the skin that are dominant and also quite easily detectable at the visual window are: melanin, oxyhemoglobin (oxygen rich blood) and deoxyhemoglobin. The intensity changes in these chromophore absorption spectra at different wavelengths can be represented within Beer-Lambert-Bouger law in such an equation[75]:

$$\begin{cases} \ln\left(\frac{I_1}{I_{01}}\right) = -l_1[\Delta C_a \cdot \varepsilon_\alpha(\lambda_1) + \Delta C_b \cdot \varepsilon_b(\lambda_1) + \Delta C_c \cdot \varepsilon_c(\lambda_1)] \\ \ln\left(\frac{I_2}{I_{02}}\right) = -l_2[\Delta C_a \cdot \varepsilon_\alpha(\lambda_2) + \Delta C_b \cdot \varepsilon_b(\lambda_2) + \Delta C_c \cdot \varepsilon_c(\lambda_2)] \\ \ln\left(\frac{I_3}{I_{03}}\right) = -l_3[\Delta C_a \cdot \varepsilon_\alpha(\lambda_3) + \Delta C_b \cdot \varepsilon_b(\lambda_3) + \Delta C_c \cdot \varepsilon_c(\lambda_3)] \end{cases}, \quad (3)$$

where:

$\varepsilon_i(\lambda_j)$ – Extinction coefficient of the three chromophores at three exploited wavelengths;

l_j – absorbtion pathlength of the skin – reemitted photons.

In the system of equations (3) it is indicated that the values are calculated for each pixel or group of pixels of the image in the formation. Equation (3) refers to the modified Beer's law of DR from the skin. Thus, not the incoming and transmitting intensities (*Io* and *I*), are compared, but the two reflected intensities, where *Io* is the reflected light from the skin next to the leison, *I* is the reflected light intensity from the pathology (leison), and also the concentration (c) in the modified version is ΔC, or the change in concentration for each of the three chromophores [76].

The example how the spectral image information is used in differentiating various chromophores is showed in Figure 20 A and B.

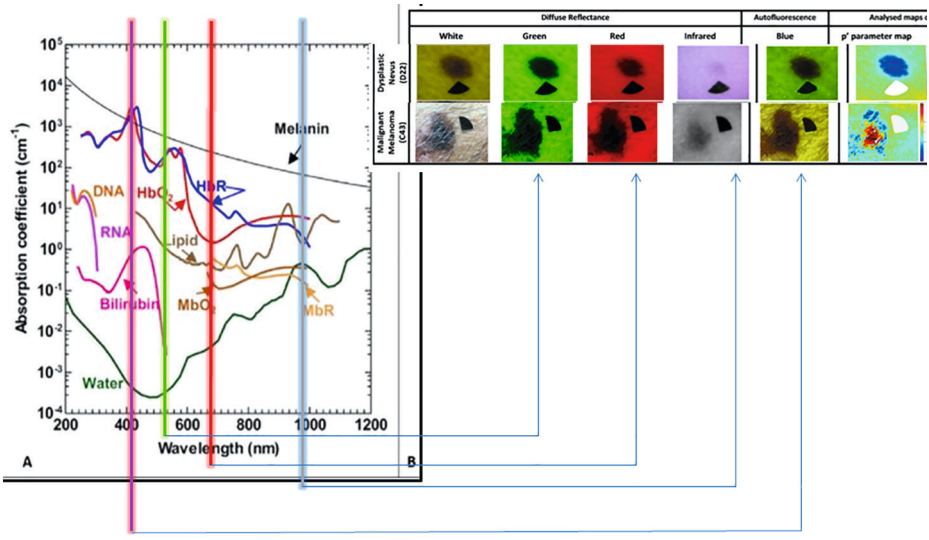

Figure 20. **(A) Absorption spectra of common endogenous chromophores in biological tissues** [77]**. (B) Cromophore distribution maps at each wavelength demonstrating the diferences between dysplastic nevus and MM. Images by M. Lange**

Using the DR features in skin imaging can be combined with fluorescence properties – demonstrated in Figure 23 with the feature of 405 nm, explained further in section 1.7.2.

1.7.2 Autofluorescence

Autofluorescence (AF) or the primary fluorescence is the fluorescence of naturally occurring substances, for example, collagen and fluorite. Most plant and animal tissues show some AF when excited with ultraviolet light (light of wavelength around 365 nm). Sometimes this AF is a nuisance as it may conceal or be confused with a specific fluorescence [78].

Fluorescence is the emission of light by a substance that has absorbed light / photon or other energy, for instance, termoluminiscence. It occurs when an excited molecule relaxes to a lower energy state (usually the ground state) through emission of a photon (see Figure 21) without a change in electron spin [79].

In most cases emitted light has a longer wavelength, and therefore lower energy than the absorbed light.

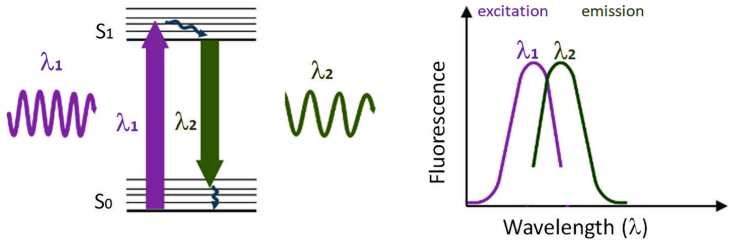

Figure 21. **Illustration of fluorescence excitation and emission. Image made with BioRender tool** [73]

AF is a characteristic of cells in biologic tissue to produce signal if induced by a specific amount of energy.

AF feature is used to visualize fluorophores of the skin in various lesions, containing, for instance: collagen, flavins, melanin, porphyrins, as a quite noticeable AF signal can be detected when induced at 405 nm illumination [6], [80]. However, the fluorophores in skin tissue are non-uniformly distributed [81].

Dermoscopic criteria for skin cancer detection *in situ*, such as increased vascularity, the presence of pigmentation, ulceration, inflammation and keratinization are related to the appearance of unique AF features of biological tissue (see an example of clinical and AF image of MM in Figure 22. More clinical examples see further in Annex 1) [P10], [82], [83], [84], [85].

The method of AF has already been shown to improve the identification of primary BCC and SCC lesions that may not be visible to the naked eye or dermoscopy [84], [86], [87], [88], [89], [90].

Considering the criteria for non-melanoma skin cancer identification, healthy skin has intense green AF at 405 nm excitation whereas cancerous areas may appear darker (see Figure 20) [84], [87].

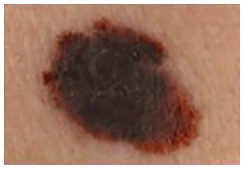

(A) Clinical color image of MM

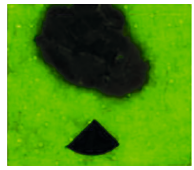

(B) AF image of MM

Figure 22. **An example of skin cancer (MM) images: (A) clinical color image and (B): surrounding healthy skin has a bright AF signal at 405 nm excitation, whereas leson in the middle has low AF signal. Photo by M. Lange**

Cancer cells proliferation require larger amount of nicotamide adenine dinucleotide (NAD) with hydrogen (H) (its green AF emission is located at 415–480 nm) thus replenishing the amount of oxidized form of NAD which possess no fluorescence [84], [91]. In addition, tumour neovascularization and elevated blood vessel permeability can lead to the loss of green AF signal due to the reabsorption and light excitation screening effects produced by blood [87]. At the dermo-epidermal junction, the AF signal originates from collagen, elastin and the related crosslinks. The stroma of BCC tumours possess disrupted structures of collagen, verified by second harmonic generation imaging, with some additional specific feature of increased AF of elastin [92].

Early detection and removal of skin cancer can significantly increase the survival time. Non-invasive methods in primary oncological diagnostics of skin tumors are still essential topics for dermatologists and oncologists worldwide. One of the non-invasive diagnostic methods is skin AF imaging and spectroscopy, based on differences of AF specific information (intensity, spectral shape and lifetime) in the tumor and surrounding normal skin [93], [94], [95], [96].

1.7.3 Combined imaging: diffuse reflection and autofluorescence

By combining the previously mentioned two imaging modalities: DR and AF in one imaging device, it is possible to get information about a wide range of chromophores (melanin, hemoglobin, etc.) (in Figure 23) that are in skin and have different absorption spectra, as well as skin fluorophores (flavins, porphyrins, keratin, etc.) that when induced with 405 nm LEDs, demonstrate AF feature and can be detected with the camera sensor (an example with MM in Figure 22) [97].

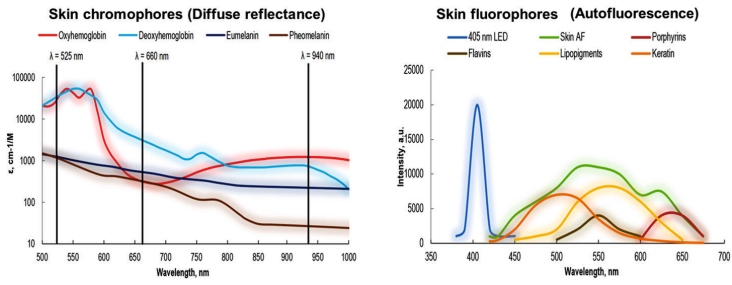

Figure 23. **Detection of skin chromophores and fluorophores by using DR and AF** [89], [98], [99], [100], [101], [102]**. Image design by E. V. Plorina**

When the skin is being illuminated by the light source, the detector (camera sensor) detects surface-reflected and diffuse reflected light, as well as AF signal from the skin, giving the information in a form of image (pixel matrix) the distribution of various chromophores and fluorophores that are in the skin (see the principle in Figure 24). In order to reduce the surface reflection from the skin, crossed polarisers are used in front of the illuminator and detector, respectively (more detailed about the device setup in section 2.1.6).

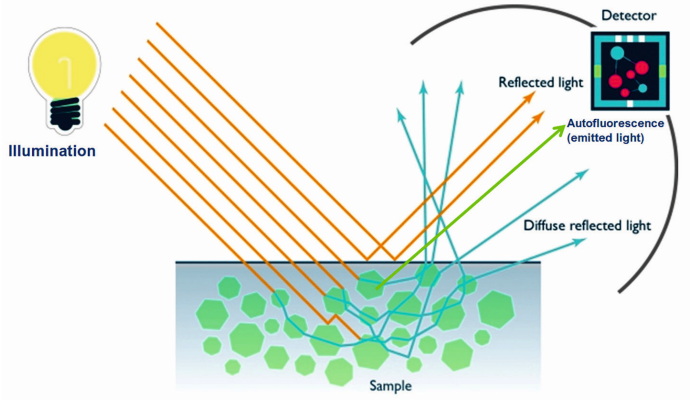

Figure 24. **The scheme illustrating the light travelling from the source to the sample (skin) and to the detector (camera), providing the spectral information** [103]

Later, analysing and comparing this information, the lesion of the skin can be evaluated depending on the spectral information of it.

1.7.4 Photoplethysmography technology

PPG is a simple and low-cost optical technique that can be used to detect blood volume changes in the microvascular bed of tissue [104].

The tissue is being illuminated continously.

Measurment is done by placing the detector right next to the illuminator or right in front of it – depending wether the reflected (a) or transmitted (b) light is being detected (see Figure 25 (a) and (b)). The PPG waveform comprises a pulsatile (alternating current – AC) physiological waveform attributed to cardiac synchronous changes in the blood volume with each heartbeat (pulsatile arterial blood), and is superimposed on a slowly varying (direct current – DC) baseline with various lower frequency components attributed to respiration, sympathetic nervous system activity and thermoregulation (tissue+capillary blood, venozus blood, non-pulsatile arterial blood) [104]. The pulsatile component (volumetric) of arterial blood was used for imaging and signal calculations (see Figure 25 A).

Pulse oximetry – one of the PPG applications – is based on the principle that blood absorbance of the pulsatile (AC) component of PPG signal changes depending on wavelength with regard to the degree of oxygenation, so ratios of the AC signal amplitudes at two wavelengths are used, for example, 660 nm (red) and 940 nm (IR) [105].

For instance, in the finger pulsoximeter the (b) variant is applied and in smart watches the (a) variant is applied. Also, it is important to note that pulsoximeter with the light passing through (variant b) is measuring blood oxygen saturation more precisely than the smart watches with reflective light measurment (b) [106].

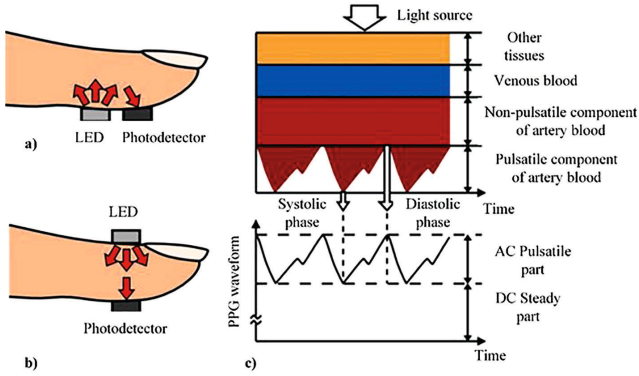

Figure 25. **The principle of photopletismography** [107]

The RA or a block is a specific anesthetic technique that inhibits nerve transmission to avoid or relieve pain. This activity reviews the indications, contraindications, complications, and other key elements related to the essential points needed by members of an interprofessional team managing the care of patients undergoing surgical procedures [108].

Regional anesthesia consists of infiltrating a peripheral nerve with an anesthetic agent and blocking transmission to avoid or relieve pain. It differs from general anesthesia as it does not affect the patient's consciousness level to relieve pain. There are several advantages over general anesthesia, such as avoidance of airway manipulation, reduced doses, side effects of systemic drugs, faster recovery time, and significantly lower pain levels after surgery [109], [110].

As the research in this thesis is mainly concentrated on upper extremity surgeries, here are examples of cutaneous nerve supply and dermatomes of hand that are administred nerve blocks before surgery (see Figure 26).

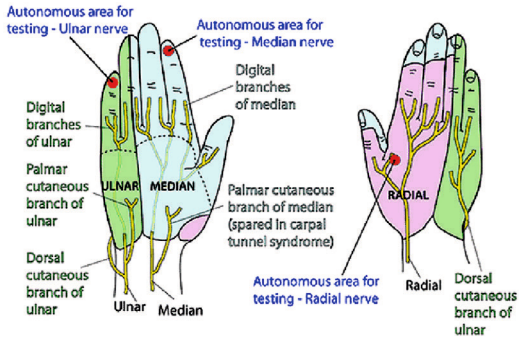

Figure 26. **Cutaneous nerve supply of hand and dermatomes** [111]

However, there are cases when the patient is unfortunately inadequate, a child or a senior, after a trauma or having issues communicating with the medical staff.

The golden standard to evaluate when and if the block has become effective after administrating the RA is to check the respective dermatome of the nerve that has been blocked. The sensory nerve fibres respond to pain, temperature and pressure, for example, it is being checked:

1) if patient is communicating, check for pain, testing with light a pinch or by applying pressure on the respective dermatome;
2) if patient feels temperature difference, using ice cubes [112].

1.7.4.1 Remote photoplethysmography imaging

In recent years there has been a growing demand in cost-effective and contactless reliable techniques for assessment of cutaneous microcirculation for both small clinics and large hospitals. Due to the advances in the microelectronics and image processing techniques, the past two decades have progressed a lot in the development of optical imaging technologies for various biomedical and clinical applications. Recently the remote PPG technique has become popular due to its simplicity and inexpensiveness [113], [114], [115], [116], [117], [118], [119], [120], [121], [P11].

The basic concept of remote PPG is to illuminate the tissue with a light source and to measure the back-scattered light with a video camera. Small light pulsations induced by blood volume changes in tissue become visible after the processing of video frames. It is possible thanks to the temporal processing of video and calculating the corresponding pixel value changes in predefined frequency range, which corresponds to the heartbeat frequency range of a healthy human (see Figure 27).

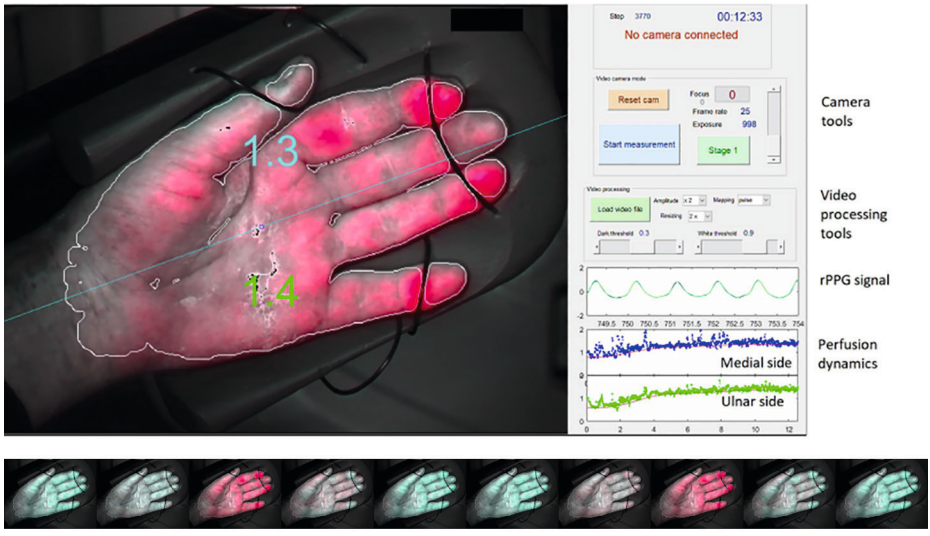

Figure 27. **(Upper): The screenshot of graphical user interface of remote PPG imaging software showing the palm division and signal reading for medial and ulnar nerve area (dermatome). (Lower): Subsequent color-magnified video frames reflecting heartbeat-induced perfusion changes. Skin areas having red color indicates more perfusion, light-blue – less perfusion** [P13]

The application of remote PPG is not restricted only by heart and respiration rate monitoring, it can be used for different clinical applications, such as monitoring of burned skin, monitoring of surgical operations, monitoring of newborns, etc. [113], [114], [116], [121], [122].

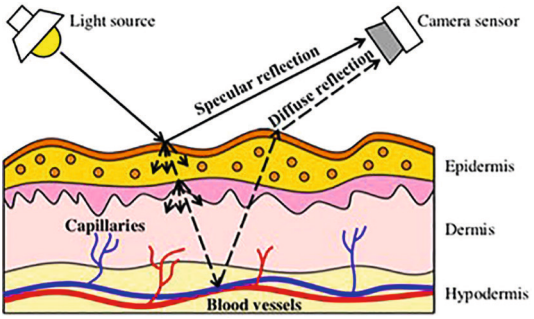

Figure 28. **Demonstration of the remote PPG principle. The skin reflection model that contains specular and diffuse reflections, where only the diffuse reflection contains pulsatile information** [123]

1.7.4.2 Evaluating the regional anesthesia with remote PPG

Determining the level and effectiveness of RA is vitally important to both: an anesthesiologist and surgeon, also knowing the RA level can protect the patient and reduce the time of surgery. Normally to detect the level of RA, usually a simple subjective (alternatives are sensitivity test and thermal test) and complicated quantitative methods (thermography, neuromyography, etc.) are used, but there is not yet a standardized method for objective RA detection and evaluation.

Similar research has been done also including the evaluation of skin local heating and arterial occlusion and topical application of vasodilatory liniment on the skin by Marcinkevics et al., 2016 [119]. The PPG system has been validated by the measurements of a laser doppler imager as a reference. The hardware comprises four bispectral light sources (530 and 810 nm) for uniform illumination of skin, video camera, and the control unit for triggering of the system. The PPG signals were calculated and the changes of perfusion index (PI) were obtained during the tests. The topical liniment and local heating tests revealed good selectivity of the system for superficial microcirculation monitoring. It is confirmed that the PPG imaging system could be used for assessment of cutaneous perfusion at two different depths, morphologically and functionally different vascular networks, and thus utilized in clinics as a cost-effective alternative to the laser doppler imager [119].

2 METHODOLOGY OF MEASUREMENTS AND DATA PROCESSING

In this section the applied methods, components of devices and technical principles used for acquiring diagnostic information have been explained.

Each activity was performed within a certain research project (referenced in sections: 2.1, 2.2 and 2.3) together with colleagues from Biophotonics Laboratory, University of Latvia and/or in collaboration with research partners from all over the world. Author's contribution within each research activity is explained at the beginnig of the respective paragraphs (Sections 2.1, 2.2 and 2.3). There are three imaging systems validated and used in this work, which further will be analysed and discussed, for easier and visual understanding, adittionally, please, see Annex 4.

2.1 Portable LED skin screening device for skin malformation diagnostics

In order to image suspicious skin lesions at one go, the two methods were combined: AF with blue/violet LEDs excitation and DR imaging, illuminating lesions with IR, red and green LEDs. In further paragraphs it is explained how AF and DR technique applications are combined in one device – the portable LED skin screening device. During patient clinical measurments various lesions were imaged: malignant, benign and also skin cancer post-operative scars.

Author's contribution within this research: imaging and patient data collection at the clinic, image analysis, systemisation of image storing and patient data, clinical evaluation adjustment with the encrypted anonymised image data, device validation at the clinical environment, enabling feedback of the device for the technical team, interpretation of the imaging results together with the clinical team.

This work was done within these research projects:

- "Portatīva ierīce ādas vēža agrīnai bezkontakta diagnostikai", 1.1.1.1/16/A/197;
- Ādas vēža agrīnas diagnostikas precizitātes uzlabošana ar neironu tīkliem (FLPP #lzp-2018/2-0052);
- Atomfizika, optiskās tehnoloģijas un medicīniskā fizika (LU Nr. AAP2016/B054).

2.1.1 Autofluorescence and diffuse reflection imaging

In this section it is explained how the two methods (AF and DR) are combined in one skin imaging device.

The portable LED skin screening device is custom-made for patient imaging at clinical environment: in a 3D printed case there is an integrated IDS (*Imaging Development Systems, GmbH*) 5MPix camera with a polarizer (oriented orthogonally relatively to the polarization of illumination), 520 nm filter and a 35mm lens. Around the camera there is a circular array of LEDs of red (663 nm), green (526 nm), IR (964 nm) for DR and violet (405 nm) LED to induce AF. There is a white light for lesion location

and for image archive purposes. In front of the LEDs there is a diffusing film, polarizer film placed in order to reduce detection of any possible residual reflection from the lesion surface. For image processing and sending to the cloud-based server there is a Raspberry Compute module and a WiFi dongle built-in within the system. The camera field of view (FOV) is 2.5 × 2 cm; for the computing software to recognize the lesion and align the images correctly, a black sector-shaped one time use sticker-like marker is being placed a few mm from the lesion with the sharp corner pointing to the lesion (see Figure 29). For more details, see 2.1.8.

2.1.2 Patient selection

During several studies included in this thesis, the patient screening took place at both: LOC and Department of Dermatology, Venereology and Dermatooncology, Semmelweis University, Hungary.

All the skin screening studies were approved by the local Ethics comittee. The patients who participated in the studies were informed about the trial and gave their full written consent.

The guidelines suggest that each patient should be screened in follow-up 3, 6 months and then 1 year after the skin cancer surgery, following an annual check-up for life at a professional well trained oncologist – dermatologist [124]. Patients with signs of pigmentation in the surgical site additionally to their dermoscopy examination were imaged with the portable LED skin screening device.

2.1.3 Image acquisition and analysis

The images of the lesions were collected using the screening device and stored in a cloud-based server. For body location clarity and archiving purposes, for some patients the lesions were also photographed using a regular digital camera in order to get bigger scale image of larger area of the body and for easier clinical evaluation. All the imaging data on the server have been fully encrypted. The patient data have been anonymized and images do not contain any personal information of the patients.

The screening device acquires images at various wavelengths in a range from 405 to 950 nm for further analysis. The time for one measurement once the lesion is located takes around 40 seconds, then about 2 minutes for the images to be analyzed in the cloud and displayed on the user interface screen. Suspicious lesions were confirmed with cytology or histology lab analysis.

2.1.4 Post-operative scar imaging

The idea of performing the imaging of post-operative MM scars comes from practicing lesion imaging at LOC during various research projects along with Dr. Alexander Derjabo. Working in a team and witnessing how important is a proper evaluation of post-operative scars, providing a visual database with color images and multispectral images led to creating an image library of all sorts of scars available from patients who came to regular follow-ups. Not really knowing what would be more valuable and useful in the future, different types of scars were imaged: post-operative scars after MM, BCC,

SCC surgeries, after tattoo removals, after different trauma, etc. The main idea is to find parameters to distinguish and evaluate if the skin cancer post-operative scar is healing well and there are no signs of possible cancer recurrence.

The AF images were analyzed using custom MATLAB (The MathWorks, Inc.) algorithms that utilize the G channel of the RGB images. First, it is attempted to distinguish scar and healthy skin regions, using segmentation. In this algorithm, it is assumed that there are three main regions in an image – the black marker, the dark scar and the light skin (see Figure 29). They can be distinguished using a range of normalized pixel values for these three regions. If the quality of the images is low, they contain additional regions or if due to different states of scar tissue (vascularization, depigmentation, etc.) these regions cannot be correctly segmented, the region of interest (ROI) of scar tissue is manually selected instead (Figure 9 (2)). In both cases the average pixel values of the scar region are normalized against the surrounding skin to take into account the patient's age, gender and sun exposure of the skin during the patient's lifetime.

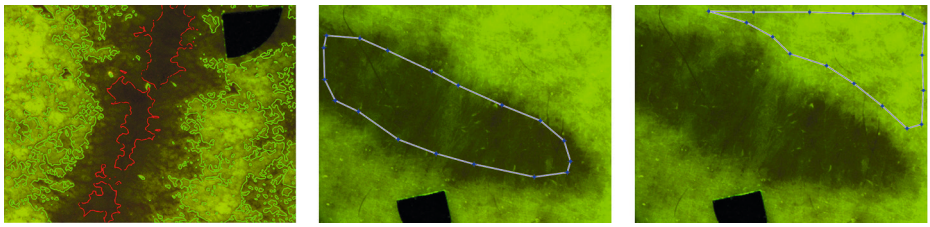

Figure 29. **Selection of ROI for analysis automatically (1) and manually for scar (2) and skin (3). Photo by: M. Lange and E. V. Plorina**

For both benign and recurrent scars an AF intensity ratio (I.R.) was calculated in order to determine the tendency of the scar to become lighter in time or to have considerably low values that could indicate recurrence. The AF I.R. is calculated:

$$AF\ Intensity\ Ratio = \frac{I_{scar}}{I_{healthy\ skin}} \tag{4}$$

The same lesions have been illuminated with red (R), green (G) and IR in order to obtain the parameter *p'* (further discussed in section 2.1.7.). This value is a screening parameter that gives an evaluation of the suspicious lesion and calculates its probability of being MM, based on DR principle which is developed by Ilze Lihacova and colleagues [P9].

2.1.5 Imaging parameters

The imaging parameters that are important are AF healthy surrounding skin to scar region I.R., its tendency to increase (if patient was screened for more than one time during the post-operative follow-up evaluation), as well as the parameter *p'* and oncologist's clinically suspected pigmentation changes in the scar (for visual purposes only, imaged with a regular digital camera or dermoscope, depending what is available).

2.1.6 Device setup

In order for the family doctors and dermatologists to use such device for skin cancer screening on suspicious skin lesions, it has to be portable, simple, accurate and fast to operate. After several years of clinical trials and consistent improvements a screening device (in Figure 30) has been created [125].

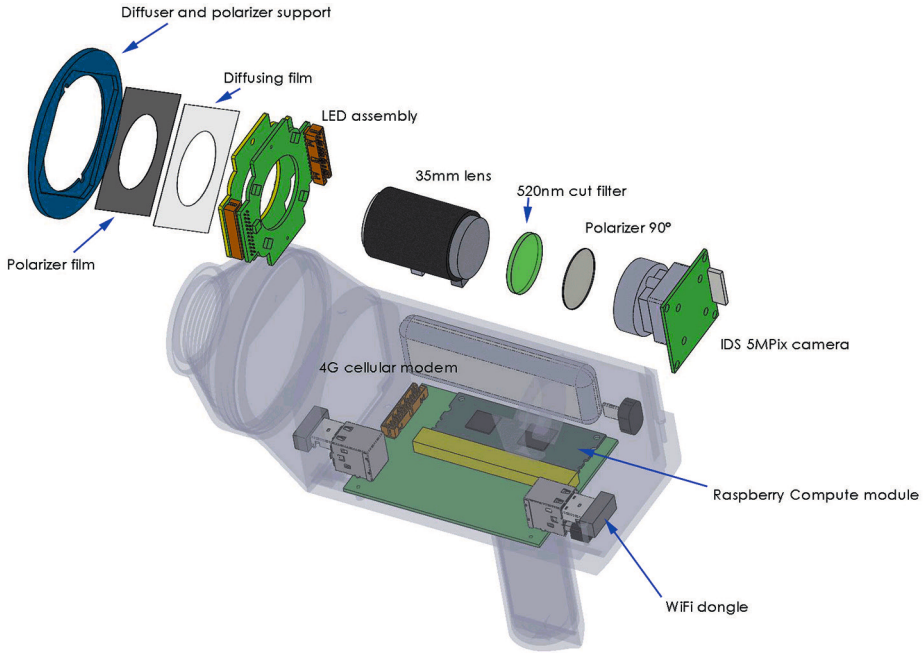

Figure 30. **The components of the portable LED skin screening device. Image design by Dmitrijs Bliznuks**

The proposed screening device (in Figure 30) consists of multispectral light emitting diode (LED) sources at specific peak wavelengths: 526 nm, 663 nm, 964 nm for DR and 405 nm to induce skin AF, as well as a white light LEDs for lesion location and visual archive. The illuminators are assembled in a LED ring. Polarizing filters are used to decrease glare effects, therefore preventing image overexposure of very reflective skin areas, as well as a filter that enables capturing of DR and fluorescence images while blocking the fluorescence inducing light. The previous prototype version has been improved into current one, emphasizing the user experience features, LED positions and better optical design parameters [P7].

The IDS 5Mix camera is used for image capturing. Afterwards, the captured images are sent to the cloud with the help of a WiFi module (see the schematics in Figure 31).

The block diagramm (Figure 31) demonstrates what components portable LED skin screening device is made of. Device's structure is modular to enable easier build and adaptation to physical design. There are 3 main blocks and 2 components, which are not part of any block: Li-on (lithium ion) battery and USB (universal serial bus) IDS camera. The battery is used to power the device, when it is not connected to external source of power.

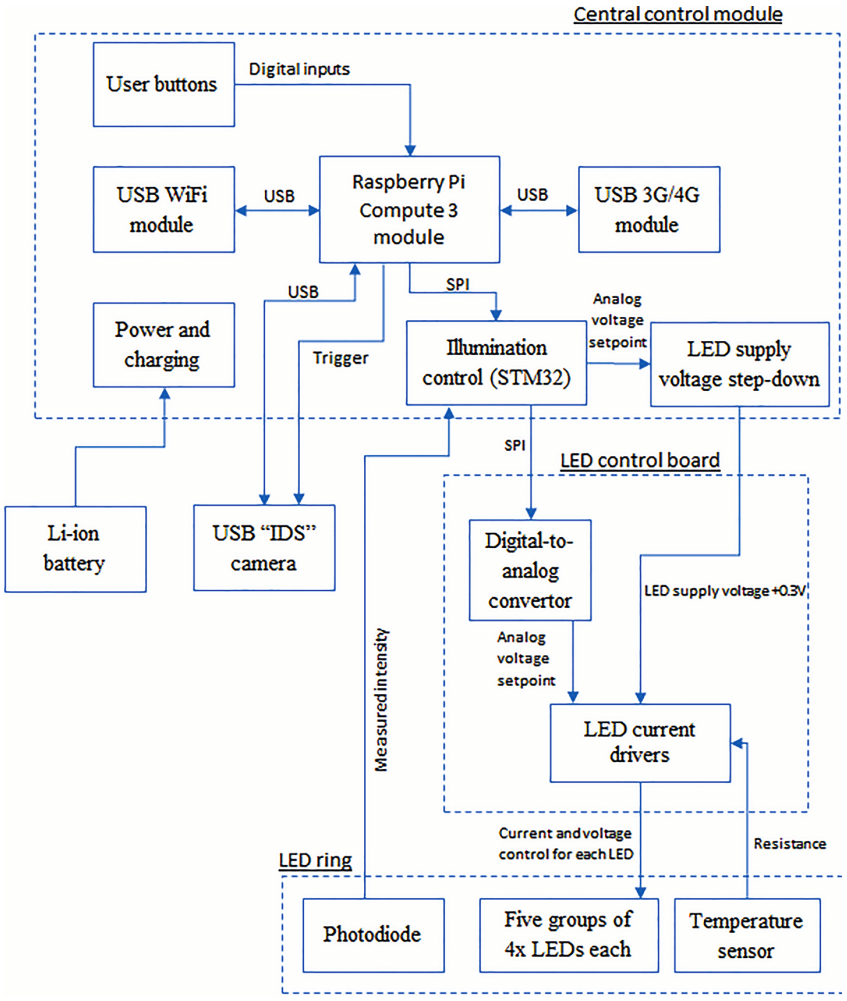

Figure 31. **Block diagramm of electronic components for portable LED skin screening device. Design by D. Bliznuks**

The IDS camera features high-quality CMOS (complementary metal-oxide-semiconductor) sensors with ultra high QSXGA (Quad Super Extended Graphics Array) resolution of 2560 × 1920 pixels. The 1/2" Bayer RGB sensor is capable of frame speeds of up to 6 frames per second at full resolution iDS LE series cameras provide a cost effective solution for many OEM (original equipment manufacturer) applications where the camera is designed into a system or instrument [126].

First of blocks is the central control module which main component is Raspbery Pi Compute3 module. It basically is a mini-computer with wireless LAN (local area network) and Bluetooth connectivity making it the ideal solution for powerful connected designs. *Raspberry pi 3* use the cheapest Boardcom BCM 2837 64 bIT ARMv7 Quad Core processor powered Singel Board Computer, running at 1200MHz and has 1GB SDRAM@400MHz (synchronous dynamic random-access memory) [127].

There are two user buttons connected to *Raspbery* board, one serves as input for triggering the imaging sequence, the other is for turning the device on and off. For connecting to server, central control board is equiped with 3G/4G (generation) router and Wi-Fi, which can provide connection to the internet.

Central control board also includes power and charging module that is responsible for charging the Li-on battery and switching the power source: either external or internal.

Main tasks of control module are triggering the IDS camera and capturing images and control of LED control board, which is the second block of the device. There is a step-down voltage converter that powers the LED control board and a ilumination control via STM32 microprocessor.

LED control board consists of LED current regulator that is feeding from step-down voltage converter, and digital to analog signal converter, which recieves digital signal from STM32 microprocessor, translates it into analog signal and regulates the LED current.

Final version is the LED board which has 20 LEDs of 4 types mounted on it, as well as photodiode and temperature sensor for feedback.

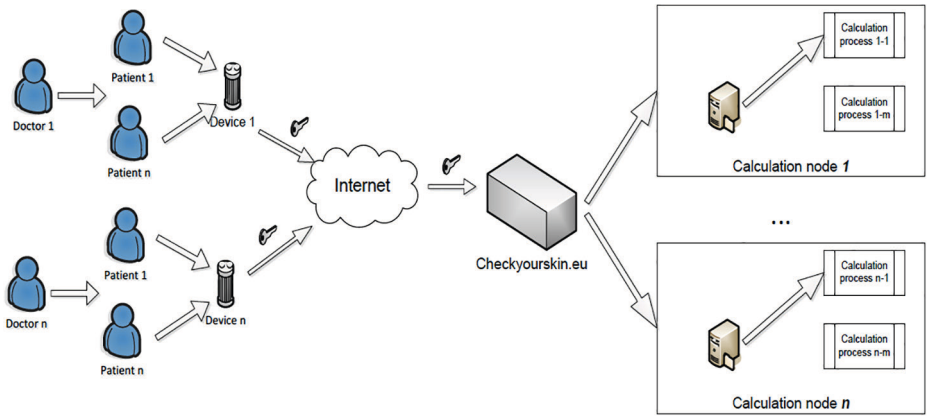

Figure 32. **Diagram of image transfer network. Design by D. Bliznuks**

The cloud-based image analysis system runs several *MATLAB (MathWorks, Inc.)* scripts according to the created algorithms that calculate specific parameters and create image maps (see in Figure 32 the "Calculation node" block); so that the doctors in just a few minutes after capturing the image could already evaluate the result in the web-based information system (IS) by logging in and viewing each patient's records and visual images of their lesions.

In Figure 33 it is demonstrated how the doctor performs the screening of the patient's suspicious lesion on the arm. In the personal computer web-based solution it is possible to preview the lesion as well as later to view the analysis of the lesion after the examination. The device is wireless, so it is handy to image various parts of the body. The imaging of one lesion after locating it takes around 30 seconds only.

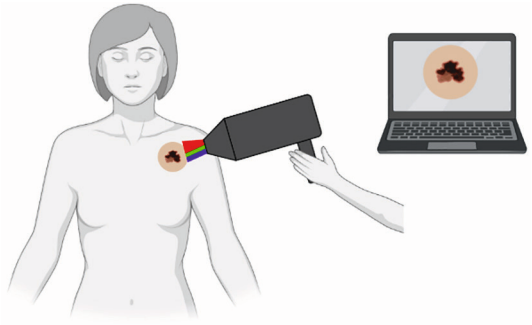

Figure 33. **Measurement set-up and procedure: the doctor captures the image of the patient's suspicious skin lesion with portable LED skin screening device. The clinical image is available on the screen, along with the resulting, analysed parameter lesion maps. Image Design by M. Lange, using BioRender tool** [73]

2.1.7 Parameter *p'*

For diagnostic purposes and determining whether the pigmented formation is MM, a p' parameter [P9] map is calculated and the image, captured under 405 nm excitation, is analyzed. DR images for lesion I and surrounding healthy skin I_{skin} (at 526 nm, 663 nm and 964 nm) are used for calculating parametric p' map:

$$p' = lg \frac{I(526) \cdot I_{skin}(663) \cdot I_{skin}(964)}{I_{skin}(526) \cdot I(663) \cdot I(964)}, \tag{5}$$

where images at 526 nm mostly characterize blood absorption, at 663 nm – melanin absorption in skin and at 964 nm – gives us information about deeper layers of the skin. The criterion for MM is that there is an area within the lesion where $p' > 1$.

Since there are cases when SK provides the same criterion as MM, it is possible to distinguish them from MM, using AF images under the 405 nm excitation [P10] SK present increased intensities within the lesion I_{lesion} in comparison with the surrounding skin I_{skin} [P2]:

$$I_{lesion}\,(405) > I_{skin}\,(405) \tag{6}$$

2.2 Smartphone AF imaging system for skin malformation diagnostics

Smartphones may become useful diagnostic tools for dermatologists and oncologists due to the wide accessibility, convenient use and relatively low cost [128], [129].

In this section it is demonstrated how a smartphone AF imaging system was designed for quick and convenient patient skin cancer screening.

Author's contribution within this research: imaging and patient data collection at the clinic, device validation at the clinical environment, interpretation of the imaging results together with the clinical team. This work was done within research project and grant: "Inovatīvas ādas diagnostiskās attēlošanas tehnoloģijas" (ERAF #2111/3-015).

2.2.1 Experimental setup

The smartphone AF imaging system setup is demonstrated in Figure 34. For parametric mapping of skin AF, a sequence of AF images under continuous 405 nm LED (light emitting diode) (model LED Engin LZ1-00UA00-U8) excitation for 20 seconds with framerate 0.5 fr/s was recorded and analyzed. Four battery-powered violet LEDs were placed within a cylindrical light-shielding wall that also ensured fixed distance (60 mm) between the smartphone camera and evenly irradiated spot (diameter 40 mm) of the examined tissue. A long pass filter (> 515 nm) was placed in front of smartphone camera to prevent detection of the LED emission. The Samsung Galaxy Note 3 smartphone was used for image acquisition with CMOS RGB image sensor with the resolution of 13 MP. The recorded R (red), G (green) and B (blue) images were separated; G- and R-images were used for imaging of skin tissue AF in the green and red spectral bands, respectively. All images were acquired with the following settings: ISO – 100, white balance – daylight, focus – manual, exposure time – fixed 200 ms [130].

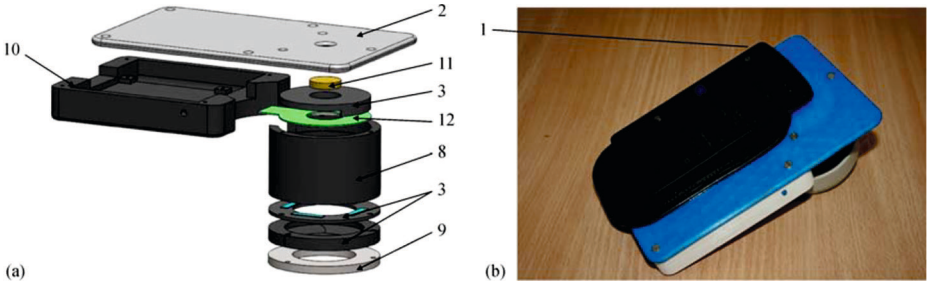

Figure 34. **(a): Smartphone AF imaging system setup with a smartphone and its components: 1 – smartphone, 2 – fixing plate with camera window, 3 – mounting rings, 8 – cylindrical screening spacer, 9 – silicone skin-contact ring, 10 – battery/electronics compartment, 11 – long-pass filter, 12 – LED ring** [130]**; (b): device prototype with the smartphone in real life** [130]

2.2.2 Image processing technique

In order to visualize the fluorophores or their groups according to the recorded AF intensity decrease rate, the following image processing expression was applied [P14]:

$$N(C) = (I_{t0}[C] - I_t[C]) \div \mathrm{I}_{t0}[\mathrm{C}], \tag{7}$$

where (C) represents normalized AF intensity decrease map for each pixel (or pixel group) during the excitation period, $I_{t0}[C]$ – AF image at the excitation start moment, $I_t[C]$ – AF image after 20 s of continuous excitation. C – color component of the RGB image.

Thus AF intensity decrease maps for separated color channels were obtained. Afterwards the information about the fluorophore distribution in the patient's skin was extracted [P14].

2.2.3 Patient selection

Overall, 50 patients with 150 different skin neoplasms were imaged at the clinic during the study. The lesion types included: SK, pigmented nevi, BCC and healthy skin.

For the detailed image analysis 13 BCC and 1 atypical nevus were selected. This study was approved by the Ethics Committee of the Institute of Experimental and Clinical Medicine, University of Latvia. All involved volunteers were informed about the study and signed the required consent form.

2.2.4 Measurement protocol

The patients with suspected benign lesions, like: SK, nevi, hemangiomas, other dermatological diseases of interest that are not cancer, as well as clinically suspected skin cancer by a professional dermatologist-oncologist: BCC and MM were informed about the study and the possibility to perform a free screening at LOC. Patients who agreed, we explained the measurement procedure and signed consent forms approved by the Ethics Committee of University of Latvia.

Then the suspected lesions were imaged with the smartphone AF imaging system [131], placing the device's silicone skin-contact ring around the lesion. The measurement was started by the push of the button and lasted for around 30 seconds in total.

After each patient the device was disinfected with an alcohol-based spray disinfectant and a special disinfecting wet wipe. The measurement assistants used single-use medical gloves during the procedure and changed them after each patient.

After each image set was captured, the user checks for the quality of the image (motion artefacts, etc.). If necessary, with the consent of the patient, the measurement was repeated. The anonymous image sets were saved, the anonymised patient data collected: sex, age, date of the visit and the clinical diagnosis of the lesion. After the surgery (if there is one performed), the anonymized histological result of the confirmed lesion diagnosis is added to the image data set.

2.3 Regional anesthesia effectiveness evaluation with PPG imaging

This work was supported by the Latvian National research program "Cyber-physical systems, ontologies and biophotonics for safe and smart city and society" (SOPHIS) under the grant agreement #10-4/VPP-4/11.

Author's contribution within this research: imaging and patient data collection at the clinic, device validation at the clinical environment and interpretation of the imaging results together with the clinical team.

Non-contact and visual monitoring options are explored to determine the moment when anesthesia has become effective and to evaluate skin perfusion due to the changes of patients AC pulse amplitude during anesthetic block administration using remote PPG method as an alternative for patients who are unresponsive or not able to communicate with the medical staff.

2.3.1 Application of remote PPG in anesthesiology

Determining the level and effectiveness of RA is vitally important. Unfortunately, there are not standardized methods available yet that could be used for any type of surgery. There is an assumption that after the administration of the local anesthetic,

when the sympathetic nerve block has been done, that leads to local vasodilation and increasing of peripheral blood flow. For other hand the peripheral circulation can be monitored by optical methods as remote PPG. In the previous projects several similar remote PPG prototypes have been developed and tested for regional anesthesia monitoring in clinical environment [116], [117], [118], [119], [120], [P11]. The surgical lamp can be used as a light source, [P11] because it is widely available in most operation theatres and can be conveniently adjusted. For this reason, a custom-made technical solution for RA monitoring was created.

For skin perfusion measurements in clinical environment a portable custom-designed remote PPG monitoring device (Figure 35) was used along with a computer with custom-developed dedicated software. A simple and effective approach for automatic real-time contactless monitoring of the palm RA effectiveness by using the created system is demonstrated. The developed remote PPG monitoring device for AR evaluation has been successfully tested in a clinical environment.

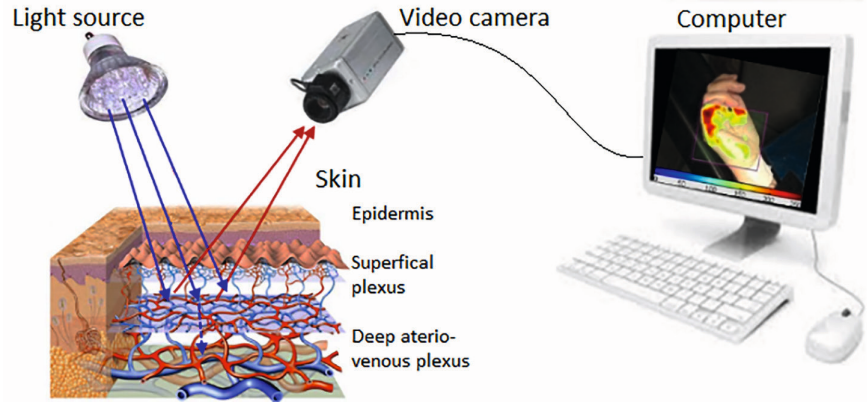

Figure 35. **The principle of remote PPG technique** [P11]

2.3.2 Remote PPG monitoring device for regional anasthesia

The remote PPG monitoring device [136] was developed in Biophotonics laboratory, Institute of Atomic Physics and Spectroscopy, University of Latvia. It was designed for use with the surgical lamp in the operation room (Figure 36). The remote PPG monitoring device consists of custom designed 3-D printed holder for surgical lamp, compact industrial camera (Ximea-xiQ, CMOSIS, monochrome, ADC-8/10/12-bits, max. resolution 640 × 480, max. framerate 502), equipped with low-distortion lens (*Edmund optics, LTD*) and optical band-pass filter (half-bandwidth 520–580 nm). Skin illuminating was performed by warm-white-light surgical lamp, color temperature 3300±200 K (ALM Prismalix PRX800 by Maquet, Getinge group). The camera was cable-connected to laptop computer. Regarding the full view of adult palm, the prototype device was oriented at 1.5 m distance from the palm surface. The video acquisition was performed in 640 × 480 resolution, 10-bit mode, 100 frames-per-second to achieve video with high resolution and high dynamic range.

(a)  (b) 

Figure 36. **The remote PPG monitoring device (a) attached to surgical lamp (b)** [P11]

2.3.3 Video processing

The remote PPG video processing algorithm was created to display the amplitude of blood volume pulsation in each pixel of the skin image. This algorithm was modified for real-time clinical assessments of skin microcirculation, utilizing an unstabilized white illumination source (such as a surgical lamp).

The primary stages of remote PPG processing involve the following: while capturing the video, the images are saved in the computer memory as an image cube with dimensions H × W × B (where H represents height, W represents width, and B represents the length of the video buffer). Subsequently, temporal processing of the image cube occurs. The intensity of the skin image varies from frame to frame due to changes in backscattered illumination induced by blood flow.

As the fast varying remote PPG component is related to the cardiac blood volume pulsations, we assume the heartbeat range of 40–180 bps. This signal was extracted by applying bandpass filter within the frequency range 0.7–3.0 Hz. Subsequently, the filtered signal and its amplitude were computed for each pixel of the image across the frame buffer to generate remote PPG amplitude maps. Ultimately, the PPG amplitude map was displayed on the computer screen, facilitating the monitoring of blood circulation in various skin zones. Throughout the acquisition process, these processing steps are iterated infinitely.

The algorithm has been optimized for speed and sequence of calculations described in [132] has been changed. The spatial filtering has been moved to the tail of the algorithm. This adjustment doesn't compromise the spatial resolution of the map but enhances computational efficiency. Throughout the RA procedure, there were instances where the subject's hand moved, potentially causing significant artifacts in the registered signal. To ensure a clear signal during measurements, a basic motion artifact remover was integrated into this algorithm: 1) PPG amplitude signal was filtered using median filter; 2) PPG amplitude values that exceeded filtered signal, were replaced by this signal; 3) the process was repeated several times.

The electrical current within the network pulsates (in Europe, the standard frequency is 50 Hz), causing the lamp to emit pulsed light at twice the current frequency. To avoid interference caused by unstable light, video acquisition was conducted at a frame rate matching the blinking frequency: 100 Hz. Despite the instability in power supply, gradual fluctuations in intensity do not impact the PPG amplitude signal,

thanks to the filtering within the frequency range of 0.7 to 3.0 Hz. To achieve higher quality of remote PPG signal acquired from the skin surface at different lighting conditions, the dynamic range of camera was extended to 10-bit mode. This takes two bytes of memory needed for one video frame.

In order to decrease the volume of data from the 16-bit 100-fps recordings, a custom algorithm was employed to compress the live video prior to storing it in the standard .avi (audio video interleave) format.

2.3.4 Measurement procedure and patient selection

The clinical measurements were performed in the TOS, Riga, Latvia under approval of the local Ethics Committee. Eight patients (aged 30–78 years) undergoing hand surgery received ultrasound guided axillary brachial plexus blocks. During the recording (see Figure 37), patients were in a supine position. The dorsal aspect of hand was comfortably adjusted in a custom made foam rubber hand support. Room temperature was 23.0±0.5 ˚C. The block was produced by administrating a combination of *Sol.Lidocaini* 2% 10 ml and *Sol.Bupivacaini* 0.5% 10 ml. After the measurement, the anesthesia level was controlled with "conventional" methods e.g. skin touch with ice.

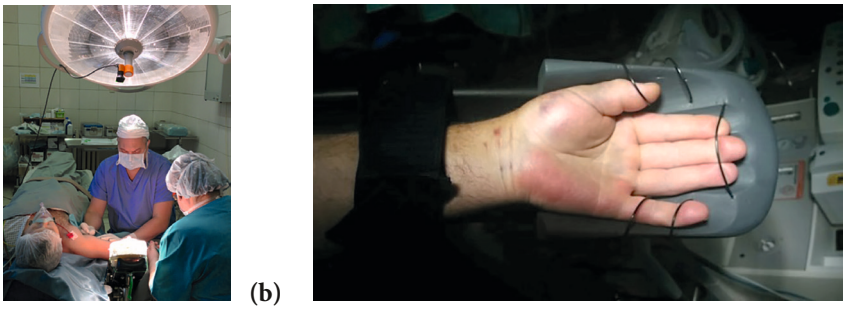

Figure 37. **Assessment of system in clinical settings. The RA procedure (a) and position of palm during measurement (b)** [P11]

Before each measurement, the surgical lamp was adjusted to reach uniformed illumination of the palm. The distance between lamp and the skin surface was approximately 1 meter. Then the camera was attached to lamp's holder and connected to the laptop computer with a 3-meter long USB-3 cable. This kind of setup is very easy to install and does not interfere with the doctor-anesthesiologist and medical staff to perform their standard RA manipulations [P11], [P13].

Video acquisition and real-time processing was performed by custom designed Matlab (Mathworks) software, described in [132]. To reduce large amount of video data, smaller ROI with image resolution of 240 × 160 pixels was chosen. Such resolution was enough to get quality PPG amplitude maps that can visualize innerved areas of palm skin supplied by single nerve (dermatomes) which were affected by RA. The video from the palm surface was acquired before and during the all stages of RA procedure, 10 minutes after the RA manipulation [P11], [P13].

3 RESULTS

In this section the most relevant results have been summarized for each subsection and device used, including references to the publications for further information. Lesion images of evaluated parameters along with clinical pictures and parameter maps are given as examples, as well.

3.1 Validation results of smartphone AF imaging system

The smartphone AF imaging system was validated in LOC, the results were described in articles [P10], [P12] and [P14] are summarized in the Table 1 for easier understanding.

In total, there were more than 400 lesions screened with smartphone AF imaging system, including malignant and benign, between years 2015 and 2018. The main interest was to find out a way to discriminate SK from MM and BCC, and other suspicious, possibly malignant lesions.

The patient flow and possibility to acquire more malignant clinical images depends on various human factors which are out of our control, so the best possible work was done with the images and data available at the time.

Table 1. **Results of malignant lesion evaluation with smartphone AF imaging system**

Benign lesions	Malignant lesions	Total amount of patients / lesions included in the study	Parameter or characteristic evaluated	Main results/ conclusions	More information found in publication or other reference
16 (pigmented nevi), 15 (SK), 2 (dysplastic nevi)	17 (BCC), 1 (MM)	51 lesions	diagnostic criterion is based on the calculation of the mean AF intensity of the examined lesion in the spectral range of 515–700 nm.	1) It is possible to differentiate SK from BCC, pigmented nevi and MM. 2) The sensitivity and specificity of the proposed method was estimated as being close to 100%. 3) The obtained high diagnostic parameters are strictly theoretical, since the groups of SK and nevi do not overlap. On the other hand, the boundary values of those groups are very close, and the reliable specificity and sensitivity of the method is in range between 90–100%. 4) In spite of the fact that SK is benign, it is frequently mistakenly suspected as a malignant lesion during BCC and MM visual diagnostics, leading to unnecessary excision.	Lihachev, A.; Lihacova I.; Plorina, E. V.; **Lange, M.**; Derjabo, A.; Spigulis, J. Differentiation of seborrheic keratosis from basal cell carcinoma, nevi and melanoma by RGB autofluorescence imaging. Biomed Opt Express, 2018. DOI: 10.1364/BOE.9.001852 **[P10]** and see Figures 36 and 37.

Table 1 continued

Benign lesions	Malignant lesions	Total amount of patients / lesions included in the study	Parameter or characteristic evaluated	Main results/ conclusions	More information found in publication or other reference
14 (dysplastic nevi), 20 (hemangiomas), 23 (SK), 4 (hyperkeratosis), 3 psoriasis, 1 dematitis, 2 dermatofibromas, 5 papillofibromas, 12 lupus erythematosus, 7 purpura, 6 bruises, 5 freckles, 3 fungal infections, 1 burn, 1 tattoo, 1 age spot, 1 vitiligo, 32 postoperative scars, 8 post cream therapy BCCs, 4 post radiation therapy scars, 2 post laser therapy scars, 1 post freezing scar, 114 reference images of healthy skin.	32 (BCC), 4 (MM), 1 (SCC), 3 (actinic keratosis)	> 300 lesions	First attempts evaluating AF intensity	With background intensity A parameter it is possible to distinguish BCC from SK, hyperkeratosis and healthy skin.	Lihachev, A.; Plorina, E. V.; Derjabo, A.; **Lange, M.;** Lihacova, I. Evaluation of skin pathologies by RGB autofluorescence imaging. In: *Progress in Biomedical Optics and Imaging – Proceedings of SPIE*. Vol. 10592. 2017. DOI:10.1117/12.2297158 **[P12]**
1 (atypical nevus)	13 (BCC)	50 patients screened, 150 malformations imaged, 14 selected for the study.		1) Smartphone AF imaging has shown potential for remote primary evaluation of cancerous or suspicious skin tissues. 2) The increased rates in the BCC tumor area most probably indicate different fluorophore content composition affected by the tumor growing process, e.g., destruction of collagen elastin cross-links along with decrease in NADH levels	Lihachev, A.; Derjabo, A.; Ferulova, I.; **Lange, M.;** Lihacova, I.; Spigulis, J. Autofluorescence imaging of basal cell carcinoma by smartphone RGB camera. J Biomed Opt., 2015; 20(12). DOI:10.1117/1 **[P14]**

In the study of distinguishing SK from other lesions with smartphone AF imaging system there were compared 5 lesion groups; the mean AF intensity was calculated

within the visual area of the lesion. The box-of-whiskers plot of AF intensity mean values for SK, pigmented nevi, BCC, and healthy skin has been depicted in Figure 36. As the results include only 2 dysplastic nevi (mean value 23.7 arbitrary or relative units (a.u.) and 43.8 a.u.) and one MM (mean value 8.9 a.u.) data, they are not depicted in Box and Whisker plot in Figure 38.

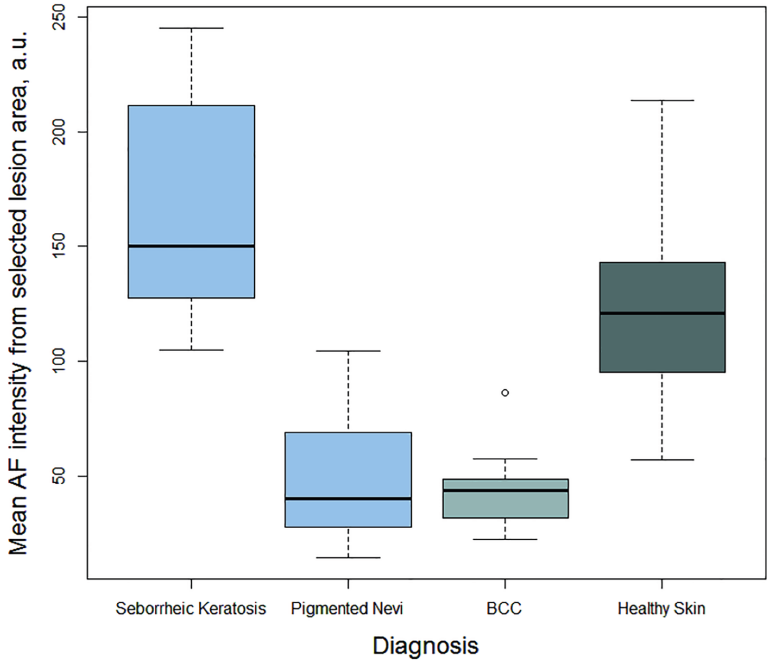

Figure 38. **Distribution of the mean autofluorescence intensity for seborrheic keratoses, pigmented nevi, BCC, and healthy skin** [P10]

In this study there were 51 lesions in total, from which visual examples are given in Figure 37. When using the smartphone AF imaging system it is not only possible to differentiate SK from other groups, but also visually SK lesions often are more prominent due to the bright AF signal (see Figure 39, the last image of SK).

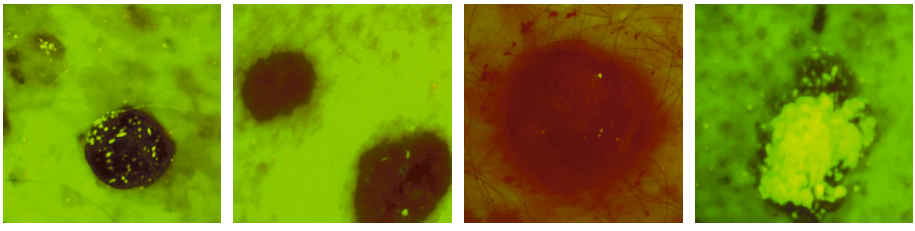

Pigmented nevus **BCC** **MM with ulceration** **SK**

Figure 39. **Visual example – comparison of analysed lesion images of filtered AF signal. From the left: pigmented nevus, BCC, MM, SK** [P10]

Testing the sensitivity and specificity of the method for SK separation from other lesion groups, the following values have been obtained: true positives (TP) were 15, true negatives (TN) were 36, false positives (FP) were 0 and false negatives (FN) were 0. Furthermore, the **Sensitivity** is TP / (TP + FN) = 15 / (15 + 0) = **100%, Specificity** is TN / (TN + FP) = 36 / (36 + 0) = **100%.** The obtained high diagnostic parameters are strictly theoretical, since the groups of SK and nevi do not overlap. On the other hand, the boundary values of those groups are very close, and the reliable specificity and sensitivity of the method with high probability is in range from 90 to 100% [P10].

3.2 Validation results of the portable LED skin screening device

This work has been supported by European Regional Development Fund projects: "Portable Device for Non-contact Early Diagnostics of Skin Cancer" under grant agreement 1.1.1.1/16/A/197 and "Development and clinical validation of a novel cost-effective multi-modal methodology for early diagnostics of skin cancers" (No. 1.1.1.2/16/I/001, agreement No. 1.1.1.2/VIAA/1/16/052).

3.2.1 Malignant lesion evaluation

In skin evaluation and skin screening the first step for patient's evaluation is to locate any suspicious lesions (the "Ugly Duckling" principle, mentioned at Section 1.2.1), clinically evaluate it and, if necesarry send for further evaluation. Here in the section about malignant lesions the research has been done, comparing malignant with benign lesions, trying to find a parameter that would significantly distinguish one from another. In Table 2. the main results and and lesions learned have been summarised of how the malignant lesions have been avaluated with the portable LED skin screening device.

Table 2. **Results of evaluating the malignant lesions**

Patients with benign lesions	Patients with malignant lesions	Total amount of patients included in the study	Parameter or characteristic evaluated	Main results/ conclusions	More information found in publication or other reference
10 (pigmented lesions)	12 (MM)	22	*p'* and *p'* distribution in 2D maps	1) The calculated sensitivity and specificity for distinguishing MM from melanocytic nevi is respectively 75% and 100%. 2) The device has a high accuracy, good visual archive possibility, and this method should be used as a yearly screening tool for new patients and for patients with skin cancer history it could be used as a reference and monitoring tool for cancer recurrence in the post-operative scars.	**Lange et al.** Skin cancer screening – better safe than sorry (2018/2020) **[P2]**

Table 2 continued

Patients with benign lesions	Patients with malignant lesions	Total amount of patients included in the study	Parameter or characteristic evaluated	Main results/ conclusions	More information found in publication or other reference
32 (nevi)	21 (MM) + Spectral images of BCC for visual comparison	> 50	p' values, p' 2D maps and visually AF signal of BCC	1) With the use of this device, it is possible to distinguish different skin cancers, including MM, from benign lesions, such as SK and pigmented nevi. 2) Using this screening device may be highly beneficial to differentiate SK and hyperkeratosis from other pigmented lesions at 405 nm illumination, as keratin emits a very strong AF signal. 3) p' parameter values are shown in order to distinguish MM from nevus. The median p' value for MM and nevus is 1.41 and 0.14, respectively. The p' values range from 0.5 to 1 and larger are considered suspicious with a high potential for MM. Usually in those very pigmented lesions that also have high vascular signal the p' values are close to 2 or even more. In contrary, for benign lesions, such as nevi, which are often appear also highly pigmented, but without high vascular signal, the p' values range from $-0.5 < p' < 0.4$.	**Lange, M.;** Kiss, N.; Fesus, L.; Plorina, E. V.; Derjabo, A.; Spigulis, J. Non-invasive LED-based screening solution for skin cancer, Proc. SPIE 11073, Clinical and Preclinical Optical Diagnostics II, 110731I, 2019. DOI: 10.1117/12.2526386 **[P5]**

The parameter p' was calculated for 12 MM (C43) and for randomly selected benign lesions: 10 dysplastic nevi or melanocytic nevi (D22). All lesions were imaged in LOC during regular patient check-ups. The MM in this study were histologically approved, the benign lesions were approved by an experienced dermato-oncologist by using a dermatoscope (*DermLite DL4*, 3Gen Inc., USA). In Figure 40 the maximal and minimal values of p' parameter are visualized [P2].

The standard threshold is set at $p' = 1$ empirically, and usually lesions with a lot of values already at $p' = 0.8$ are considered suspicious. For MM most of the values should be positive and above value 1, in that case, unless it is noise (signals from hair, movement artefacts or image stabilization error), the negative p' values showed no correlation between the diagnoses. For benign lesions (D22) both the p' min and p' max values are below $p' = 1$, indicating that the lesion most probably is not MM. The calculated sensitivity and specificity for distinguishing MM from melanocytic nevi is 75% and 100%, respectively [P2]. An example comparing benign and cancerous lesions, clinical images and parameter p' map differences are demonstrated in Figure 41.

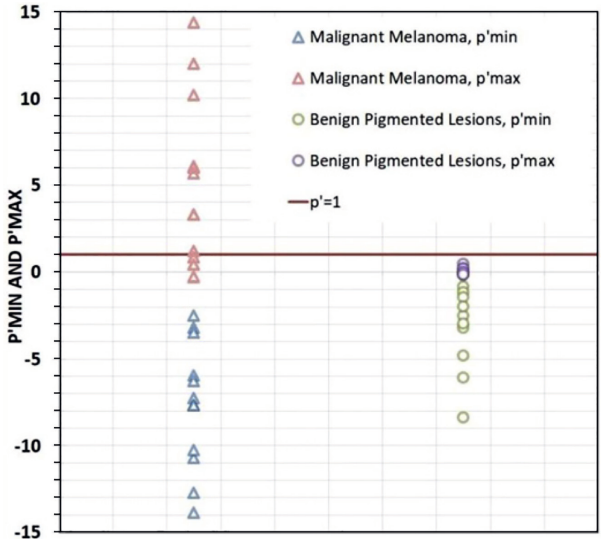

Figure 40. **The evaluation of parameter *p′* comparing MM and benign lesions maximum and minimum values and the threshold at *p′* = 1** [P2]

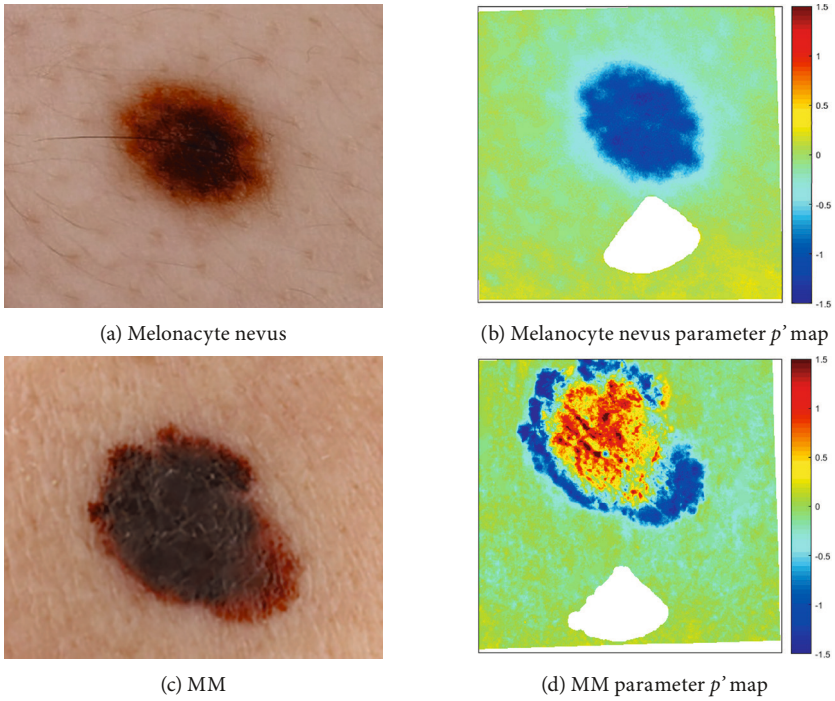

(a) Melonacyte nevus

(b) Melanocyte nevus parameter *p'* map

(c) MM

(d) MM parameter *p'* map

Figure 41. **Two examples with melanocyte nevus (a) and MM (c), showing the different parameter *p′* maps of each lesion (b) and (d). The scale is in relative units. Clinical images (a) and (c) by Dr. Szabolcs Bozsányi, parameter *p′* maps retrieved by Marta Lanģe**

In the Figure 42 (or Annex 1 for a larger image) the comparison of various skin lesions is shown. As the parameter p' has been created for MM evaluation, it describes mostly the possibility of the lesion to be MM. As seen on the 2D distribution for MM the amount of values larger than 1 (red colour) clearly shows the lesion to be MM, even though visually in the white and green channel MM and BCC look similar: as dark pigmented lesions with irregular shapes. The SK, as expected, shows greater AF intensity than the surrounding skin. Hemangioma can be distinguished most of the times visually, but also in the p' parameter map the negative values have very high negative peaks due to the vascular signal.

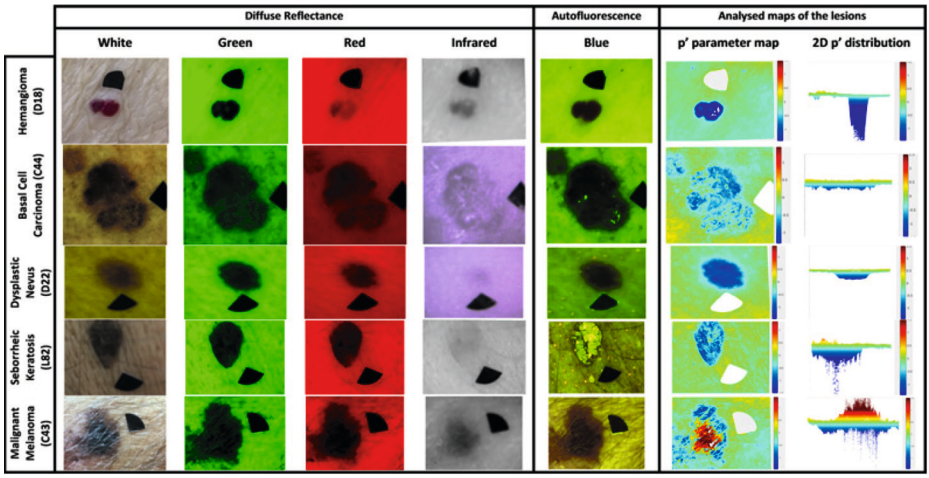

Figure 42. **Possibility to distinguish various lesions: Hemangioma, BCC, Dysplastic Nevus, SK, MM at various illuminated modes: (from the left): DR at white light, green (526 nm), red (663 nm), infrared (964 nm); Auto fluorescence induced by violet (405 nm) light; Analyzed image maps: p' parameter map and p' parameter distribution in 2D** [P2]

The distinguishing method for BCC is still under development, because visually these lesions can be very different in pigmentation and subtypes. Also, there are cases when the physician can doubt dysplastic nevus for MM. In that case for long term observation this visual evaluation method is useful, because MM have areas with values $p' > 1$, whereas dysplastic nevus has big amount of values in the negative (blue area values $p' < 0$) [P2].

In Figure 43 the results of p' parameter are shown in order to distinguish MM from nevus.

The median p' value for MM and nevus is 1.41 and 0.14, respectively. The p' values range from 0.5 to 1 and larger are considered suspicious with a high potential for MM. Usually in those very pigmented lesions that also have high vascular signal the p' values are close to 2 or even more. In contrary, for benign lesions, such as nevi, which are often appear also highly pigmented, but without high vascular signal, the p' values range from $-0.5 < p' < 0.4$.

In real-life clinical practice, for family doctors with very limited dermatological expertise, it is often a challenge to distinguish benign lesions, such as nevi and SK from

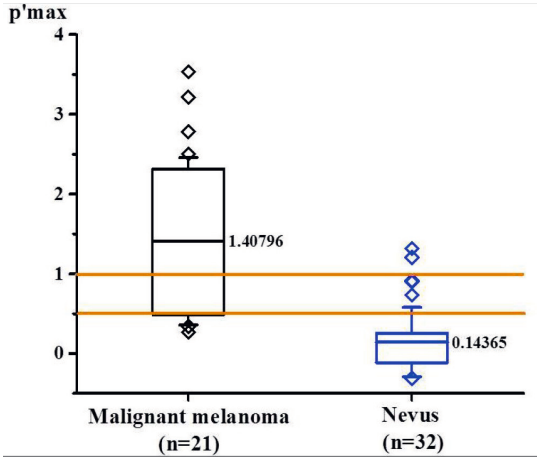

Figure 43. **Results of parameter *p'* values for MM with confirmed histology compared with benign nevus** [P5]

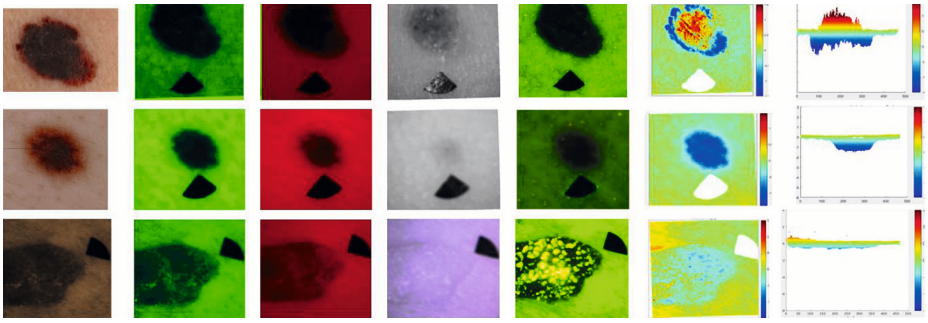

Figure 44. **An example of MM (upper line), nevus (middle line) and SK (lower line) images and parameter maps from the left: clinical colour image, green (λ = 525 nm), red (λ = 660 nm), infrared (λ = 940 nm), violet (λ = 405 nm) for AF and the resulting parameter map showing parameter *p'* of the lesions, and the 2D distribution of *p'*** [P6]

MM. Therefore, using this screening device may be highly beneficial to differentiate SK and hyperkeratosis from other pigmented lesions at 405 nm illumination, as keratin emits a very strong AF signal (see Figure 43, lower line of SK images).

After the acquisition of multispectral images, they are transferred to a cloud-based service (scalable Matlab computing nodes) and automatically analysed in order to create parameter *p'* maps. All skin lesions are imaged at various wavelengths (see Figures 42 and 44). An adhesive marker in a shape of a triangle is being placed on the patients' skin for scaling and image alignment during the post-processing phase.

For patients who came in for a follow-up appointment, images of the post-operative scars were captured (scars from cryotherapy, the use of topical imiquimod cream, radiation therapy – after BCC removal and scars after surgically removed BCC and MM, and others). The scars were imaged with the same modality and the AF images were analysed to perceive any changes compared to the healthy background skin and the scar tissue.

3.2.2 Post-operative scar evaluation

In this section there is a summary of results from several studies evaluating post-operative scars. **Benign scar** is a scar that heals well and no abnormal cell growth is being found during the check-ups. **Recurrent scar** is a scar where after the surgery the dermatologist observed a suspicious cell growth and a reoperation and/or histology was performed in the lesion.

The results of published data for post-operative scar evaluation are summarized in Table 3.

Table 3. **Results of post-operative scar evaluation**

Patients with benign scars	Patients with re-current scars	Total amount of patients included in the study	Age range of the scars	Lesion types (clinical diagnosis)	Main results/ conclusions	Full info found in the publication or other reference
		>30	several months up to 20 years after the surgical proce-dure.	BCC, benign lesions.	Results in study state that AF trend does not correspond to the normal AF trend for healing scar.	**M. Lange,** et al., "Evaluating the aging of the scars after cancer removal by using multispectral diagnostic device" (2018) **[P8]**
9	4	13	6 months to 7 years 9 months	BCC, SK, hyper-keratosis, dermato-fibroma, etc.	1) A parameter to evaluate skin cancer recurrence θ was introduced. 2) For most patients, the old scars had the lowest θ values and the new scars possessed the larg-est θ values. It means that new scars undergo sig-nificant AF increase during the wound healing process and the change in old scar AF is slower.	Tamošiūnas, M., Plorina, E. V., **Lange, M.**, et al. Autofluorescence imaging for recur-rence detection in skin cancer postop-erative scars. *J Biophoton-ics*, 2020; 13(3): e201900162. DOI:10.1002/ jbio.201900162 **[P3]**
9	3	12	1 month to 137 months (11 years and 5 months)	BCC, MM, other benign surgical scars.	1) Spectral image analysis shows decreased **AF intensity ratio** values in the scars with the skin cancer recurrence. 2) There are still some challenges, for instance, automatic scar area segmenta-tion, because of pigmented, sun damaged healthy skin, vascular structures, etc.	**Lange, M.**, Bozsányi, S., Plorina, E. V., Lihachev, A., Der-jabo , A. Spectral imaging as a tool for the evaluation of skin cancer post-operative scars. Proc.SPIE, 11585. 2020. DOI: 10.1117/12.2575704 **[P4]**

Table 3 continued

Patients with benign scars	Patients with re-current scars	Total amount of patients included in the study	Age range of the scars	Lesion types (clinical diagnosis)	Main results/ conclusions	Full info found in the publication or other reference
2	5	10	1 month to 4 months	MM	1) During the stages of the wound healing the chromophores in the skin and the scar change, and the changes of AF intensity ratio does not have a specific trend during the first 4 months. 2) AF images stored in patient records could give valuable information during dynamic observation of the patient in longer time.	**Marta Lange**, Szabolcs Bozsányi, Emilija V. Plorina, Norbert Kiss, Nora N. Varga, Ilze Lihacova, and Alexey Lihachev, "Skin cancer post-operative scar evaluation using autofluorescence features", Proc. SPIE 12226, Applications of Digital Image Processing XLV, 1222618 (3 October 2022). DOI:10.1117/12.2633932 **[P1]**

3.2.2.1 Visual evaluation and advantages of post-operative scar imaging

In the beginning of post-operative scar evaluation journey, a great number of healthy or benign scars were imaged to try and see if there is any pattern for AF ratio when the scar heals well. A study was done [P8] and multispectral images evaluated of healthy healing scars (Figure 45) after various surgeries (see the results in Figure 45).

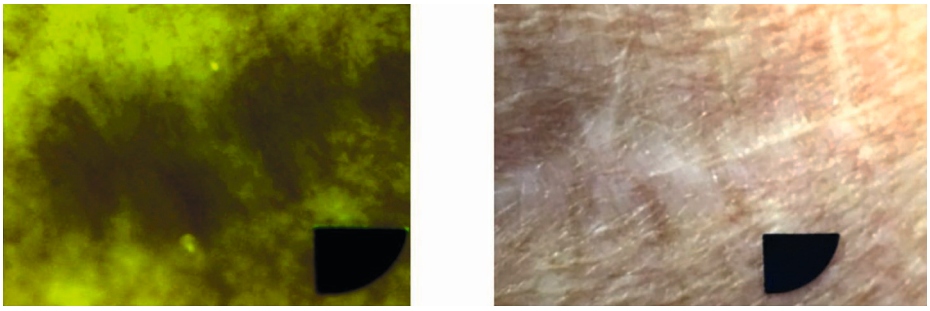

Figure 45. **An example of well healing post-operative scar. Male, 81 y.o with a 7 years old scar on upper right arm after BCC surgical removal. Left: Scar image with paper marker at 405 nm light exposure; Right: picture with regular camera at the white light exposure** [P8]

When calculating the AF ratio of the scar (Formula 2) in time, the AF should increase; post-operative scars from patient age group of 25 to 85 y.o., the aging range of the scars were from several months up to 20 years after the surgical procedure (Figure 46).

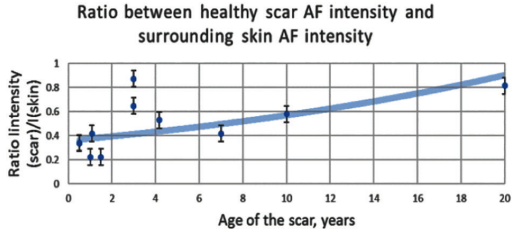

Figure 46. **Healthy scar tissue AF trend** [P8]

The first results reveal slight increase of AF trent in time, however here the patients imaged were of Fitzpatrick skin type 1 to 2, but the screening device first prototype had some illumination issues that could have affected the image quality, therefore probably the big data scattering is present.

Afterwards, another post-operative study [P3] took place in order to create an indicator for possible cancer recurrence in the scar that would identify variation of autofluorescence in post-operative scar in time. Results revieled that after two measurement sessions of 13 patients data show the significant increase in scar AF intensity associated with the scar age (Figure 47).

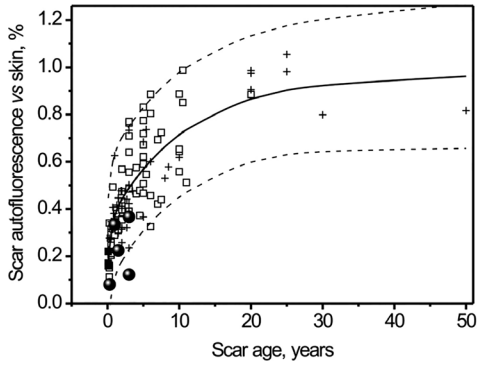

Figure 47. **Comparison of scar autofluorescence intensities during postoperative period: data points (•) represent scars after BCC excision surgery and (+) indicate other benign lesions that had been removed. Data show the significant increase in scar autofluorescence intensity associated with the scar age. 95% prediction interval for autofluorescence values is indicated by the dashed lines. Data points (•) show normalized autofluorescence of recurrent BCC** [P3]

Next, there was a dataset with scar images studied [P4] of 12 patients with benign and recurrent scars, but after different types of scars: surgical, laser and irradiation treatments of BCC, and surgical removal of MM. The results show that the recurrent patient cases stick out of the AF trend, as well as some cases of benign scar cases, really not showing strong increasing AF trend (outside of the 95% confidence level area) (see Figure 48 of Annex 2 for better quality), however, it was a great experience to create a protocol, work with patient scar images from Latvia and Hungary, validate and improve the measurement sequence and image analysis and realize that for a more

successful study a larger patient number and bigger time period would be needed, as well as more images with recurrent post-operative scars, which is not always available due to hospitals inner restrictions, as well as ethical reasons.

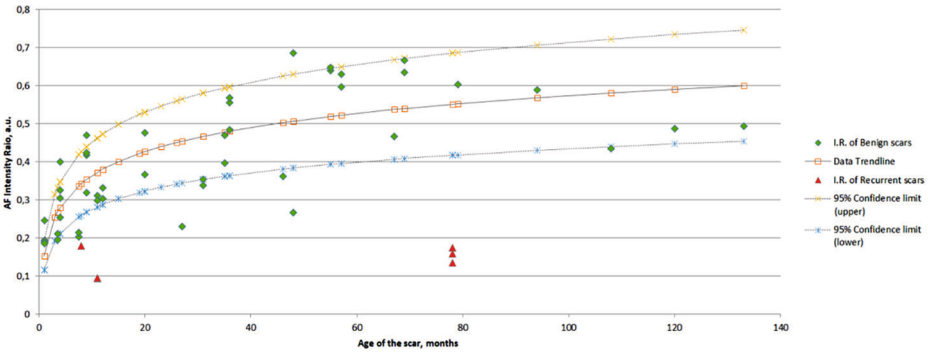

Figure 48. **AF intensity ratio (I.R.) showing the distribution of benign scars (green points) and recurrent scars (red triangles). Data trendline shows the tendency of benign scar AF I.R to increase with time, the lower and upper dashed curves demonstrate the 95% confidence level of the benign scar AF I.R. distribution** [P4]

Lastly, a study [P1] in collaboration with Semmelweis University, Department of Dermatology, Venerology and Dermatooncology, Budapest, Hungary from 2021 till 2022 was done to compare healthy and recurrent MM post-operative scars, but in a relatively shorter time (up to 4 months post-op). In Figure 49 there are two examples of surgical scars after MM surgery. The field of view for the screening device is 2 × 2.5 cm, so the scar must be imaged piece-by-piece. By doing that, the user (dermatologist / general practitioner) can not only evaluate the calculated AF ratio, but also visually spot some pigment changes or extra fluorescent fluorophores (like keratin, pores, etc.), but also pigmented areas that are not visible by a naked eye.

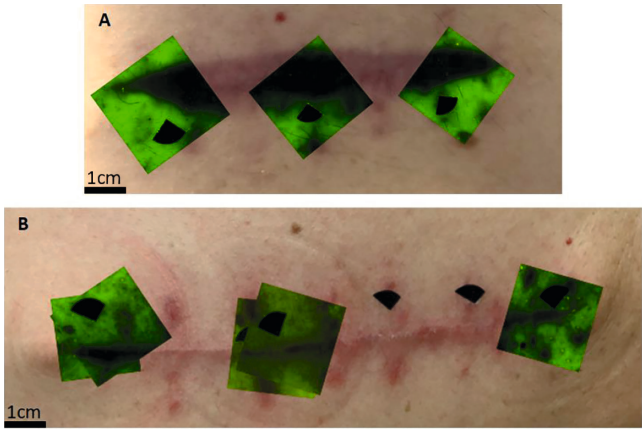

Figure 49. **Examples of two patient post-operative scars (A) and (B). For both images on the background is the colored picture of the skin and on top of it are fragments of AF images** [P1]

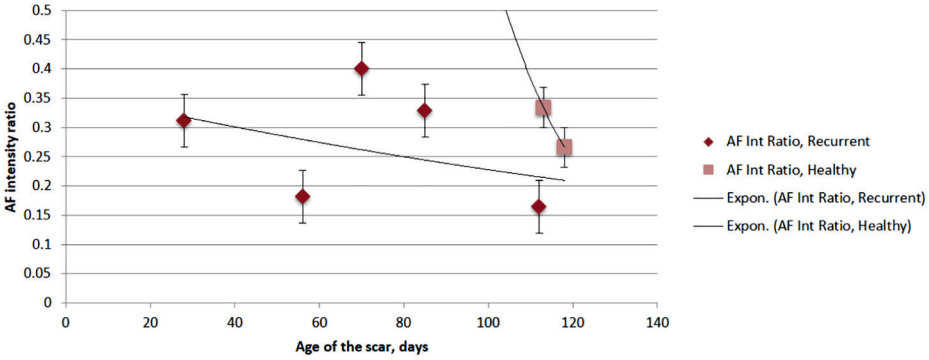

Figure 50. **Autofluorescence intensity ratio between scar tissue and healthy skin. Comparison: scars after MM surgery showing AF intensity values of recurrent scar (n = 5) and healthy scars (n = 2)** [P1]

Summing up the AF ratio for the 7 patients whose scar images were available at the end of the study (see Figure 50), the resulting datapoints did not show a specific trend. During the stages of the wound healing the chromophores in the skin and the scar change, and the changes of AF intensity ratio does not have a specific trend during the first 4 months, but for the first time there was a possibility to image scars right after surgery and have an experience in these kinds of images. AF images stored in patient records could give valuable information during dynamic observation of the patient in longer time.

3.3 Validation results of the remote PPG monitoring device

In order to validate the remote PPG monitoring device, clinical approbation was done at TOS in Riga, Latvia (LU and TOS Contract No. 6012-A53/112 of 12th of November, 2015) [P11], [133], [134], [P13].

This work was supported by the Latvian National research program SOPHIS under the grant agreement #10-4/VPP-4/11.

Local anesthetic affects the sympathetic vascular tone by resulting in vasodilation and subsequent rising of microcirculation intensity in the palm skin. This leads to the increase of amplitude of fast-varying remote PPG signal detected by remote PPG monitoring device. Signal waveforms recorded from the middle part of the palm before and after the anesthesia procedure are shown in Figure 51. The remote PPG signal is weak at baseline (before RA) for most of patients. In some cases, this signal is near to camera noise level. After the successful administrating of local anesthetic, the signal amplitude becomes high enough to detect effect of RA.

The remote PPG signal dynamics during the measurement of patient's palm is shown in Figure 52, the upper graph shows the beat-to-beat amplitude dynamics while the lower graph shows the slow-varying remote PPG component. The gradual increase of perfusion and subsequent remote PPG amplitude was observed a few minutes after the administration of local anesthetics (on the 6th minute), where the plateau phase was reached approximately 10 minutes later [P11].

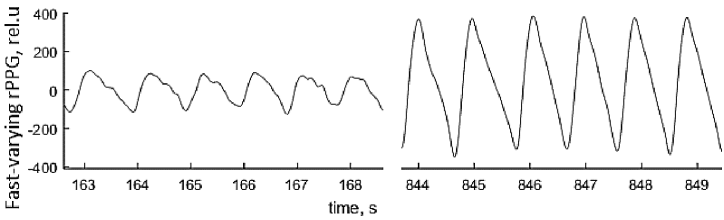

Figure 51. **The palm remote PPG signal waveforms (relative units) before (left) and after (right) the administrating of local anesthetic** [P11]

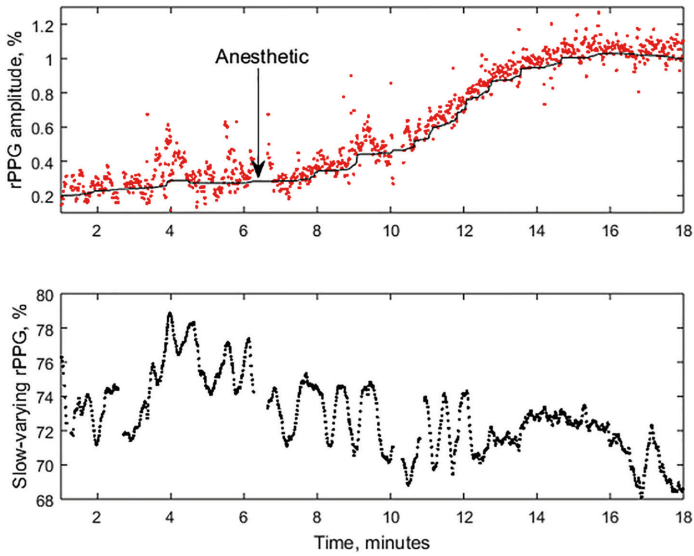

Figure 52. **The ROI averaged amplitude of fast-varying remote PPG signal (above) and slow-varying signal (below) during the RA procedure. The signals show % values of full dynamic range of camera** [P11]

Variations of slow-varying remote PPG signal was affected mainly by non-stabilized light which reached 9% from full dynamic range of camera. Although the power supply was not stable, slow variations of light intensity did not affect the fast-varying remote PPG signal in the near-heartbeat frequency range, because the high dynamic range camera allows capturing video frames with wide range of light intensities [P11].

In Figure 53 there are screenshots of palm video fused with thresholded PPG amplitude maps in the different time moments, before and after the RA procedure. The maps show the spatial distribution of skin microcirculation in the palm. As the local anesthetic affects four different nerves, subsequent microcirculation changes of four different skin zones (dermatomes) should be observed [14]. The PPG amplitude maps showed increase of microcirculation in dermatomes, and the intensity of maps increased immediately after the administering of local anesthetics (see Figure 53 stages 2 to 6) [P11].

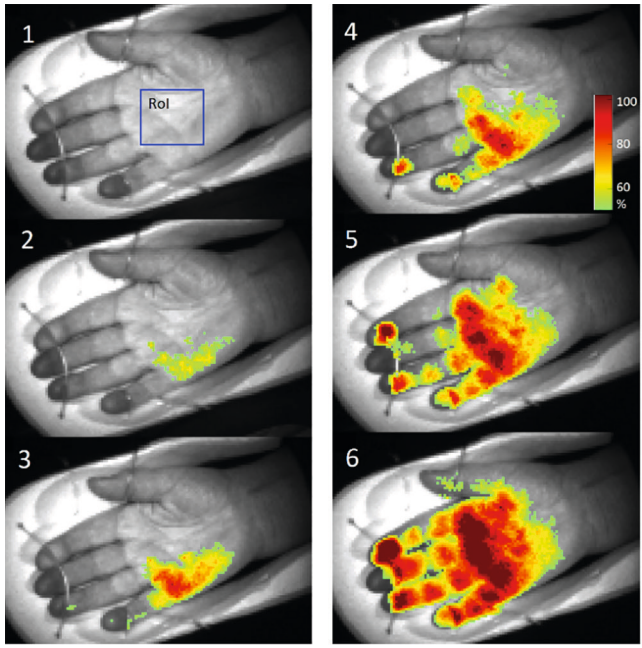

Figure 53. **PPG amplitude maps before (1) and after the administration of local anesthetics, after 1 (2), 3 (3), 5 (4), 6 (5) and 7 minutes (6)** [P11]

The perfusion response slightly differs across the patients, depending on the heterogeneity of the group of patients and the variance of anesthetic procedure. The PPG amplitude maximum value (100%) was found empirically: from the subject having best RA effect, and 50% of PPG amplitude maximum value was suggested as the threshold of a successful anesthesia. The effectiveness of RA was expressed by PPG amplitude signal maxima/minima ratio, which is different from subject to subject [P11], [P13].

Table 4. **Results of regional anasthesia effectiveness evaluation**

Total amount of patients / lesions included in the study	Parameter or characteristic evaluated	Main results/ conclusions	Full info found in publication or other reference
7 patients	Perfusion changes ΔP (%)	1) The advantage of remote PPG monitoring device is the simplicity and ease to use it in a clinical environment. This simple system consisting of the surgical lamp, video camera and computer can be easily adjusted for non-contact monitoring of microcirculation for any application, including regional anesthesia. 2) An efficient remote PPG algorithm for unsupervised monitoring of regional anesthesia effectiveness in two dermatomes of palm.	Rubins, U., Miscuks, A., Marcinkevics, Z., **Lange, M**. Remote photoplethysmography system for unsupervised monitoring regional anesthesia effectiveness. Progress in Biomedical Optics and Imaging. Proceedings of SPIE. Vol. 10592. 2017. **[P13]**

Table 4 continued

Total amount of patients / lesions included in the study	Parameter or characteristic evaluated	Main results/ conclusions	Full info found in publication or other reference
		3) The computing performance tests showed ability of remote PPG monitoring device to process video and performing palm recognition and perfusion map calculations in real-time. 4) The perfusion changes (%) for all patients ranged from 54% to 1432% (ulnar nerve) and from 72% to 1238% (medial nerve) – the necessary threshold for RA effectiveness could be evaluated in the future with a bigger data pool.	
8 patients (age range 30–78)	PPG amplitude changes in time (relative units) in dermatomes of patient's palm. **PPG amplitude ratio** as a parameter.	1) The standard surgical lamp can be used as a light source together with the high dynamic range camera for remote monitoring of skin microcirculation. 2) PPG amplitude ratio could be an indicator for RA evaluation in the future.	Rubins, U., Miscuks, A., **Lange, M**. Simple and convenient remote photoplethysmography system for monitoring regional anesthesia effectiveness. EMBEC & NBC 2017. EMBEC 2017, NBC 2017. IFMBE Proceedings. Vol. 65. Springer, Singapore, 2018. DOI: 10.1007/978-981-10-5122-7_95 **[P11]**

4 DISCUSSION

4.1 Smartphone autofluorescence imaging system

The smartphone AF imaging system usage and data processing method seems to have a good potential for non-invasive differentiation of BCC from SK and can be implemented as a fast screening method of skin non-pigmented pathologies. However, the image processing method requires the high computational load that requires certain time to calculate the output result. Above mentioned problem could be solved by transferring of obtained images to the cloud based platform, thereby enabling to realize the resource intensive image processing during the fixed time.

During several years of data selection at LOC and during discussions with practicing dermatologists, a very clear trend is that it would be great for dermatologists to have a device – compatible with their smartphone with what they could quickly capture patient's lesions within seconds, but at controlled, same illuminated settings. All this could be achieved with an app on smartphone with a combination with the mountable device with illuminators – like the one explained in this work. In order to make it more user friendly, light and quickly to use, as well as to go through medical device approval would require time and effort, and a completely separate project. Still, it is what dermatologists and general practitioners, especially in rural areas, would be happy to use for quick skin screening.

For the technical setup there are, of course, challenges, for instance: motion artefacts, power supply problems, blood perfusion changes because of the pressure of the device against the skin, and user experience in general, as well as others. Besides that, it is a great first attempt for a smartphone solution in skin screening and dermatology diagnostics field.

4.2 Portable LED skin screening device

The proposed setup and device can be used as a screening tool at a general practitioner's office, as well as an extra help for a dermatologist when deciding on the most appropriate procedure or treatment option depending on the diagnosis and situation. The device has good visual archive possibility, and this method should be used as a yearly screening tool for new patients and for patients with skin cancer history it could be used as a reference and monitoring tool for cancer recurrence in the post-operative scars. Considering the relatively high skin cancer incidence in Latvia, it is suggested that family doctors draw more attention to their patients and encourage them to attend dermatologists and do self-check-ups regularly.

As the proposed skin screening system is non-invasive, meaning that the preliminary diagnosis can be done without performing unnecessary biopsy in the initial screening stage, also it is easy to use for the physician and the measurement for one lesion takes around 30 seconds, for the patient it is fast and non-painful, so it can be easily implemented in a national oncology early-diagnosis programme to lower the incidence of skin cancer in Latvia and other countries in the world where the population is at high risk for skin cancer.

Along with outreaching to the general public and informing patients about reducing risks of getting skin cancer and changing the lifestyle, there should be extra guidelines and training provided for general practitioners, so that they could screen their patients more efficiently using their experience and various kinds of diagnostic tools [P2].

4.3 Screening of post-operative scars

This screening method is aiming to give the dermatologist or family doctor extra information when evaluating healing post-operative skin cancer scars. Spectral image analysis shows decreased AF intensity ratio values in the scars with the skin cancer recurrence. It is useful for scar AF evaluation and visual image achieving in a longer time period during patient follow-up to determine the possible cancer recurrence earlier, which is possible with this non-invasive, multispectral method compared to subjective, visual assessment.

There are still some challenges, for instance, automatic scar area segmentation, because of pigmented, sun damaged healthy skin, vascular structures, etc.

With this method, pigmented and abnormal cell detection in scars, using AF intensity evaluation in time can lead to a chance to detect skin cancer recurrence in post-operative scars as early as possible [P4].

In the studied patient scar images the age of the scars varies from a few days after surgery to several decades after surgery, so these are only the first attempts to understand the features and characteristics of AF ratio for post-operative scar healing process using multispectral imaging.

This combination of visual assessment and scar screening evaluating AF features gives a visual and measurable insight of how well the scar is healing and helps to identify possible signs of cancer recurrence.

4.4 Remote PPG monitoring device

The results of remote PPG monitoring device approbation in the clinic gave insights and feedback on what measurements could be performed in the further studies and what would be the best parameters to take into account in order to evaluate RA effectiveness, for instance, during upper extremity surgeries.

The research [P11], [P13] does not yet answer the question: how is it possible to detect the minimum signal level, when the local anesthetic affects peripheral microcirculation and what is the maximum level of such signal? Nevertheless, the effectiveness of RA could be expressed through the remote PPG signal changes at different stages of RA.

The advantage of remote PPG monitoring device is the simplicity and ease to use in a clinical environment. Every operating room has a surgical lamp as a light source that is suitable for remote PPG illumination. This simple system consisting of the surgical lamp, video camera and computer can be adjusted for non-contact monitoring of microcirculation for any application, including RA.

Future plans include designing a wireless remote PPG device for more convenient using in clinical environment [P11], [P13].

By providing a larger patient datapool would significantly improve remote PPG monitoring accuracy and would contribute towards more successful RA effectiveness evaluation. This is important for a lot of patient groups. As seen later, during COVID-19 pandemic, such remote technologies become very handy and essential in operation theatres – reducing the risk of spreading infection, gathering patient vital signs and other data with non-contact diagnostic tools.

5 CONCLUSIONS

1) **The portable LED skin screening device** was successfully used in both clinics in Latvia and in Hungary. The portable device is convenient to use for both dermatologists and general practitioners, the measurement for one lesion takes around 40 seconds and the *p'* parameter map of the lesion is shown a couple of minutes later on the physician's interface for each patient with the suggested evaluation of the lesion, that assist the physician to make decision about further treatment or referral.The calculated sensitivity and specificity for distinguishing MM from melanocytic nevi is respectively 75% and 100%. The device has visual archive possibility, and this method should be used as a yearly screening tool for new patients and for patients with skin cancer history it could be used as a reference and monitoring tool for cancer recurrence in the post-operative scars.
2) The method of using the portable LED skin screening device opens opportunity to screen for skin cancer at primary care level. It can help differentiate benign skin malformations that are commonly mistaken for skin cancer.
3) Skin cancer recurrence unfortunately is an issue, as well as late cancer diagnostics, so the post-operative scar evaluation is essential. The portable LED skin screening device not only provides visual image archive for each patient, but also gives spectral information about the healing process of the post-operative scar and possible new pigmentation that could be recurrent malignant process.There are however a few challenges, like, patient dynamic screening, widening the scope of types of lesions, availability of patients, availability of doctors wanting to take extra time performing the screening, quality of images: segmentation, artefacts: moving, hair, extended pores, etc.
4) AF intensity ratio could be an indicator for the healing stage of the scar; however more data is needed to justify that. During the stages of the wound healing the chromophores in the skin and the scar change, and the changes of AF intensity ratio does not have a specific trend during the first 4 months.
5) The images stored in patient records could give valuable information during dynamic observation of the patient in longer time.
6) **Smartphone AF imaging system** has shown potential for primary evaluation of cancerous or suspicious skin lesions. This technique adequately represents planar distribution of AF intensities in malignant and healthy tissues. This technique could be useful for primary evaluation of BCC, such as determination of precise excision margins prior to surgery.
7) The analysis of 405 nm LED excited AF images captured by smartphone AF imaging system enabled to discriminate SK from BCC, MM, pigmented and dysplastic nevi with sensitivity and specificity close to 100%. In spite of the fact that SK is benign, it is frequently mistakenly suspected as a malignant lesion during BCC and MM visual diagnostics, leading to unnecessary excision, burden to healthcare and wasteful use of resources.
8) The smartphone AF imaging system further could be implemented as a routine method for increasing the diagnostic accuracy of suspicious lesions. It is crucial in

skin cancer diagnostics, as well as for full body examination for timely detection for any possible cancer recurrence.

9) **The remote PPG monitoring device** was approved in clinical environment during regional anesthesia procedures. The results showed that the standard surgical lamp can be used as a light source together with the high dynamic range camera for remote monitoring of skin microcirculation.

THESIS FOR THE DEFENSE

1) The technological solutions offered in the work provide an opportunity to quickly and successfully distinguish skin melanoma from visually similar-looking benign formations. The smartphone autofluorescence imaging system has a sensitivity and specificity close to 100%, distinguishing seborrheic keratosis, while the portable light emitting diode skin screening device has a sensitivity of 75% and a specificity of 100%, distinguishing malignant melanoma from melanocyte nevus.
2) The developed screening protocol for skin cancer post-operative scars, using the portable light emitting diode skin screening device allows to objectively characterize the scar healing process and provides quantitative and visual information about its degree of pigmentation, which helps to evaluate the possibility of recurrence of cancer.
3) The remote photoplethysmography anesthesia monitoring device has been approved as an imaging method for using in the operating room during upper extremity surgeries while evaluating the moment when regional anesthesia becomes effective.
4) The effectiveness of the three technical solutions: smartphone autofluorescence imaging system, portable light emitting diode skin screening device and remote photoplethysmography anesthesia monitoring device and the developed diagnostic procedures have been successfully confirmed and validated in the clinical environment and can be recommended for a wider implementation in hospitals and clinics.

LIST OF PUBLICATIONS

[**P1**] **Lange, M.,** Bozsányi, S., Plorina, E. V., Kiss, N., Varga, N. N., Lihacova, I., and Lihachev, A. "Skin cancer post-operative scar evaluation using autofluorescence features", Proc. SPIE 12226, Applications of Digital Image Processing XLV, 1222618 (3 October 2022). DOI: 10.1117/12.2633932

[**P2**] **Lange, M.**, Plorina, E. V., Lihacova, I., Spigulis, J. Skin cancer screening – better safe than sorry. SHS Web Conf. 85 02003. 2020. DOI: 10.1051/shsconf/20208502003

[**P3**] Tamošiūnas, M., Plorina, E., **Lange, M.**, et al. Autofluorescence imaging for recurrence detection in skin cancer postoperative scars. J Biophotonics, 2020, 13(3): e201900162. DOI:10.1002/jbio.201900162

[**P4**] **Lange, M.,** Bozsányi, S., Plorina, E. V., Lihachev, A., Derjabo, A. Spectral imaging as a tool for the evaluation of skin cancer post-operative scars. Proc. SPIE, 11585, Biophotonics-Riga, 2020, 1158506. DOI: 10.1117/12.2575704

[**P5**] **Lange, M.,** Kiss, N., Fesus, L., Plorina, E. V., Derjabo, A., Spigulis, J. Non-invasive LED-based screening solution for skin cancer, Proc. SPIE 11073, Clinical and Preclinical Optical Diagnostics II, 110731I, 2019. DOI: 10.1117/12.2526386

[**P6**] Lihachev, A., Plorina, E. V., **Lange, M.,** Lihacova, I., Derjabo, A., and Bliznuks, D. "Imaging of LED-excited autofluorescence photobleaching rates for skin lesion diagnostics". In Clinical and Preclinical Optical Diagnostics II, Vol. EB101 of SPIE Proceedings (Optica Publishing Group, 2019), paper 11073_63. DOI: 10.1117/12.2526260

[**P7**] Plorina, E. V.; Bliznuks, D.; Lihachev, A.; Derjabo, A.; Ošiņa, I.; Lihacova, I.; **Lange, M.** Optical design improvement for noncontact skin cancer diagnostic device. Proc. SPIE 10685, Biophotonics: Photonic Solutions for Better Health Care VI, 2018, 1068542, 147. DOI: 10.1117/12.2307125.

[**P8**] **Lange, M.**, Lihachev, A., Plorina, E. V., Derjabo, A., Lihacova, I., Osina, I.; Bliznuks, D., Spigulis, J. Evaluating the aging of the scars after cancer removal by using multispectral diagnostic device. *Biophotonics Congress: Biomedical Optics Congress 2018*. OSA Technical Digest. 2018. DOI: 10.1364/TRANSLATIONAL.2018.JTh3A.7

[**P9**] Lihacova, I., Bolochko, K., Plorina, E. V., **Lange, M.,** Lihachev, A., Bliznuks, D., Derjabo, A. A method for skin malformation classification by combining multispectral and skin autofluorescence imaging. Proc. SPIE 10685, Biophotonics: Photonic Solutions for Better Health Care VI, 1068535. 2018. DOI: 10.1117/12.230620

[**P10**] Lihachev, A., Lihacova, I., Plorina, E. V., **Lange, M.,** Derjabo, A., and Spigulis, J. Differentiation of seborrheic keratosis from basal cell carcinoma, nevi and melanoma by RGB autofluorescence imaging. *Biomedical optics express*, 2018, 9(4), 1852–1858. DOI: 10.1364/BOE.9.001852

[**P11**] Rubins, U., Miscuks, A., **Lange, M.** Simple and convenient remote photoplethysmography system for 2. DOI: 10.1117/1.JBO.20.12.120502

PARTICIPATION IN CONFERENCES

Oral presentations:

[C1] **Lange, M.**, Bozsányi, S., Plorina, E. V., Kiss, N., Lihacova, I., Lihacev, A. "Autofluorescence features can help dermatologists to evaluate skin cancer post-operative scars" at 81st International Scientific Conference of the University of Latvia, 2023, Riga, Latvia.

[C2] **Lange, M.**, Bozsányi, S., Plorina, E. V., Kiss, N., Varga, N. N., Lihacova, I., and Lihachev, A. "Skin cancer post-operative scar evaluation using autofluorescence features", SPIE Optics and Photonics 2022, San Diego, USA.

[C3] **Lange, M**., Bozsányi, S., Plorina, E. V., Lihachev, A., Derjabo, A. "Spectral imaging as a tool for the evaluation of skin cancer post-operative scars", Biophotonics Riga, Latvia, 2020.

[C4] **Lange, M**., Kiss, N., Fesus, L., Plorina, E.V., Derjabo, A., Spigulis, J. "Non-invasive LED-based screening solution for skin cancer", SPIE European Conferences on Biomedical Optics 2019 (24.06.2019.–28.06.2019, Munich, Garmany).

[C5] **Lange, M.,** Plorina, E. V., Derjabo, A., Spigulis, J. "Multispectral imaging device for non-invasive skin lesion diagnostics", "IONS NANJING" (2th of May – 2nd of June, 2019, China).

[C6] **Lange, M.**, Rubīns, U., Lihachev, A., Bļizņuks, D. "Optical, Non-Invasive Diagnostic Imaging Methods" in Riga Stradins University scientific conference, 2018 (22nd–23rd of March, Riga, Latvia).

[C7] **Lange, M.**, Bliznuks, D., Lihachev, A., Plorina, E. V., Lihacova, I., Spigulis, J. "Non-invasive optical skin evaluation device for cancer screening" in Developments in Optics and Communications" (12–13th of April, 2018, Riga, Latvia).

[C8] **Lange, M.**, Plorina, E. V., Lihacova, I., and Derjabo, A. "Skin cancer screening – better safe than sorry" in The 7th conference "Society. Health. Welfare" 2018 (10–12th of October, Riga, Latvia).

[C9] **Lange, M.**, Zeidaks, M., Plorina, E. V., Lacis, M., Panke, K. "Mobile device for skin screening" in World Congress on Medical Physics and Biomedical Engineering 2018 (3–8 June, 2018, Prague Czech Republic).

[C10] **Lange, M.**, Rubins, U., Miscuks, A. "The use of remote photoplethysmography system for regional anesthesia monitoring in operating room" in DOC Riga 2017, 6–7 April, Riga, Latvia.

Poster presentations:

[CP1] **Lange, M.**, Bozsanyi, S., Plorina, E. V., Kiss, N., Lihacova, I., Lihacev, A. "Autofluorescence features can help dermatologists to evaluate skin cancer post-operative scars" at 81st International Scientific Conference of the University of Latvia, 2023, Riga, Latvia.

[CP2] **Lange, M.**, Bozsányi, S., Plorina, E. V., Kiss, N., Varga, N. N., Lihacova, I., and Lihachev, A., "Skin cancer post-operative scar evaluation using autofluorescence features", SPIE Optics and Photonics 2022, San Diego, USA.

[**CP3**] **Lange, M.**; Bozsányi, S.; Plorina, E. V.; Lihachev, A.; Derjabo, A. "Spectral imaging as a tool for the evaluation of skin cancer post-operative scars", Biophotonics Riga, Latvia, 2020.

[**CP4**] **Lange, M.**; Kiss, N.; Fesus, L.; Plorina, E. V.; Derjabo, A.; Spigulis, J. "Non-invasive LED-based screening solution for skin cancer", SPIE European Conferences on Biomedical Optics, 2019 (24.06.2019.–28.06.2019, Munich, Garmany).

[**CP5**] **Lange, M.**, Plorina, E. V., Derjabo, A., Spigulis, J. "Multispectral imaging device for non-invasive skin lesion diagnostics", "IONS NANJING" (2th of May – 2nd of June, 2019,China).

[**CP6**] **Lange, M.**, Rubīns, U., Lihachev, A., Bļizņuks, D. "Optical, Non-Invasive Diagnostic Imaging Methods" in Riga Stradins University scientific conference, 2018, (22nd-23rd of March, Riga, Latvia).

[**CP7**] **Lange, M.**, Bliznuks, D., Lihachev, A., Plorina, E. V., Lihacova, I., Spigulis, J. "Non-invasive optical skin evaluation device for cancer screening" in Developments in Optics and Communications" (12th–13th of April, 2018, Riga, Latvia).

[**CP8**] **Lange, M.**, Plorina, E. V., Lihacova, I., and Derjabo, A. "Skin cancer screening – better safe than sorry" in The 7th conference "Society. Health. Welfare.", 2018 (10–12th of October, Riga, Latvia).

[**CP9**] **Lange, M.**, Zeidaks, M., Plorina, E. V., Lacis, M., Panke, K. "Mobile device for skin screening" in World Congress on Medical Physics and Biomedical Engineering 2018 (3–8 June, 2018, Prague Czech Republic).

[**CP10**] **Lange, M.**, Rubins, U., Miscuks, A. "The use of remote photoplethysmography system for regional anesthesia monitoring in operating room" in DOC Riga 2017, April 6–7, Riga, Latvia.

Contests and other events that promote the topic of the thesis:

1) **Golden Award** in IFMBE-Sponsored Student Design Competition of World Congress on Medical Physics and Biomedical Engineering 2018 (3–8 June, 2018, Prague Czech Republic) (in a team).
2) **1st place** in 4th Riga-Cambridge Venture camp with business idea for non-invasive skin screening device (15th of December, 2018, Riga, Latvia) (in a team).
3) **Third prize** winner of THE EMBEC17 & NBC17 YOUNG INVESTIGATORS COMPETITION with "*Simple and convenient remote photoplethysmography system for monitoring regional anesthesia effectiveness*" *oral presentation, 2017 (individual).*
4) **Peoples' Choice Talk Prize** *for presentation* "Remote regional anesthesia monitoring with photoplethysmography system" in *IONS KOALA* (Conference on Optics, Atoms and Laser Applications), Brisbane, Australia, 2017 (individual).
5) **Acknoweledgment Prize** of Latvian Academy of Sciences for scientific success in 2018 about the work in project "Portable Device for Early Contactless Diagnosis of Skin Cancer" (in a team).

Other science related activities about thesis topic:

- Presentation "Ādas veidojumu skrīnings / Skin Screening" at an outreach event for general public "Zināšanu agora" at University of Latvia, fall of 2019.
- Main organiser of free skin screening event for general public regarding melanoma awareness month "Ādas skrīninga diena / Skin Screening Day", at University of Latvia, May of 2019.
- Participation in National Radio discussion about latest medical technologies "Nākotnē medicīna kļūs personalizēta un krietni precīzāka katram cilvēkam / In the future, medicine will become personalized and much more accurate for each person" Latvijas Radio 1st Channel, 11th of April, 2019.
- Main organiser and Conference Chair at Scientific Student Conference "Developments of Optics and Communications Riga" in 2015 and 2017, Riga, Latvia.

REFERENCES

[1] A. M. Roberts, *The Complete Human Body*. Dorling Kindersley Limited, 2010.

[2] User "Madhero88," "Skin layers," 2011. [Online]. Available: https://en.wikipedia.org/wiki/File:Skin_layers.png. [Accessed: 09-Jun-2023].

[3] W. Damsky and M. Bosenberg, "Melanocytic nevi and melanoma: unraveling a complex relationship," *Oncogene*, vol. 36 (42), 2017, pp. 5771–5792.

[4] U. Wollina, "Recent advances in managing and understanding seborrheic keratosis," *F1000Research*, vol. 8, 2019.

[5] "Seborrheic Keratosis," *Yale Medicine*. [Online]. Available: https://www.yalemedicine.org/conditions/seborrheic-keratosis. [Accessed: 21-Jun-2023].

[6] M. Monici, "Cell and tissue autofluorescence research and diagnostic applications," *Biotechnology annual review*, vol. 11, 2005, pp. 227–256.

[7] "Hemangioma," *Cleveland Clinic*. [Online]. Available: https://my.clevelandclinic.org/health/diseases/23365-hemangioma.

[8] D. Turbert, "What Is Hemangioma?," 2022. [Online]. Available: https://www.aao.org/eye-health/diseases/hemangioma. [Accessed: 06-Jun-2023].

[9] B. L. Horecker, "THE ABSORPTION SPECTRA OF HEMOGLOBIN AND ITS DERIVATIVES IN THE VISIBLE AND NEAR INFRA-RED REGIONS," *Journal of Biological Chemistry*, vol. 148, no. 1, 1943, pp. 173–183.

[10] "Photoaging (Sun Damage)," *Yale Medicine*. [Online]. Available: https://www.yalemedicine.org/conditions/sun-damage. [Accessed: 01-Jun-2023].

[11] "Sun Damaged Skin." [Online]. Available: https://media.istockphoto.com/photos/dermoscopy-of-sun-damaged-skin-picture-id693844100?k=6&m=693844100&s=170667a&w=0&h=vXsgtAxPa6HlblcpBNgrBu97JaUMT_qBmVkOANkhZx0=.

[12] "Skin Cancer." [Online]. Available: https://www.cancer.org/cancer/skin-cancer.html.

[13] "Cancer Screening," *World Health Organisation*. [Online]. Available: https://www.who.int/cancer/prevention/diagnosis-screening/en/.

[14] "The Official Federal Cancer Statistics. Data Visualisations," *Centers for Disease Control and Prevention*. [Online]. Available: https://gis.cdc.gov/Cancer/USCS/#/AtAGlance/. [Accessed: 01-Mar-2022].

[15] "Statistikas dati par onkoloģiskajiem pacientiem, 2010–2017", 2018. [Online]. Available: https://www.spkc.gov.lv/lv/statistika-un-petijumi/statistika/veselibas-aprupes-statistika1.

[16] "Ļaundabīgi audzēji," *SPKC*. [Online]. Available: https://statistika.spkc.gov.lv/Resources/PX/Databases/Health/Metadati/ONKO_Registra_metadati_lv.html.

[17] "Signs and Symptoms of Melanoma Skin Cancer," *American Cancer society*, 2019. [Online]. Available: https://www.cancer.org/cancer/melanoma-skin-cancer/detection-diagnosis-staging/signs-and-symptoms.html.

[18] "Skin cancer statistics," *World Cancer Research Fund International*, 2022. [Online]. Available: https://www.wcrf.org/cancer-trends/skin-cancer-statistics/.

[19] C. S. M. Wong, R. C. Strange, and J. T. Lear, "Basal cell carcinoma," *BMJ (Clinical research ed.)*, vol. 327, no. 7418, Oct. 2003, pp. 794–798.

[20] Ronald P. Rapini, *Practical Dermatopathology*. Elsevier Health Sciences.

[21] "Cancer Facts & Figures 2022," 2022. [Online]. Available: https://www.cancer.org/content/dam/cancer-org/research/cancer-facts-and-statistics/annual-cancer-facts-and-figures/2022/2022-cancer-facts-and-figures.pdf [Accessed: 26-Jul-2022].

[22] "ICD-10 Version:2016," 2016. [Online]. Available: https://icd.who.int/browse10/2016/en.

[23] "Latvijas veselības aprūpes statistikas gadagrāmata 2017". Rīga, 2018.

[24] G. Rozentāle, I. Zvaigznīte, and M. Štāle, "Sabiedrības veselības stratēģijas mērķu sasniegšanas izvērtējums". Rīga, 2010.

[25] Ministry of Health of Latvia, "Cancer prevention," 2017. [Online]. Available: http://www.vm.gov.lv/lv/tava_veseliba/sievietem/valsts_apmaksata_veza_savlaicigas_atklasanas_programma/.

[26] "Necepies! Pasargā sevi no ādas vēža!", *The Centre for Disease Prevention and Control of Latvia*, 2018. [Online]. Available: https://www.spkc.gov.lv/lv/tavai-veselibai/kampanas/necepies-pasarga-sevi-no-adas-. [Accessed: 20-Sep-2001].

[27] M. Štāle, A. Treide, and G. Rožkalne, "Neinfekciju slimības – saslimstība, mirstība, riska faktori. Situācija Latvijā 2006.–2015. gadā", 2016.

[28] H. W. Walling, S. W. Fosko, P. A. Geraminejad, and E. Al., "Aggressive basal cell carcinoma: Presentation, pathogenesis, and management," *Cancer Metastasis Rev*, no. 23, 2004, pp. 389–402.

[29] M. M. Stuart, S. E., Schoen, P., Jin, C., Parvataneni, R., Arron, S., Linos, E., et al. Chren, "Tumor recurrence of keratinocyte carcinomas judged appropriate for Mohs micrographic surgery using Appropriate Use Criteria," *Journal of the American Academy of Dermatology*, vol. 76, no. 6, 2017.

[30] A. M. Farhi D, Dupin N, Palangié A, Carlotti A, "Incomplete Excision of Basal Cell Carcinoma: Rate and Associated Factors among 362 Consecutive Cases," *Dermatol Surg.*, vol. 33, no. 10, 2007, pp. 1207–1214.

[31] Koolen, P. G. L., Matos, T. R., Ibrahim, A. M. S., Sun, J., Lee, B. T., Frankenthaler, R. A., and Lin, S. J., "Recurrence Rates Over 20 Years in the Treatment of Malignant Melanoma: Immediate Versus Delayed Reconstruction," *Plastic and Reconstructive Surgery – Global Open*, vol. 7, no. 5, 2017.

[32] M. J. Lin, V. Mar, C. McLean, R. Wolfe, and J. W. Kelly, "Diagnostic accuracy of malignant melanoma according to subtype," *The Australasian journal of dermatology*, vol. 55, no. 1, Feb. 2014, pp. 35–42.

[33] L. L. Yu and P. J. Heenan, "The morphological features of locally recurrent melanoma and cutaneous metastases of melanoma," *Human Pathology*, vol. 30, no. 5, 1999, pp. 551–555.

[34] A. NH, "Wound healing process," 2016.

[35] "Medical gallery of Mikael Häggström 2014," *WikiJournal of Medicine,* 1(2), 2014.

[36] T. Fitzpatrick, "The validity and practicality of sun-reactive skin types I through VI", *Arch Dermatol*, vol. 6, no. 124, pp. 869–871.

[37] J. D'Orazio, S. Jarrett, A. Amaro-Ortiz, and T. Scott, "UV Radiation and the Skin," *International Journal of Molecular Sciences*, vol. 14, no. 6, 2013.

[38] "Skin Cancer in People with Dark Skin Tones," *Health Union, LLC*. [Online]. Available: https://skincancer.net/basics/dark-skin-tones-risk-factor.

[39] G. Chaplin, "Geographic distribution of environmental factors influencing human skin coloration," *American journal of physical anthropology*, vol. 125, no. 3, Nov. 2004, pp. 292–302.

[40] T. Weyrich, et al., "Analysis of Human Faces Using a Measurement-Based Skin Reflectance Model", *ACM Trans. Graph.*, vol. 25, no. 3, 2006, pp. 1013–1024.

[41] D. Baltina, S. Donina, S. Januskevics, I. Kudaba, A. Derjabo, and S. Maksimova, "Klīniskās vadlīnijas "Ādas vēža un melanomas diagnostika, ārstēšana un dinamiskā novērošana"". Rīga, 2015.

[42] "No Title," *Melanomas pacientu atbalsta biedrība "Soli priekšā melanomai."* [Online.] Available: https://solipriekšamelanomai.lv/kontakti-2/.

[43] M. Boniol, P. Autier, and S. Gandini, "Melanoma mortality following skin cancer screening in Germany," *BMJ Open*, vol. 5, 2015.

[44] WHO, *National cancer control programmes : policies and managerial guidelines*, 2nd ed. Geneva, 2002.

[45] N. Calonge, D. B. Petitti, and T. G. DeWitt, "Screening for Skin Cancer: U.S. Preventive Services Task Force Recommendation Statement," *Annals of Internal Medicine*, vol. 150, no. 3, pp. 188–194.

[46] S. Allen, "Melanoma Screening Saves Lives." [Online]. Available: https://www.skincancer.org/skin-cancer-information/melanoma/melanoma-prevention-guidelines/melanoma-screening-saves-lives.

[47] *IARC monographs on the evaluation of carcinogenic risks to humans*. Lyon, France: International Agency for Research on Cancer, 1992.

[48] Veselības ministrija, *Higiēnas prasības kosmētiskā iedeguma pakalpojuma sniegšanai*. Rīga, Latvia: Ministru kabinets, 2019.

[49] "CLOUD PACS." [Online]. Available: https://datamed.lv/en/services/cloud-pacs.html.

[50] "Artificial intelligence in radiology." [Online]. Available: https://datamed.lv/en/services/artificial-intelligence-in-radiology.html.

[51] W. Stolz, P. Bilek, M. Landthaler, T. Merkle, and O. Braun-Falco, "SKIN SURFACE MICROSCOPY," *The Lancet*, vol. 334, no. 8667, 1989, pp. 864–865.

[52] "HEINE." [Online]. Available: https://www.heine.com/en/products/dermatoscopes-and-digital-documentation/ dermatoscopes/detail/28744-heine-delta-20t-dermatoscope.

[53] "Dermatoscope." [Online]. Available: https://www.distrimed.com/images/imagesmulti/116021_7_b.jpg.

[54] G. Argenziano and H. P. Soyer, "Dermoscopy of pigmented skin lesions – a valuable tool for early," *The Lancet Oncology*, vol. 2, no. 7, Jul. 2001, pp. 443–449.

[55] J. Levy, D. L. Barrett, N. Harris, J. J. Jeong, X. Yang, and S. C. Chen, "High-frequency ultrasound in clinical dermatology: a review," *The ultrasound journal*, vol. 13, no. 1, Apr. 2021, p. 24.

[56] "Ultrasound," *National Institute of Biomedical Imaging and Bioengineering*. [Online]. Available: https://www.nibib.nih.gov/science-education/science-topics/ultrasound.

[57] K. D. Bhatt, S. A. Tambe, H. R. Jerajani, and R. S. Dhurat, "Utility of high-frequency ultrasonography in the diagnosis of benign and malignant skin tumors," *Indian journal of dermatology, venereology and leprology*, vol. 83, no. 2, 2017, pp. 162–182.

[58] J. Welzel, E. Lankenau, R. Birngruber, and R. Engelhardt, "Optical coherence tomography of the human skin," *Journal of the American Academy of Dermatology*, vol. 37, no. 6, Dec. 1997, pp. 958–963.

[59] "Patient Scan OCT," *Skin Cancer Network*. [Online]. Available: https://www.skincarenetwork.co.uk/wp-content/uploads/2018/01/patient-scan.jpg.

[60] M. Kislevitz, Y. Akgul, C. Wamsley, J. Hoopman, and J. Kenkel, "Use of Optical Coherence Tomography (OCT) in Aesthetic Skin Assessment-A Short Review," *Lasers in surgery and medicine*, vol. 52, no. 8, Oct. 2020, pp. 699–704.

[61] J. Holmes, S. Hattersley, N. Stone, F. Bazant-Hegemark, and H. B. M. D., "Multi-channel Fourier domain OCT system with superior lateral resolution for biomedical applications," in *Coherence Domain Optical Methods and Optical Coherence Tomography in Biomedicine XII*, 2008, vol. 6847, p. 68470O.

[62] "LINE-FIELD CONFOCAL OPTICAL COHERENCE TOMOGRAPHY (LC-OCT)," *Damae Medical*. [Online]. Available: https://damae-medical.com/files/Brochure_deepLive.pdf.

[63] A. J. Coleman, T. J. Richardson, G. Orchard, A. Uddin, M. J. Choi, and K. E. Lacy, "Histological correlates of optical coherence tomography in non-melanoma skin cancer," *Skin research and technology : official journal of International Society for Bioengineering and the Skin (ISBS) [and] International Society for Digital Imaging of Skin (ISDIS) [and] International Society for Skin Imaging (ISSI)*, vol. 19, no. 1, Feb. 2013, pp. 10–19.

[64] A. Dubois et al., "Line-field confocal optical coherence tomography for high-resolution noninvasive imaging of skin tumors," *Journal of biomedical optics*, vol. 23, no. 10, Oct. 2018, pp. 1–9.

[65] "FotoFinder." [Online]. Available: https://www.fotofinder.de.

[66] D. N. Dorrell and L. C. Strowd, "Skin Cancer Detection Technology," *Dermatologic clinics*, vol. 37, no. 4, Oct. 2019, pp. 527–536.

[67] "Class 2 Device Recall MelaFind," *FDA*. [Online]. Available: https://www.accessdata.fda.gov/scripts/cdrh/cfdocs/cfRES/res.cfm?id=136172.

[68] R. R. Winkelmann, A. S. Farberg, A. M. Glazer, and D. S. Rigel, "Noninvasive Technologies for the Diagnosis of Cutaneous Melanoma," *Dermatologic clinics*, vol. 35, no. 4, Oct. 2017, pp. 453–456.

[69] F. M. Walter et al., "Effect of adding a diagnostic aid to best practice to manage suspicious pigmented lesions in primary care: randomised controlled trial," *BMJ (Clinical research ed.)*, vol. 345, Jul. 2012, p. e4110.

[70] S. Pratavieira, C. T. Andrade, A. G. Salvio, V. S. Bagnato, and C. Kurachi, "Optical Imaging as Auxiliary Tool in Skin Cancer Diagnosis," in *Skin Cancers*. C. A. M. La Porta, Ed. Rijeka: IntechOpen, 2011.

[71] A. J. Moy and J. W. Tunnell, "Chapter 17 – Diffuse Reflectance Spectroscopy and Imaging," in *Imaging in Dermatology*, M. R. Hamblin, P. Avci, and G. K. Gupta, eds. Boston: Academic Press, 2016, pp. 203–215.

[72] S. Xu, "Skin Image Synthesis Based on Pigment Concentration Distribution," *DEStech Transactions on Computer Science and Engineering*, Mar. 2017.

[73] "BioRender tool." [Online]. Available: https://www.biorender.com.

[74] W. West, "Absorption of electromagnetic radiation," *Access Science*, 2014.

[75] J. Spigulis, I. Oshina, A. Berzina, and A. Bykov, "Smartphone snapshot mapping of skin chromophores under triple-wavelength laser illumination," *Journal of Biomedical Optics*, vol. 22, no. 9, Mar. 2017, p. 91508.

[76] I. Oshina and J. Spigulis, "Beer–Lambert law for optical tissue diagnostics: current state of the art and the main limitations," *Journal of Biomedical Optics*, vol. 26, no. 10, 2021, p. 100901.

[77] J. Yao and L. V Wang, "Sensitivity of photoacoustic microscopy," *Photoacoustics*, vol. 2, no. 2, Jun. 2014, pp. 87–101.

[78] F. W. D. Rost, *Fluorescence microscopy. Vol. II*. Cambridge University Press, 1995.

[79] P. N. M. Raja, "4.5: Photoluminescence, Phosphorescence, and Fluorescence Spectroscopy." [Online]. Available: https://chem.libretexts.org/Bookshelves/Analytical_Chemistry/Physical_Methods_in_Chemistry_and_Nano_Science_(Barron)/04%3A_Chemical_Speciation/4.05%3A_Photoluminescence_Phosphorescence_and_Fluorescence_Spectroscopy.

[80] C. M. C. Volgenant, M. H. van der Veen, J. J. de Soet, and J. M. ten Cate, "Effect of metalloporphyrins on red autofluorescence from oral bacteria," *European journal of oral sciences*, vol. 121, no. 3 Pt 1, Jun. 2013, pp. 156–161.

[81] H. Zeng, C. E. MacAulay, D. I. M. M.D., and B. Palcic, "Novel microspectrophotometer and its biomedical applications," *Optical Engineering*, vol. 32, no. 8, Aug. 1993, pp. 1809–1814.

[82] N. L. Lacz, R. A. Schwartz, and G. Kihiczak, "Epidermolytic hyperkeratosis: a keratin 1 or 10 mutational event", *International journal of dermatology*, vol. 44, no. 1, Jan. 2005, pp. 1–6.

[83] B. P. Korge, J. G. Compton, P. M. Steinert, and D. Mischke, "The two size alleles of human keratin 1 are due to a deletion in the glycine-rich carboxyl-terminal V2 subdomain," *The Journal of investigative dermatology*, vol. 99, no. 6, Dec. 1992, pp. 697–702.

[84] A. Reolid et al., "Annular epidermolytic ichthyosis: An exceptional mild subtype of epidermolytic ichthyosis without genotype and phenotype correlation", *JAAD case reports*, vol. 6, no. 1. United States, Jan. 2020, pp. 46–50.

[85] V. P. Sybert et al., "Cyclic ichthyosis with epidermolytic hyperkeratosis: A phenotype conferred by mutations in the 2B domain of keratin K1," *American journal of human genetics*, vol. 64, no. 3, Mar. 1999, pp. 732–738.

[86] A. Terron-Kwiatkowski et al., "Atypical epidermolytic palmoplantar keratoderma presentation associated with a mutation in the keratin 1 gene", *British Journal of Dermatology*, vol. 150, 2004.

[87] Y. Wu and J. Y. Qu, "Autofluorescence spectroscopy of epithelial tissues," *Journal of biomedical optics*, vol. 11, no. 5, 2006, p. 54023.

[88] N. Kiss et al., "Quantitative Analysis on Ex Vivo Nonlinear Microscopy Images of Basal Cell Carcinoma Samples in Comparison to Healthy Skin," *Pathology oncology research : POR*, vol. 25, no. 3, Jul. 2019, pp. 1015–1021.

[89] I. Bliznakova, E. G. Borisova, and L. Avramov, "Laser- and Light-Induced Autofluorescence Spectroscopy of Human Skin in Dependence on Excitation Wavelengths," *Acta Physica Polonica A*, vol. 112, 2007, pp. 1131–1136.

[90] A. Hotz et al., "Expanding the Clinical and Genetic Spectrum of KRT1, KRT2 and KRT10 Mutations in Keratinopathic Ichthyosis," *Acta dermato-venereologica*, vol. 96, no. 4, 2016, pp. 473–478.

[91] J. H. Yim, K. H. Jeong, and M. K. Shin, "Comparative study of skin autofluorescence expression in atopic dermatitis and psoriasis: A prospective in vivo study," *Skin research and technology : official journal of International Society for Bioengineering and the Skin (ISBS) [and] International Society for Digital Imaging of Skin (ISDIS) [and] International Society for Skin Imaging (ISSI)*, vol. 23, no. 2, May 2017, pp. 169–175.

[92] S. J. Lin, et al., "Discrimination of basal cell carcinoma from normal dermal stroma by quantitative multiphoton imaging," *Opt. Lett.*, vol. 31, no. 18, Sep. 2006, pp. 2756–2758.

[93] E. G. Borisova, L. P. Angelova, and E. P. Pavlova, "Endogenous and Exogenous Fluorescence Skin Cancer Diagnostics for Clinical Applications," *J. Quantum Electron.*, vol. 20, no. 2, 2014.

[94] M. Panjehpour, C. E. Julius, M. N. Phan, T. Vo-Dinh, and S. Overholt, "Laser-Induced Fluorescence Spectroscopy for In Vivo Diagnosis of Non-melanoma Skin Cancers", *Lasers Surg Med*, vol. 31, no. 5, 2002, pp. 367–373.

[95] N. P. Galletly et al., "Fluorescence lifetime imaging distinguishes basal cell carcinoma from surrounding uninvolved skin," *Br J Dermatol*, vol. 159, no. 1, 2008, pp. 152–161.

[96] D. Chorvat and A. Chorvatova, "Multi-wavelength fluorescence lifetime spectroscopy: a new approach to the study of endogenous fluorescence in living cells and tissues," *Laser Phys Lett.*, vol. 6, no. 3, 2009, pp. 175–193.

[97] S. Chen, C. Zhu, C. Hoe-Kong Chui, G. Sheoran, B. K. Tan, and Q. Liu, "Spectral diffuse reflectance and autofluorescence imaging can perform early prediction of blood vessel occlusion in skin flaps," *Journal of biophotonics*, vol. 10, no. 12, Dec. 2017, pp. 1665–1675.

[98] "Optical Absorption of Hemoglobin." [Online]. Available: https://omlc.org/spectra/hemoglobin/.

[99] S. Jacques, "Extinction Coefficient of Melanin." [Online]. Available: https://omlc.org/spectra/melanin/extcoeff.html.

[100] Lumex, "Datasheet of SML-LXL8047UVC." [Online]. Available: https://www.lumex.com/datasheet/SML-LXL8047UVC.

[101] A. C. Croce and G. Bottiroli, "Autofluorescence spectroscopy and imaging: a tool for biomedical research and diagnosis," *European journal of histochemistry : EJH*, vol. 58, no. 4, 2014, p. 2461.

[102] Marcu, Laura; French, P. M. W., Elson, D. S., *Fluorescence Lifetime Spectroscopy and Imaging Principles and Applications in Biomedical Diagnostics*. CRC Press, 2015.

[103] C. Macdonald, "Principle of NIR diffuse reflectance spectroscopy," 2016. [Online]. Available: https://www.pulpandpapercanada.com/canadian-mills-opt-for-fitnir-analyzers-1100000232/.

[104] J. Allen, "Photoplethysmography and its application in clinical physiological measurement", *Physiological measurement*, vol. 28, no. 3, Mar. 2007, pp. R1–39.

[105] A. Jubran, "Pulse oximetry," *Critical care (London, England)*, vol. 3, no. 2, 1999, pp. R11–R17.

[106] V. Song, "How to measure your SpO2 on your smartwatch," *The Verge*, 2022. [Online]. Available: https://www.theverge.com/23031829/how-to-measure-spo2-smartwatch.

[107] T. Tamura, Y. Maeda, M. Sekine, and M. Yoshida, "Wearable Photoplethysmographic Sensors-Past and Present," *Electronics*, vol. 3, no. 2, 2014, pp. 282–302.

[108] T. B. Folino and S. K. Mahboobi, "Regional Anesthetic Blocks," Treasure Island (FL), 2023.

[109] J. Li, D. Lam, H. King, E. Credaroli, E. Harmon, and N. Vadivelu, "Novel Regional Anesthesia for Outpatient Surgery," *Current pain and headache reports*, vol. 23, no. 10, Aug. 2019, p. 69.

[110] J. L. Yurgil, C. D. Hulsopple, and J. C. Leggit, "Nerve Blocks: Part I. Upper Extremity," *American family physician*, vol. 101, no. 11, Jun. 2020, pp. 654–664.

[111] "Cutaneous Nerve Supply of Hand," *Instant Anatomy*. [Online]. Available: https://www.instantanatomy.net/arm/nerves/dermatomes.html.

[112] "Assessment of sensory block. Dermatome assessment," *The Royal Children's Hospital Melbourne*, 2000. [Online]. Available: https://www.rch.org.au/anaes/pain_management/Assessment_of_sensory_block/.

[113] W. Verkruysse, L. O. Svaasand, and J. S. Nelson, "Remote plethysmographic imagingusing ambient light," *Opt. Express*, vol. 16, no. 26, 2008, pp. 21, 434–421, 445.

[114] M. Kumar and A. Veeraraghavan, A. Sabharwal, "DistancePPG: Robust non-contact vital signs monitoring using a camera," *Biomed. Opt. Express*, vol. 5, no. 6, 2015, pp. 1565–1588.

[115] A. A. Kamshilin, S. Miridonov, V. Teplov, and E. Saarenheimo, R. Nippolainen, "Photoplethysmographic imaging of high spatial resolution," *Biomed. Opt. Express*, vol. 2, no. 4, 2011, pp. 996–1006.

[116] J. Spigulis, "Biophotonic technologies for non-invasive assessment of skin condition and blood microcirculation," *Latv. J. Phys. Tech. Sci.*, vol. 5, no. 49, 2012, p. 63.

[117] U. Rubins, A. Miscuks, O. Rubenis, R. Erts, and A. Grabovskis, "The analysis of blood flow changes under local anesthetic input using non-contact technique," *Proc. 3rd Int. Conf. on BioMedical Engineering and Informatics*, vol. 2, 2010, pp. 601–604.

[118] U. Rubins, J. Spigulis, and A. Miscuks, "Application of colour magnification technique for revealing skin microcirculation changes under regional anaesthetic input," *Proc. SPIE*, no. 9032, 2013, pp. 1–5.

[119] Z. Marcinkevics, U. Rubins, J. Zaharans, A. Miscuks, E. Urtane, and L. Ozolina-Moll, "Imaging photoplethysmography for clinical assessment of cutaneous microcirculation at two different depths," *J. Biomed. Opt. 35005*, vol. 21, no. 3, 2016.

[120] U. Rubins, J. Spigulis, and A. Miscuks, "Photoplethysmography imaging algorithm for continuous monitoring of regional anesthesia," *ESTIMedia'16 Proc. of 14th ACM/IEEE Symposium on Embedded Systems for Real- Time Multimedia*, pp. 67–71.

[121] W. T. Wu, H. Rubinstein, M. Shih, E. Guttag, J. Durand, F. Freeman, "Eulerian Video Magnification for Revealing Subtle Changes in the World," *ACM Transactions on Graphics, Proc. SIGGRAPH*, Vol. 31, No. 4, 2012.

[122] S. Hu, J. Zheng, V. Chouliaras, and R. Summers, "Feasibility of imaging photoplethysmography," 2010.

[123] W. Wang, A. C. den Brinker, S. Stuijk, and G. de Haan, "Algorithmic Principles of Remote PPG," *IEEE Transactions on Biomedical Engineering*, vol. 64, no. 7, 2017, pp. 1479–1491.

[124] "NCCN Clinical Practice Guidelines in Oncology: Melanoma. v.3", 2020.

[125] P. Osipovs, D. Bliznuks, and A. Lihachev, "Cloud infrastructure for skin cancer scalable detection system," *Proc. SPIE 10679*, vol. Optics, Ph, no. Proc. SPIE 10679, 2018.

[126] "New iDS uEye LE cameras." [Online]. Available: https://www.adept.net.au/news/newsletter/200807-jul/board_camera.shtml.

[127] "Raspberry Pi 3 Model B." [Online]. Available: https://www.raspberrypi.com/products/raspberry-pi-3-model-b/.

[128] "Number of smartphone users* worldwide from 2012 to 2018 (in billions)." [Online]. Available: http://www.statista.com/statistics/330695/number-of-smartphone-users-worldwide/.

[129] S. A. Lamel, K. M. Haldeman, H. Ely, C. L. Kovarik, H. Pak, and A. W. Armstrong, "Application of mobile teledermatology for skin cancer screening," *J Am Acad Dermatol*, vol. 67, no. 4, 2012, pp. 576–581.

[130] J. Spigulis, "In vivo skin imaging prototypes 'made in Latvia," *Frontiers of Optoelectronics*, vol. 10, no. 3, 2017, pp. 255–266.

[131] I. Kuzmina, M. Lacis, J. Spigulis, A. Berzina, and L. Valeine, "Study of smartphone suitability for mapping of skin chromophores," *Journal of Biomedical Optics*, vol. 20, no. 9, 2015, p. 90503.

[132] U. Rubīns, J.Spīgulis, and A. Miščuks, "Photoplethysmography imaging algorithm for continuous monitoring of regional anesthesia," in *2016 14th ACM/IEEE Symposium on Embedded Systems For Real-time Multimedia (ESTIMedia)*, 2016, pp. 1–5.

[133] M. Lange, U. Rubins, and M. Aleksejs, "The use of remote photoplethysmography system for regional anesthesia monitoring in operating room," in *Book of Abstracts of 13th International Young Scientist conference Developments in Optics and Communications 2017*, 2017.

[134] M. Lange, U. Rubins, A. Lihachev, and D. Bliznuks, "Optical, non-invasive diagnostic imaging methods," in *Book of Abstracts of "Rīga Stradiņš University Scientific Conference 2018"*, 2018.

[135] SPKC, "Health Statistics Database," 2023. [Online]. Available: https://statistika.spkc.gov.lv/pxweb/lv/Health/Health__Saslimstiba_Slimibu_Izplatiba__Onkologija/?tablelist=true. [Accessed: 25-Jan-2024].

ACKNOWLEDGEMENTS

I am deeply grateful for the opportunity to explore the wide horizons of medical physics research topics, especially biophotonics, and happy to be a part of this PhD journey!

All that would not have been possible without the intelligent, hard-working and supporting colleagues, team members and collaborators at University of Latvia (LU) and Riga Technical University, especially colleagues at Institute of Atomic Physics and Spectroscopy, LU. I am deeply grateful for the support to my thesis supervisor Prof. Janis Spigulis. The clinical approbation of the equipment created at the Biophotonics laboratory would have not been possible without the collaborations of hospitals: LOC and TOS, and very supportive medical doctors: Dr. Alexnder Derjabo, Dr. Aleksejs Miščuks, and others. I am blessed to have met wonderful collaboration partners and researchers around the world who have inspired and helped me in this work. A great shoutout to the medical team in Dermatology Department at Semmelweis University, Hungary who always provided support with patient imaging, data collection, medical advice and other solutions on how to get things done better. All the work would have not been possible without the patients who volunteered to get their skin lesions imaged while often dealing with the incredibly hard battle of skin cancer.

While people and ideas always come first, this work would have been possible without the generous financial and resourceful support, so here are the received grants for participation in research projects:

- LU doktorantūras kapacitātes stiprināšana jaunā doktorantūras modeļa ietvarā, project No. 8.2.2.0/20/I/006, LU registration No. ESS2021/434.
- Ātrā mikroorganismu aktivitātes noteikšana ar optisko bez-kontakta metodi (FLPP #lzp-2018/2-0051);
- Ādas vēža agrīnas diagnostikas precizitātes uzlabošana ar neironu tīkliem (FLPP #lzp-2018/2-0052);
- Atomfizika, optiskās tehnoloģijas un medicīniskā fizika (LU registration No. AAP2016/B054);
- Portatīva ierīce ādas vēža agrīnai bezkontakta diagnostikai / European Regional Development Fund project "Portable Device for Non-contact Early Diagnostics of Skin Cancer" (ERAF #1.1.1.1/16/A/197);
- Biofotonika: attēlošana, diagnostika un monitorings (VPP SOPHIS #10-4/VPP-4/11);
- Inovatīvas ādas diagnostiskās attēlošanas tehnoloģijas (ERAF #2111/3-015).
- European Regional Development Fund project "Innovative technologies for optical skin diagnostics" (2014/0041/2DP/2.1.1.1.0/14/APIA/VIAA/015).

Also, financial support received for attending and presenting at conferences, symposiums and contests:

- Department of Physics, University of Latvia annual PhD student support of for attending conferences,
- SPIE Student Conference Support grant,
- OSA Student Conference Support grant,

- ERAF support "Integrētie nacionālā līmeņa pasākumi Latvijas pētniecības un attīstības interešu pārstāvības stiprināšanai Eiropas pētniecības telpā" (No. 1.1.1.5/17/I/002),
- LSA Scientific Fund State Grant (2017), etc.

Last and the most sincere gratitude to my family for supporting me throughout this journey, for the patience and love. An enormous gratitude to my friends who are always an inspiration, support and reason to keep doing the work, to get up even after falling down. I am forever grateful to my grandfather Raimonds who was a physics teacher and was the first one showing me the amazing and exciting world of engineering, and always reminding that physics is and will be in our lives every step of the way.

ANNEX 1

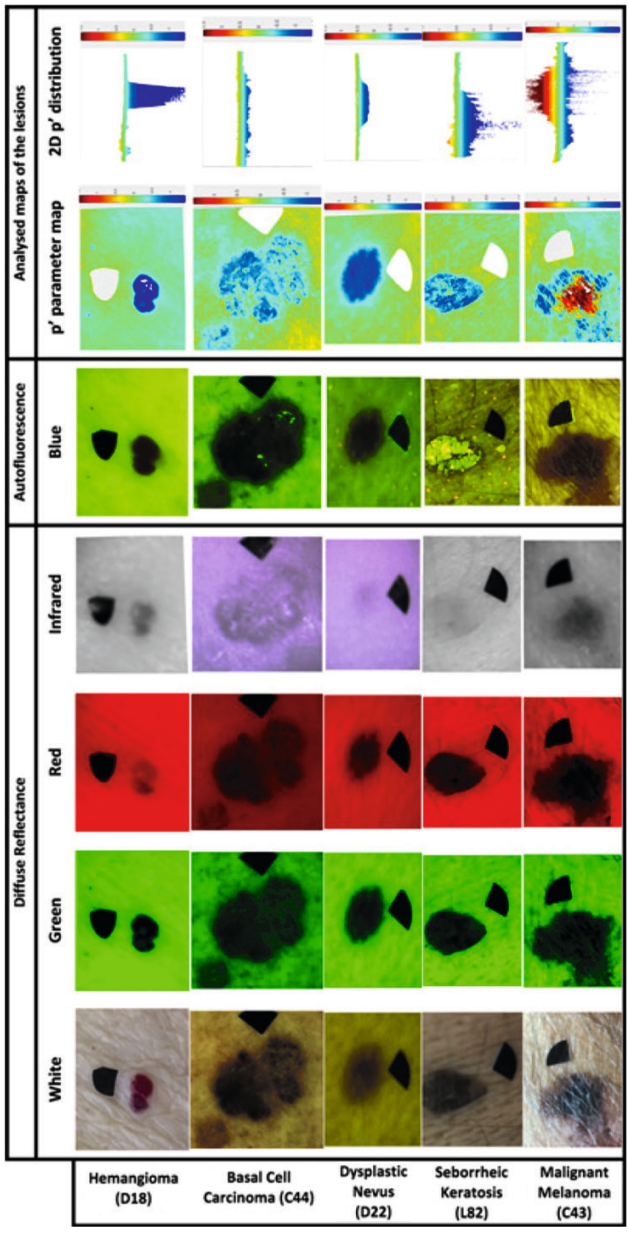

Possibility to distinguish various lesions: Hemangioma, BCC, Dysplastic Nevus, SK, MM at various illuminated modes: (from the left): Diffuse reflectance at white light, green (526 nm), red (663 nm), infrared (964 nm); Auto fluorescence induced by violet (405 nm) light; Analysed image maps: p' parameter map and p' parameter distribution in 2D [P2]

ANNEX 2

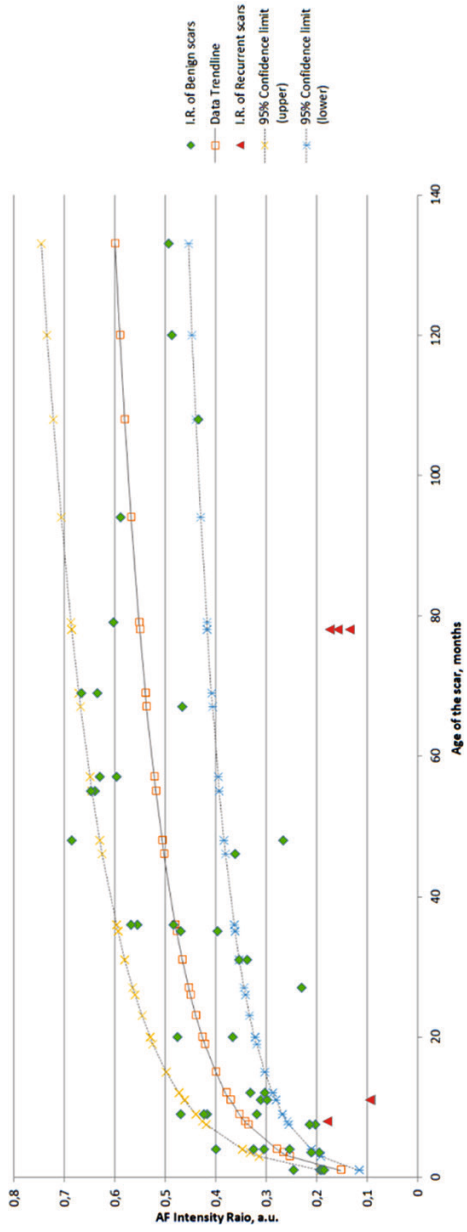

AF intensity ratio (I.R.) showing the distribution of benign scars (green points) and recurrent scars (red triangles). Data trendline shows the tendency of benign scar AF I.R to increase with time, the lower and upper dashed curves demonstrate the 95% confidence level of the benign scar AF I.R. distribution [P4]

ANNEX 3

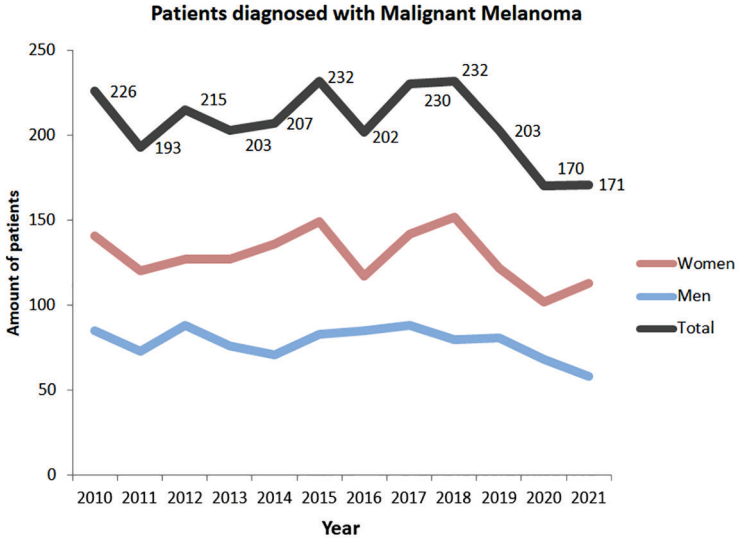

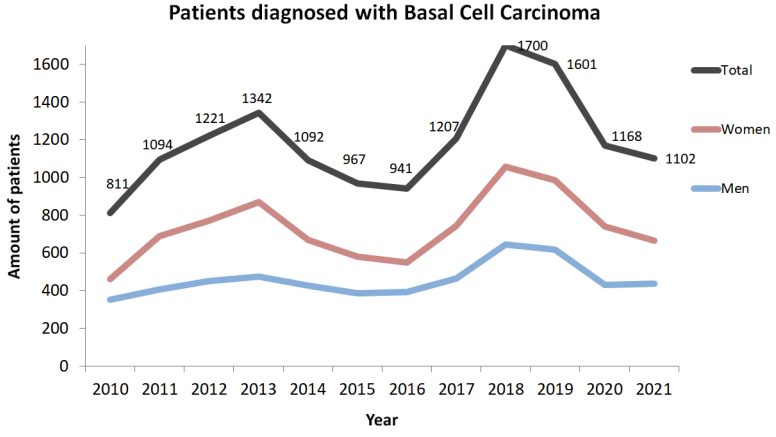

(Updated from SPKC at 31.10.2023.) Skin cancer statistics in Latvia from 2010 till 2021: incidence for MM (on the left) and BCC (on the right); the absolute amount of patients with first-time diagnosis. Note from the source SPKC: In period 2015–2016 there is a drop of data due to the fact that a number of patient data was taken out of the archive because of wrong IDs, also data about period 2018–2021 is preliminary [135]

ANNEX 4

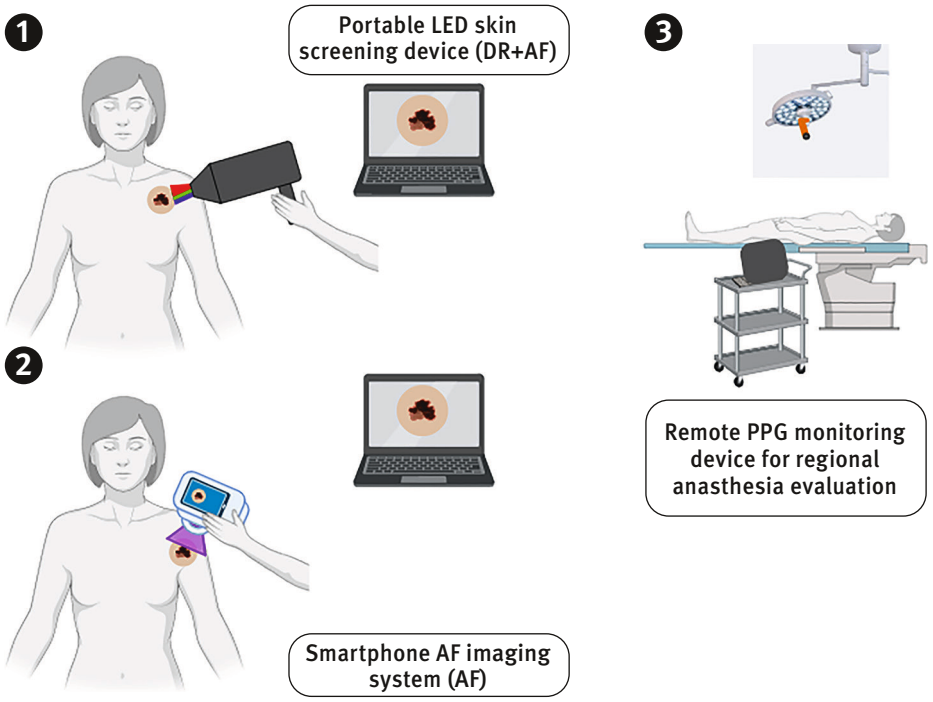

This thesis consists of three parts, validating three imaging systems at a clinical setting: 1) a portable light-emitting diode skin screening device; 2) smartphone autofluorescence imaging system; 3) remote photoplethysmography monitoring device for assessment of regional anesthesia